Coordination Chemistry Reviews 532 (2025) 216506

Contents lists available at ScienceDirect

Coordination Chemistry Reviews

journal homepage: www.elsevier.com/locate/ccr

Fabrication of MOF-based Nanozyme sensor arrays and their application in disease diagnosis

Mengmeng Wang [a,1], Hongjin Zhang [c,1], Shuangshuang Yan [d], Yutian Zhou [c], Xinli Guo [c], Dongying An [c], Wenbin Zhong [c], Yang Zhang [a,b,*]

[a] *Shenyang Key Laboratory of Medical Molecular Theranostic Probes in School of Pharmacy, Shenyang Medical College, 146 Huanghe North Avenue, Shenyang 110034, China*

[b] *Liaoning Province Key Laboratory for Phenomics of Human Ethnic Specificity and Critical Illness, Shenyang Medical College, 146 Huanghe North Avenue, Shenyang 110034, China*

[c] *School of Basic Medicine, Shenyang Medical College, 146 Huanghe North Avenue, Shenyang 110034, China*

[d] *School of Public Health, Shenyang Medical College, 146 Huanghe North Avenue, Shenyang 110034, China*

Abbreviations: MOFs, metal-organic frameworks; HRP, horseradish peroxidase; ALP, alkaline phosphatase; ACP, acid phosphatase; POCT, point-of-care testing; 3,5-DTBC, 3,5-di-tert-butylcatechol; PVP, polyvinylpyrrolidone; BA, benzoic acid; TA, terephthalic acid; MB, methylene blue; ROS, reactive oxygen specie; AuNSt, Au nanostars; SERS, surface-enhanced Raman scattering; ALD, atomic layer deposition; BPA, bisphenol A; CAT, Catalase; SOD, superoxide dismutase; Gox, glucose oxidase; PNIPAM, polymer (N-isopropylacrylamide); PDT, photodynamic therapy; PSMOF, photoresponsive MOF-based nanozyme; LAC, laccase; ESR, electron spin resonance; OPD, *o*-phenylenediamine; ABTS, 2,2′-azino-bis(3-ethylbenzothiazoline-6-sulfonic acid); TAOH, TA with •OH yields 2-hydroxyterephthalic acid; TME, tumor microenvironment; ZMTP, metal-organic framework nanozyme; ABEI, N-(4-aminobutyl)-N-(ethylisobutyramide); ECL, electrochemiluminescence; Ab1, anti-MUC1 antibody; HQ, hydroquinone; CC, catechol; SPE, screen-printed electrode; Rct, charge transfer resistance; CV, cyclic voltammetry; EIS, electrochemical impedance spectroscopy; LOD, limit of detection; SPR, surface plasmon resonance sensors; FRET, Förster resonance energy transfer; m-AP, meta-Aminophenol; p-AP, para-Aminophenol; PADs, paper-based analytical devices; PBA, phenylboronic acid; VP, *Vibrio parahaemolyticus*; Au NPs, gold nanoparticles; TDNs, tetrahedral DNA nanostructures; PAMAM, Poly(amidoamine) dendrimers; ICT, intramolecular charge transfer; TFTP, 2,3,5,6-tetrafluorothiophenol; 2,4-DNP, 2,4-dinitrophenol; IFE, inner filter effect; PVA, polyvinyl alcohol hydrogel; 2,6-NDC, 2,6-naphthalenedicarboxylic acid; TCs, tetracyclines; 2D MOF, two-dimensional MOF; Ni-MOF, nickel MOF; SEB, Staphylococcal enterotoxin B; H, histidine; hG, hemin-G-quadruplex deoxyribonuclease; AChE, acetylcholinesterase; TCh, thiocholine; MSBs, microspheres; ELISA, Enzyme-linked immunosorbent assay; CEA, anti-cancer embryonic antigen; SA-HRP, streptavidin-horseradish peroxidase; POD, peroxidase; Ach, acetylcholine; UsAuNPs, ultrasmall gold nanoparticles; ChOx, choline oxidase; Ops, Organophosphorus pesticides; POC, point-of-care; HPLC, high-performance liquid chromatography; mPEG, modifying both with polyethylene glycol; DAB, 3,3′-diaminobenzidine; AuNP, gold nanoparticle; PSA, prostate-specific antigen; AFP, alpha-fetoprotein; CA 15–3, cancer antigen 15–3; CA 125, cancer antigen 125; NSE, neuron-specific enolase; PEC, photoelectrochemical; GO, graphene oxide; CHA, catalytic hairpin assembly; E2, estradiol; CVD, Cardiovascular disease; cTnI, Cardiac troponin I; AMI, acute myocardial infarction; MMOF, magnetic metal-organic framework; SPGE, screen-printed gold electrode; NP1, nanoprobes 1; BQ, benzoquinone; Zn-MOF, zinc-based metal-organic framework; pCTAB, polymer membrane of hexadecyltrimethylammonium bromide; DES, deep eutectic solvent; MIPs, molecularly imprinted polymers; Fe-MOF, iron-based MOFs; PD-L1, death-ligand 1; FITC, fluorescein isothiocyanate; RDPP, Ru(dpp)3]Cl2); AS, atherosclerosis; MRI, magnetic resonance imaging; ZIFs, zeolitic imidazolate frameworks; LDI MS, laser desorption/ionization mass spectrometry; CAD, coronary artery disease; AD, Alzheimer's disease; ALS, Amyotrophic Lateral Sclerosis; Aβ, Amyloid-β; 2-MIM, 2-methylimidazole; BPNS, N-(6-(benzo[*d*]thiazol-2-yl)pyridin-3-yl)-5-(dimethylamino)naphthalene-1- sulfonamide; CLSM, confocal laser scanning microscopy; ThT, thioflavin T; Fer, ferrocene; Ab2, secondary antibody; ECL-RET, electrochemiluminescence resonance energy transfer (ECL-RET); GSH, glutathione; Fc-Cu-MOF, ferrocene-functionalized copper MOFs; CuCl, cuprous chloride; 4-MBN, 4-mercaptobutyronitrile; IS, internal standard; NRs, nanorods; LMG, malachite green; c-CuMOF, chiral Cu(II)-metal-organic framework; TNT, TiO2 nanotube arrays; Eu-MOF, Eu-metal organic framework; UA, Uric acid; UiO-PSM, post-modified metal-organic framework; DAP, 2,3-diaminophenazine; AA, ascorbic acid; DA, dopamine; 5-HT, serotonin; PCR, Polymerase Chain Reaction; CRP, C-reactive protein; PCT, procalcitonin; IL-6, interleukin-6; MAFs, fluorescent MOFs; LFA, lateral flow immunoassay; VOCs, volatile organic compounds; 3H-2B, 3-hydroxy-2-butanone; Co_3O_4/ZnO SPs, cobalt-doped zinc oxide superparticles; MRSA, Methicillin-resistant *Staphylococcus aureus*; Bi-MOF, bismuth metal-organic framework; RSV, respiratory syncytial virus; P-DNA, DNA probes; PET, photoinduced electron transfer; FAM, carboxyfluorescein; ROX, 5(6)-carboxyrhodamine triethylammonium salt; DENV, Dengue virus; ZIKV, Zika virus; SPCE, screen-printed carbon electrode; c-MOFs, conductive MOFs; Exo I, Exonuclease I; NPC, nasopharyngeal carcinoma; AuSPE, gold nanoelectrode; RA, rheumatoid arthritis; RONS, reactive oxygen and nitrogen species; UP, UiO-66-PSM; UPF, UiO-66-PSM-Fe; COPD, chronic obstructive pulmonary disease; Co-MOF, cobalt metal-organic framework; PA, phytic acid; TVB-N, volatile basic nitrogen; *E*-noses, electronic noses; PCA, Principal Component Analysis; ANN, Artificial Neural Networks; SVM, Support Vector Machines; SURMOFs, Surface Mounted MOFs; PDMS, polydimethylsiloxane.

* Corresponding author at: Shenyang Key Laboratory of Medical Molecular Theranostic Probes in School of Pharmacy, Shenyang Medical College, 146 Huanghe North Avenue, Shenyang 110034, China.

E-mail address: zhangyang@qdu.edu.cn (Y. Zhang).

[1] These authors contributed equally to this work.

https://doi.org/10.1016/j.ccr.2025.216506

Received 6 December 2024; Received in revised form 30 January 2025; Accepted 31 January 2025

Available online 18 February 2025

ARTICLE INFO

Keywords:
Nanozyme
MOF
Sensor arrays
Disease diagnosis

ABSTRACT

Nanomaterials with enzyme-like activities are crucial in biosensing, disease diagnosis, and treatment due to their advantages of low costs, ease of synthesis, high stabilities, and tunable activities. Among them, nanozymes based on metal-organic frameworks (MOFs) attract significant attention because of their unique structural characteristics and compositions. In this review, we analyze the regulation mechanisms and catalytic properties of MOF-based nanozymes, focusing on the latest research advancements in sensor development and biomedical applications. Additionally, we briefly explore the potential applications of these nanozymes in smart assistive technologies. Furthermore, we identify the current challenges and limitations, propose viable solutions to address these problems, and position sensors fabricated using MOF-based nanozymes as effective alternatives in disease diagnosis. Ultimately, this review provides guidance for researchers to effectively utilize MOF-based nanozymes in the field of biomedicine.

1. Introduction

Natural enzymes serve as highly efficient catalysts within organisms, exhibiting not only high catalytic activities but also substrate specificities. This enables them to rapidly convert specific substrates into quantifiable substances. When employed in biological sensing systems, the designed reactions are initiated by the presence of target molecules, enabling the generated products to serve as rapid, potentially quantifiable indicators of the presence of the target molecules. Commonly used biological enzymes in laboratory diagnostic tools include horseradish peroxidase (HRP), alkaline phosphatase, and acid phosphatase [1–3]. However, the application of these enzymes in sensing systems is limited by their poor stabilities, high costs, and complex production processes [4–6]. Notably, most of these enzymes are proteins, which are susceptible to denaturation or degradation due to environmental changes in pH, temperature, the presence of proteases, etc., and thus, their catalytic performances are often adversely affected under certain physiological conditions [7,8].

Nanozymes, as artificially engineered nanomaterials, display catalytic functionalities and characteristics akin to those of natural enzymes. Compared to natural enzymes, nanobiocatalysts exhibit several advantages, such as environmental compatibilities, ease of synthesis, extended stabilities, and capacities for repeated utilization, thus overcoming the inherent constraints of natural enzymes. In 2007, Yan et al. [9] reported that magnetic Fe_3O_4 nanoparticles (NPs) exhibit peroxidase-like (POD-like) activities, marking a rapid advancement in the field of nanozymes. Subsequent research identified various materials, such as metal oxides, metal nanoparticles, 2D materials, and MOFs, with diverse enzyme-like activities [10–13]. MOFs, which comprise metal ions or clusters coordinated with organic ligands, form crystalline materials with porous structures [14]. The pores offer abundant active sites, enabling MOFs to effectively mimic enzyme activities. By selecting appropriate ligands and metal ions, the structures of MOFs can be tailored to optimize their catalytic performances and selectivities. Nanozymes are widely utilized in sensor development, particularly in biosensing and -assays [15,16], due to their enzyme-mimicking efficiencies. The forms, sizes, and modifications of MOFs also affect their performances [17], underscoring the importance of studying the syntheses and structures of MOF-based nanozymes to comprehensively understand their catalytic capacities. Given the multi-enzyme activities and tunable structures of MOF-based nanozymes, they display significant potential for use in various sensing platforms, such as enzyme-linked immunosensors and electrochemical and optical biosensors [18–21]. Furthermore, MOF-based nanozymes can be employed in enzyme cascade analysis and point-of-care testing (POCT) to enhance diagnostic efficiency [22,23]. In clinical disease diagnosis, the highly controllable pore structures and surface functionalization properties of MOF-based nanozymes enable the specific capture and identification of particular biomolecular markers, such as disease biomarkers or drug metabolites. These biomolecular markers are primarily used in diagnosing cancer, cardiovascular, infectious, and neurodegenerative diseases, and metabolic disorders [24–31]. Several valuable reviews cover extensive research in this field. However, no reviews are currently published that summarize the latest advancements in MOF-based nanozymes in the early diagnosis of major diseases, which is crucial in the timely prevention and treatment of related illnesses.

In this review, we investigate the current advancements and prospects of MOF-based nanozymes in biosensing and disease diagnostics (Scheme 1). Section 2 analyzes the regulation of MOF-based nanozymes and factors influencing their enzymatic activities. Section 3 summarizes the catalytic mechanisms of MOF-based nanozymes, elucidating how they leverage their porous MOF structures and surface functionalization properties to mimic and enhance enzymatic catalysis. Section 4 categorizes the sensors fabricated using MOF-based nanozymes, including their applications in POCT, and furthermore, Section 5 provides an in-depth review of the applications of MOF-based nanozymes in clinical disease diagnosis. Finally, we analyze the application of machine learning in sensor development and the current obstacles and potential for clinical application in disease detection.

2. Regulation of MOF-based nanozymes

2.1. Pore and quantity

The pore structures of MOFs determine their capacities to accommodate substrate molecules and the diffusion characteristics of the substrate molecules, thus influencing the rates and efficiencies of catalytic reactions. Hence, the performances of MOF-based nanozymes are directly affected by the pore sizes of their porous structures, e.g., Tian et al. [32] manipulated the pore size of p-WO_3 to regulate the catalytic activity of in-situ-assembled MOF-818 and its catalytic performance in the oxidation of 3,5-di-*tert*-butylcatechol (3,5-DTBC). The maximum reaction rate (V_{max}) of MOF-818 in oxidizing 3,5-DTBC increased, peaking at a pore size of 400 nm, as the pore size of p-WO_3 was increased from 230 to 400 nm. However, upon further enlargement of the pore size, V_{max} began to decline. This was attributed to the effective assembly of MOF-818 within the pore channels of p-WO_3 when the pore size reached 400 nm, providing an appropriate confined environment. This environment not only facilitated the rapid diffusion of substrates into the pore channels of *p*-WO_3 but also enhanced the effective collisions between the nanozyme and substrate, thus significantly increasing the catalytic activity. Hyeongtae et al. designed the layered porous structure of LIG@Cu_3HHTP_2 to effectively exploit its large surface area and porosity, enabling the rapid detection of NO_2 [33]. Furthermore, the pore size significantly influences the sensing performance of a MOF in terms of chiral selectivity [34]. IRMOF-74-II-Mg-C-Tb, with a larger pore size, exhibited superior adsorption and detection capacities for larger chiral molecules, whereas IRMOF-74-I-Mg-C-Tb was more suitable for use in detecting smaller chiral molecules. This indicates the potential for realizing the selective, efficient detection of target molecules with different sizes by regulating the pore size. Remarkably, Wang et al. [35] reported that the regular pore structures of MOFs also influence their catalytic efficiencies.

2.2. Size

The activities of nanozymes are influenced by their particle sizes. Nanozymes based on MOFs commonly occur in 2D and 3D forms, such as dodecahedral (ZIF-67) and hemin-based (PCN-222(Fe) structures [36,37]. Two-dimensional MOF-based nanozymes exhibit superior catalytic performances compared to those of their 3D counterparts, mainly due to the smaller substrate diffusion barriers of 2D nanozymes [38]. These enable substrate molecules to smoothly traverse the nanozyme channels, rapidly reaching the active sites and significantly enhancing the catalytic efficiencies. Lu et al. [39] successfully synthesized Zr-MOF-PVP nanozymes with diameters of 45 nm, using polyvinylpyrrolidone (PVP) as a surface modifier. Compared to that of conventionally synthesized Zr-MOF (600 nm), the Zr-MOF-PVP nanozymes displayed significantly enhanced POD-like activities [40]. This is because smaller particle sizes typically correspond to higher specific surface areas, providing more active sites for substrate adsorption and reaction, thus enhancing the catalytic activity. Conato et al. investigated the synthesis of MIL-88B(Fe) MOFs using varying concentrations of benzoic acid (BA, 0.25–10 times the concentration of terephthalic acid (TA) [41]. By adjusting the BA concentration, the particle size and shape of MIL-88B (Fe) can be effectively controlled. Lower BA concentrations (0.25–0.5 times that of TA) result in rod- and spindle-shaped MIL-88B(Fe), whereas higher concentrations (approximately 10 times that of TA) lead to the formation of octahedral and spherical MIL-88B(Fe) structures. The smaller crystals (spindle- and rod-shaped) exhibit higher adsorption capacities and faster adsorption rates for methylene blue (MB) (Fig. 1A). The larger crystals (octahedral and spherical) display excellent catalytic performances, degrading >90 % of MB within 20 min, which is attributed to the increased levels of exposure and accessibility of the active sites due to microstructural defects. Furthermore, higher concentrations of BA induce missing linker defects, increasing the number of active iron centers and thus enhancing the catalytic activity (Fig. 1B). Additionally, Ahmed et al. [42] reported that the sizes of NPs were crucial in the conversion of CO_2 into valuable hydrocarbons. Smaller iron NPs were favorable in hydrogenation reactions, whereas larger particles were more suitable for the chemical adsorption of CO_2.

2.3. Morphology

In addition to size, morphology is a key factor influencing the catalytic activity of a nanozyme. Numerous studies reported close relationships between the morphologies of nanomaterials and their enzyme-like activities when designing efficient nanozymes [43,44]. Xu et al. [45] synthesized and characterized spherical, cubic, and rod-shaped Mn_3O_4 NPs with {101}, {200}, and {103} crystal facets, respectively. They investigated the design of nanozymes based on different shapes of Mn_3O_4 and their potential for use in treating Parkinson's disease. The Mn_3O_4 nanorods ({103} crystal facets) exhibited excellent enzyme-like activities in scavenging reactive oxygen species (ROS). Similarly, Singh et al. studied the enzyme activities of Mn_3O_4 nanostructures with various morphologies (including nanoflowers and -sheets, cubes, polyhedrons, and hexagonal plates), revealing that nanoflower-shaped Mn_3O_4 exhibited the highest enzyme-like activity, indicating the

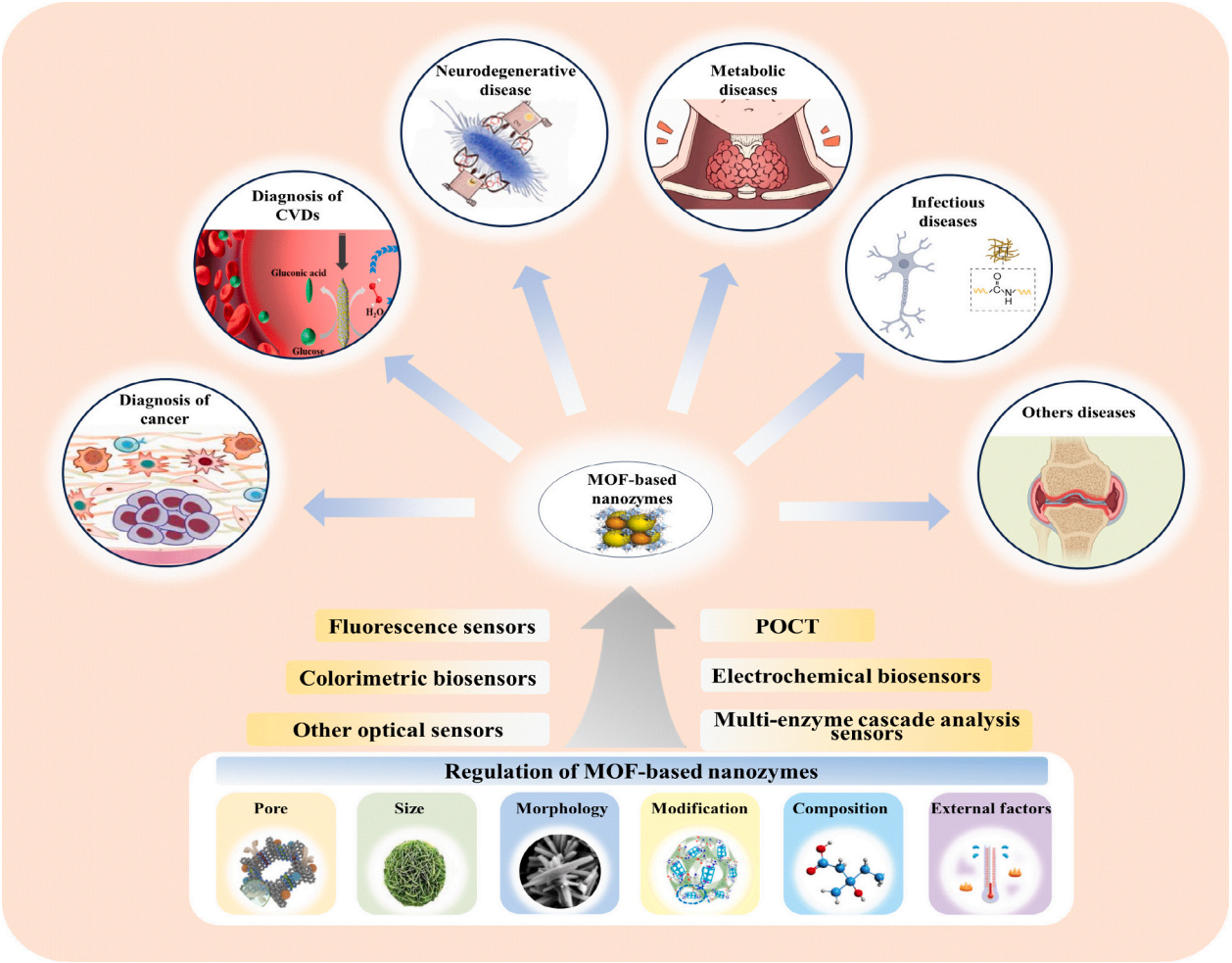

Scheme 1. Schematic diagram of the regulation of MOF-based nanozymes and their applications in disease diagnosis.

A

Effect of the pore size of p-WO_3 on the catalytic performance of MOF-818.

Catalytic system	V_{max}(μM s^{-1})	K_m(mM)	k_{cat}(s^{-1})	k_{cat}/K_m(mM^{-1} s^{-1})	Oxidation yield of 3,5-DTBC (%)
MOF-818@p-WO_3-1	1.96	2.36	11.53	4.88	35.1
MOF-818@p-WO_3-2	2.15	2.11	12.65	5.99	41.4
MOF-818@p-WO_3-3	5.35	1.42	31.47	22.16	95.2
MOF-818@p-WO_3-4	2.63	1.98	15.47	7.81	52.5

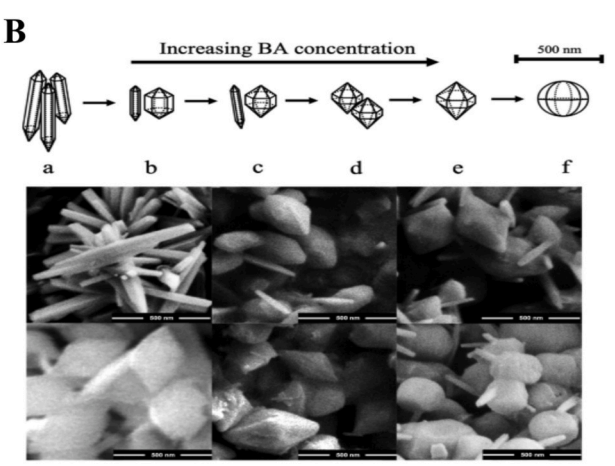

Fig. 1. Regulation of size and pore in metal-based nanozymes. (A) Catalytic reaction rate of MOF-818 in *p*-WO_3–1, *p*-WO_3–2, *p*-WO_3–3, or *p*-WO_3–4 with varying concentration of 3,5-DTBC. Reprinted with permission from Ref. [32]. (B) The synthesis of BA-MIL-88B(Fe) particles at various modulator concentrations captured through SEM images. Reprinted with permission from Ref. [41].

substantial morphology dependence [46]. Notably, changes in the morphologies of several nanozymes do not necessarily affect their enzyme activities. Cao et al. [47] reported that the formation of a Au—Hg alloy disrupted the sharp surface morphologies of Au nanostars (AuNSt), reducing their numbers of hot spots and significantly diminishing their capacities for Raman enhancement without deteriorating their catalytic activities. Ultimately, they successfully utilized the catalytic activity and surface-enhanced Raman scattering (SERS) effect of AuNSt in detecting Hg^{2+} in seawater. Remarkably, the morphologies of nanozymes not only affect their catalytic activities but may also influence their selectivities [48].

2.4. Modification

The activities of MOF-based nanozymes can be effectively modulated and their functionalities can be enhanced, while maintaining their MOF structures [49]. The enzyme-like activities of MOF-based nanozymes are highly sensitive to surface modifications. Among seven types of bimetallic NPs synthesized using the MIL-101 MOF as a stable carrier (Cu—Pd, Ni—Ru, Co—Pt, Cu—Pt), the POD-like activity of 9.5 wt% Cu-Pd@MIL-101 was the highest, surpassing those of bare Au NPs by a factor of 12.73 [50]. Zhang et al. synthesized 1Al/MIL-100(Fe) nanozymes via cyclic Al_2O_3 atomic layer deposition, and they exhibit enhanced POD-like activities compared to those of unmodified MIL-100 (Fe) nanozymes (Fig. 2A and B) [51]. This enhancement is attributed to the generation of more hydroxyl radicals by 1Al/MIL-100(Fe) nanozymes (Fig. 2C). Furthermore, the catalytic effects of these nanozymes are inhibited by glutathione (GSH), leading to the development of a highly sensitive colorimetric GSH sensor with a detection limit of 2.2 nM (Fig. 2D). Zhang et al. [52] encapsulated a hemin/bovine serum albumin co-assembly (Hemin@BSA) within a zeolitic imidazolate framework (ZIF-8) to form Hemin@BSA@ZIF-8 nanozymes, which exhibited increased POD activities. The enzyme activities of the modified nanozymes were enhanced via confinement effects, thus accelerating substrate transfer and internal catalytic cycling, enabling the sensitive detection of small molecules, such as H_2O_2, glucose, and bisphenol A. Remarkably, surface modifications of MOF-based nanozymes with multiple enzyme activities can selectively influence the activity of one enzyme without affecting those of the others [53]. Moreover, integrating antioxidant nanozymes into MOFs can regulate neuronal differentiation and improve oxidative stress, offering a novel approach to utilizing nanozymes in promoting neural regeneration [54].

2.5. Composition

MOFs, which are nanomaterials containing metal atoms and ligands, are commonly modified by doping with metal ions and synthesizing complexes to regulate nanozyme activity [55]. For example, Xu et al. [56] reported a simple method of preparing metal-adenosine triphosphate (metal-ATP) NPs, with enzyme activities that could be modulated via metal doping. Cu-ATP NPs exhibited only POD-like activities, whereas Fe^{3+}-doped Cu-ATP NPs displayed excellent POD activities and reduced POD-like activities. Upon introducing Mn^{2+} ions as regulators to balance the enzyme-like activities, the CuMnFe-ATP NPs exhibited significant POD- and catalase-like (CAT-like) activities. Another study reported that MOF-818 containing a trinuclear copper center exhibited a significantly enhanced catechol (CC) oxidase-like activity compared to that of copper-free MOF-818 [57]. Remarkably, hybridization is an effective strategy for use in fabricating nanomaterials with multiple enzyme activities, e.g., by incorporating platinum NPs with CAT-like activities and manganese (III) porphyrin with a superoxide dismutase (SOD) activity into a zirconium-based MOF (PCN-222), an integrated dual-enzyme nanozyme system (Pt@PCN-222Mn) was developed, with the catalytic functions of SOD and CAT [58].

2.6. External factors

Similar to those of natural enzymes, the optimal catalytic activities of nanozymes are also influenced by external factors, such as pH, temperature, and light [59,60]. However, compared to those of natural enzymes, most nanozymes exhibit enhanced tolerances over wider pH ranges. Generally, nanomaterials with multiple enzyme activities are more likely to display POD-like activities at a low pH and CAT- and SOD-like characteristics at a high pH. Chen et al. [61] designed a nanozyme with dual enzyme activities (Ni-MOF), which can be dynamically regulated based on changes in pH. Under slightly acidic conditions, this nanozyme displays a POD-like activity, reacting with hydrogen peroxide to generate hydroxyl radicals and effectively killing bacteria. In neutral environments, the nanozyme exhibits an SOD activity, clearing excess ROS and promoting the transformation of macrophages into M2-like macrophages (Fig. 3A). Therefore, different pH values can result in the manifestation of different enzyme-like activities by the same nanozyme. Building on this, Liu et al. [62] used 2D Cu-TCPP(Fe) nanosheets as a POD-like system and immobilized glucose oxidase (GOx) on their surfaces via physical adsorption. During the GOx catalytic reaction, large amounts of gluconic acid and hydrogen peroxide are produced. The generated gluconic acid effectively lowers the pH from 7 to 3–4,

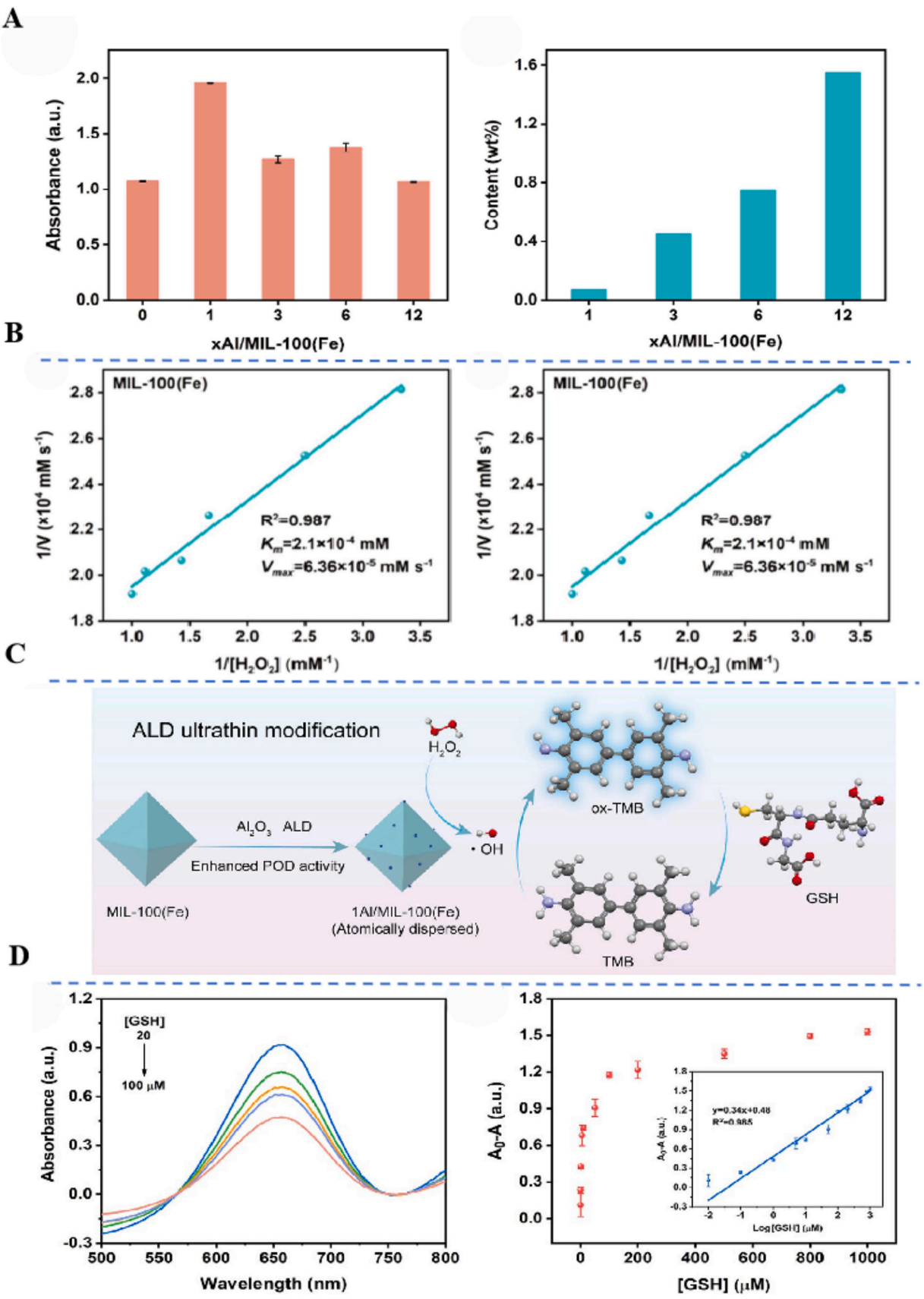

Fig. 2. (A) Comparison of peroxidase-like activity catalyzed by 1Al/MIL-100(Fe) nanozymes. (B) The relationship between the initial reaction rate and [H_2O_2] for 10 min of incubation on two nanozymes, MIL-100(Fe) and 1Al/MIL-100(Fe). (C) The reaction mechanism of 1Al/MIL-100(Fe). (D) The correlation between absorbance change and GSH concentration. Reprinted with permission from Ref. [51].

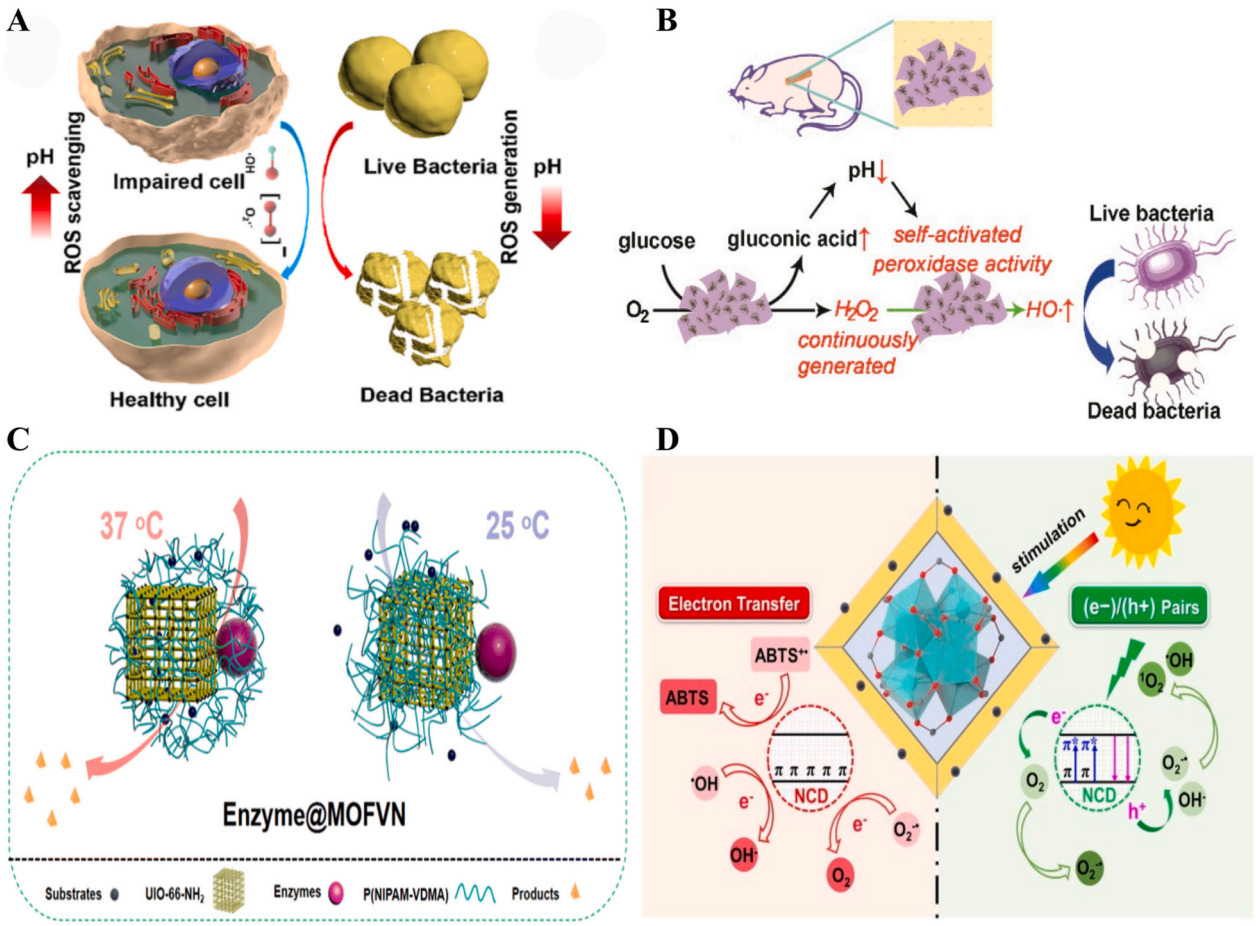

Fig. 3. (A) The mechanism by which Ni-MOF promotes macrophage transformation. Reprinted with permission from Ref. [61]. (B) The antibacterial mechanism of the 2D MOF/GOx hybrid nanocatalyst as a benign and self-activated cascade reagent. Reprinted with permission from Ref. [62]. (C) thermo-responsive polymer effect on the catalytic activity of the enzymes@MOFVN-based nano-reactors at different temperatures. Reprinted with permission from Ref. [65]. (D) Mechanisms of generating or consuming reactive oxygen species by NCDs/UiO-66 under light and dark conditions. Reprinted with permission from Ref. [69].

significantly enhancing the POD-like activity (Fig. 3B).

Temperature fluctuations can influence the catalytic performances and reaction kinetics of nanozymes, thus regulating their enzyme activities [63]. Nanozymes with multiple enzymatic activities exhibit distinct optimal temperatures for the catalytic activities, with their activities typically increasing with temperature until reaching the optimal points, e.g., Luo et al. reported a novel MOF (Ce-BPyDC) with significant OXD and POD activities, revealing the clear dependences of the enzyme activities on the temperature [64]. As the temperature increased, the OXD activity gradually increased, but it significantly decreased when the temperature was >40 °C. Similarly, Qiao et al. [65] immobilized a temperature-sensitive polymer (poly(*N*-isopropylacrylamide) (PNIPAM)) on a MOF, followed by the attachment of different enzymes onto this composite, successfully fabricating polymer-MOF@enzyme nanoreactors (Fig. 3C). The results indicated that temperature variations significantly influence the catalytic activities of five nanozymes, including TRY@MOFVN, Glnase@MOFVN, and HRP@MOFVN. Integrating photoactive molecules into MOFs enables the fabrication of photoresponsive MOF-based nanozymes. These nanozymes can activate enzyme-catalyzed reactions under specific wavelengths or light stimuli, generating ROS and modulating their catalytic properties. These characteristics endow them with high levels of potential for application in various fields, including drug delivery, photodynamic therapy, and the regulation of light-initiated biochemical processes, thus promoting the deep integration of biomedicine and nanotechnology [66–68]. Liu et al. [70] synthesized a photoresponsive MOF-based nanozyme (PSMOF) that exhibited an excellent OXD activity under visible light, efficiently catalyzing substrate oxidation. Furthermore, the photoresponsive nature of PSMOF enabled flexible control of its OXD activity by modulating the activation of the light source. Another study revealed the characteristics of a light-regulated nanozyme composite material (NCDs/UiO-66) [69]. Under darkness, NCDs/UiO-66 displays a significant antioxidant capacity, effectively scavenging ROS and free radicals. Conversely, under light, this composite material exhibits pro-oxidative properties, generating ROS and displaying a POD-like activity. By toggling the (de) activation of the light, this system realizes controllable switching between pro-oxidative and antioxidant activities (Fig. 3D). This novel regulatory mechanism holds promise for use in overcoming the limitations of traditional unidirectional enzyme regulation, offering novel possibilities for future practical applications.

3. Catalytic mechanisms

The catalytic mechanisms of MOF-based nanozymes rely on the metal active sites within their structures, which can catalyze the chemical transformations of various substrates under different environmental conditions, exhibiting enzyme-like activities, such as those of OXD, POD, CAT, SOD, GPx, laccase, and hydrolase [71,72]. The catalytic mechanisms of oxidase-like MOF-based nanozymes primarily involve the utilization of specific active site structures and chemical properties to efficiently catalyze substrate conversion via steps including substrate binding, oxidation, electron transfer, and product release. During this process, dissolved O_2 typically acts as an electron acceptor in the reactions, leading to the generation of key intermediates, such as $^1O_2$

and $O_2\bullet^-$. These intermediates are commonly employed in catalyzing substrate oxidation. The different active intermediates can be confirmed via experimental methods, such as reaction-state trapping assays and electron spin resonance studies. Chromogenic substances, such as 3,3′,5,5′-tetramethylbenzidine (TMB), *o*-phenylenediamine (OPD), and 2,2′-azino-bis(3-ethylbenzothiazoline-6-sulfonic acid) (ABTS), are often used to evaluate the performances of nanozymes in terms of substrate oxidation. Additionally, OPD can serve as a typical substrate for oxidase-like nanozymes, e.g., Sha et al. [73] developed a copper-based MOF nanozyme (MOF-L(D)-His-Cu) based on chiral histidine coordination, which mimics the structure and activity of natural CC oxidase and catalyzes the conversion of 3,5-DTBC to 3,5-di-*tert*-butyl-*p*-benzoquinone (Fig. 4A). The catalytic mechanism involves the dehydrogenation and oxidation of CC, transferring electrons to O_2 via copper redox cycling to generate H_2O_2 (Fig. 4B). Similarly, nanozymes with POD-like activities catalyze substrates similar to those of oxidoreductases. In contrast, the metal centers (e.g., Fe, Cu, and Ni) within POD-like nanozymes catalyze H_2O_2 decomposition. This process typically involves electron transfer, reducing H_2O_2 to H_2O while generating oxidized metal centers and ·OH or $O_2\bullet^-$. The resulting products further undergo redox reactions with TMB, leading to the oxidation of the amino moiety of TMB, which can be easily detected using ultraviolet-visible spectrophotometry, e.g., for the first time, our research group synthesized a controllable hollow-structure trinuclear MOF with a POD-like activity and modified it with tetracycline-specific (TC-specific) oligonucleotides (apt-NiCoFe-MOF-74) [74]. Using this nanozyme, a dual-signal (colorimetric and fluorescent) sensor for TC antibiotics was developed, enabling specific detection. The colorimetric sensor exploited the POD-like activity to catalyze the generation of blue oxtetramethylbenzidine in the presence of H_2O_2. Additionally, reaction trapping studies were conducted to elucidate the catalytic mechanism of apt-NiCoFe-MOF-74. The results indicated that apt-NiCoFe-MOF-74 catalyzed H_2O_2 decomposition to produce •OH, which could be trapped by terephthalic acid (TA). The reaction of TA with •OH yielded 2-hydroxyterephthalic acid with a distinct fluorescence signal at 430 nm. Furthermore, in another study, the POD-like activities of bimetallic MOF-based nanozymes significantly exceeded those of monometallic MOF-based nanozymes. This difference is due to the introduction of the new metal, enhancing the synergistic interactions between active sites, thus significantly increasing the electron transfer capacity and promoting •OH generation (Fig. 4C) [75]. ROS mainly comprise H_2O_2, •OH, $^1O_2$, and $O_2\bullet^-$ [76].

CAT is an essential oxidoreductase in the human body, playing a crucial role in removing ROS, protecting cell membranes, and inhibiting tumor cell proliferation. MOF-based nanozymes with CAT-like activities can decompose H_2O_2 into H_2O and O_2, e.g., Zhang et al. [77] uniformly decorated PCN-224 with Pt nanozymes and investigated its performance. PCN-224-Pt exhibited a significant CAT-like activity, facilitating the decomposition of H_2O_2 into O_2 in hypoxic tumor regions, while promoting $^1O_2$ generation. In another study, MOF-Au nanozymes catalyzed the conversion of H_2O_2 to O_2 to oxygenate the tumor microenvironment (TME). Notably, the cascade reaction of SOD and CAT is one of the most typical antioxidant pathways in nature, where SOD catalyzes the conversion of $O_2\bullet^-$ to H_2O_2 and O_2, and the conversion of H_2O_2 to O_2 is then catalyzed by CAT [58]. Yang et al. [78] combined Zn ions with Mn-TCPP to synthesize a MOF nanozyme (ZMTP) with a SOD activity. In this process, the Zn ions enhance the redox potential of the Mn-TCPP metal center, endowing ZMTP with SOD and CAT activities. The catalytic mechanism of ZMTP involves the first disproportionation of $O_2\bullet^-$ driven by single electron transfer between Mn(III) and Mn(II) and outer-sphere proton-coupled electron transfer, followed by the disproportionation of H_2O_2 based on double electron transfer between Mn(III) and Mn(V) and inner-sphere proton-coupled electron transfer (Fig. 4D). Recent studies reveal that several MOF-based nanozymes can mimic the activities of hydrolytic enzymes, such as proteases and organophosphorus hydrolases. Most Zr-based MOF-based nanozymes exhibit the capacity to hydrolyze P—O bonds [79,80]. The catalytic activities of these MOFs are primarily attributed to strongly acidic Zr(IV), which activates the coordinated phosphate species, and the presence of multiple Lewis-acidic Zr-OH-Zr linkages, resembling the Zn-OH-Zn active sites of natural phosphatases [81,82]. Additionally, different intermediates may be generated during catalytic reactions involving MOF-based nanozymes with multiple enzyme activities, influencing their overall reaction pathways and efficiencies.

4. Construction of MOF nanozyme-based sensors

MOF-based nanozymes are widely utilized in developing biosensors due to their excellent catalytic performances and highly tunable structures. Common types of MOF-based sensors currently include electrochemical and optical biosensors, enzyme-linked immunosorbent assays, and sensors based on multi-enzyme cascade analysis (Table 1). Furthermore, the use of nanozymes in developing POCT systems for application in modern medical diagnostics and disease monitoring is extensive.

4.1. Electrochemical biosensors

MOFs with large surface areas, high porosities, and excellent biocompatibilities serve as ideal platforms for the stable immobilization of biomolecules, leading to amplified electrochemical signals. Applying such nanozymes in electrochemical detection has significantly advanced biosensing technology. The working mechanisms can be broadly categorized as two types. The first type exploits the exceptional electrocatalytic properties of MOFs to generate electrochemical signals [112], whereas the second type involves the activation or coupling of relevant molecules to serve as the electrochemical signals [113]. The outstanding electrocatalytic performances of MOFs may be attributed to their electroactive components, e.g., metal ions and organic ligands. The metal centers within MOFs facilitate electron transfer reactions, thus promoting redox reactions, e.g., metal ions, such as copper, iron, and manganese ions, within MOFs provide pathways for electron transfer, enhancing their catalytic performances [114]. Additionally, the high permeabilities of MOFs facilitate electrochemical redox processes and accelerate the internal diffusion of ions within their solid matrices [115]. The organic ligands of MOFs not only contribute to structural stability but also influence electron transfer via their coordination effects [116]. Several ligands can form stable coordination environments with metal centers, facilitating electron transfer between the metal centers and substrates. Furthermore, the 3D framework structures of MOFs offer large specific surface areas, promoting the proximities and reactions of substrate molecules. The pore structure of the framework aids in electron migration between metal centers, enhancing the overall catalytic efficiency. These exceptional characteristics of MOF-based nanozymes underscore their enormous potential for use in electrochemical biosensors. Wang et al. [117] utilized *N*-(4-aminobutyl)-*N*-(ethylisobutyramide) (ABEI) as an organic bridging ligand, effectively immobilizing it within a MOF, resulting in the synthesis of a nanozyme denoted ABEI/MIL-101(Fe) with a POD-like activity. Utilizing ABEI/MIL-101(Fe) as a signal probe in conjunction with AgPt hollow nanospheres, an electrochemiluminescence (ECL) immunosensor was developed for use in detecting the tumor biomarker MUC1, realizing a low detection limit of 1.6 fg/mL, as shown in Fig. 5A. ABEI exhibits a low chemiluminescence intensity (approximately 500 a.u.), but it significantly increases to 5900 a.u. upon adding H_2O_2, which is attributed to H_2O_2 serving as an effective co-reactant for ABEI. The anti-MUC1 antibody (Ab1) was immobilized on the electrode surface modified with AgPt hollow nanospheres. The large surface areas of the AgPt hollow nanospheres enable increased antibody loading and accelerated electron transfer, facilitating the specific capture of the MUC1 antigen while further enhancing the ECL signal. In contrast, Xu et al. [86] developed an enzyme-free high-performance glucose sensor. As depicted in Fig. 5B, the sensor integrates a conductive Ni/Co bimetallic MOF onto carbon

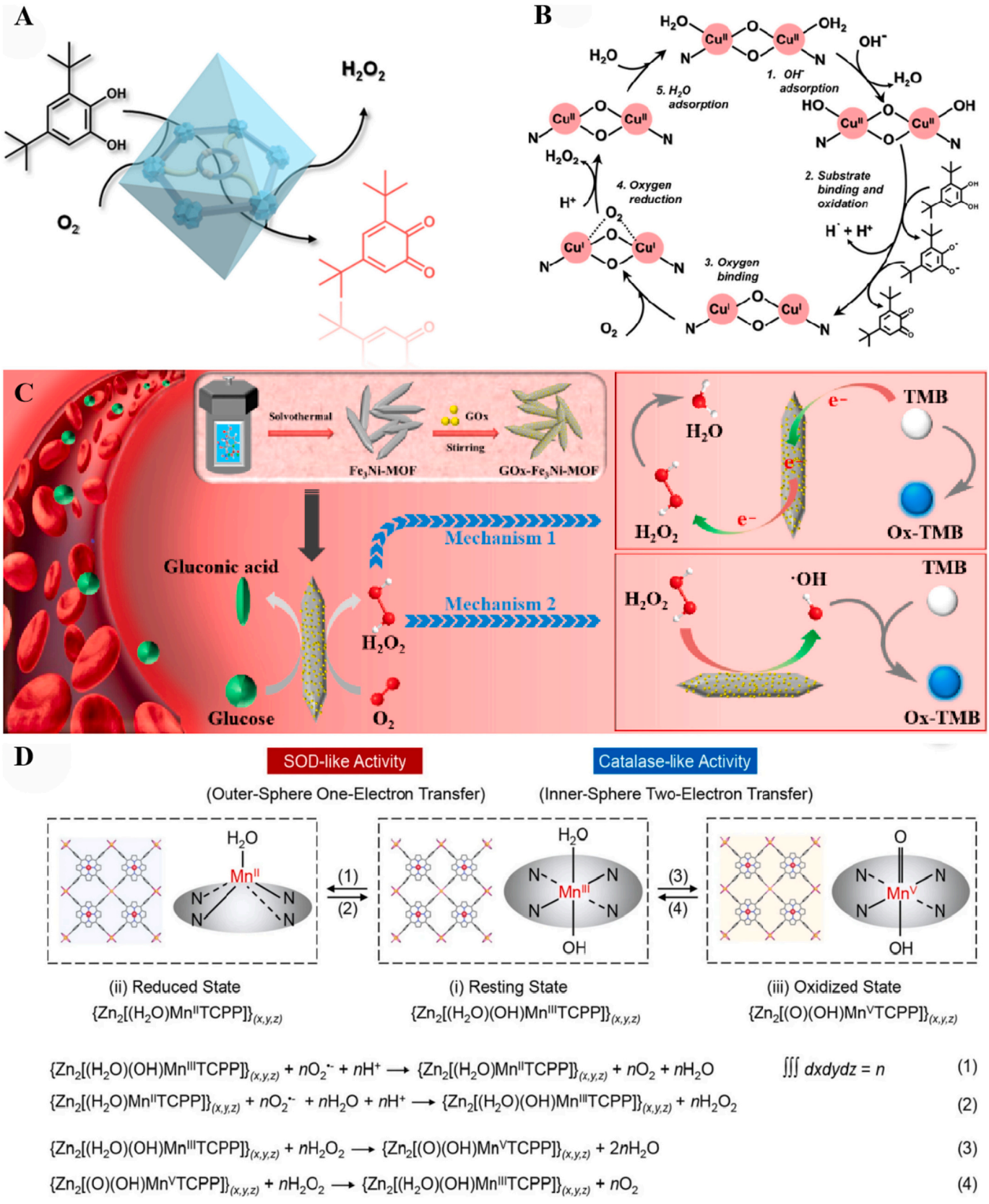

$$\{Zn_2[(H_2O)(OH)Mn^{III}TCPP]\}_{(x,y,z)} + nO_2^{\bullet-} + nH^+ \longrightarrow \{Zn_2[(H_2O)Mn^{II}TCPP]\}_{(x,y,z)} + nO_2 + nH_2O \qquad \iiint dxdydz = n \qquad (1)$$

$$\{Zn_2[(H_2O)Mn^{II}TCPP]\}_{(x,y,z)} + nO_2^{\bullet-} + nH_2O + nH^+ \longrightarrow \{Zn_2[(H_2O)(OH)Mn^{III}TCPP]\}_{(x,y,z)} + nH_2O_2 \qquad (2)$$

$$\{Zn_2[(H_2O)(OH)Mn^{III}TCPP]\}_{(x,y,z)} + nH_2O_2 \longrightarrow \{Zn_2[(O)(OH)Mn^{V}TCPP]\}_{(x,y,z)} + 2nH_2O \qquad (3)$$

$$\{Zn_2[(O)(OH)Mn^{V}TCPP]\}_{(x,y,z)} + nH_2O_2 \longrightarrow \{Zn_2[(H_2O)(OH)Mn^{III}TCPP]\}_{(x,y,z)} + nO_2 \qquad (4)$$

Fig. 4. (A) Schematic diagram of the catechol oxidase-like activity of MOF-HisCu and (B) mechanistic cycleforcatechol oxidase-like activity of MOF-His-Cu. Reprinted with permission from Ref. [73]. (C) Schematic diagram of the synthesis and application of Fe_3Ni-MOF/Gox.Reprinted with permission from Ref. [75]. (D) Schematic for the interconversion among resting, reduced, and oxidized states of ZMTP nanosheet, as well as the detailed chemical reactions in each step of conversion. Reprinted with permission from Ref. [78].

Table 1
Biosensing applications of MOFs.

Enzymes	Detection method	Analyte	Linear range	Refs.
MOF@Pt@MOF	Electrochemistry	miRNAs	10^{-9}–10^{-3} IM	[83]
Fc-Zn-MOF	Electrochemistry	Aβ	10^{-4}-100 ng/mL	[84]
Zr-MOF@AuCu	Electrochemistry	GSH	10 pM^{-1} mM	[85]
Ni/Co(HHTP)MOF/CC	Electrochemistry	Glucose	0.30 μM-2.31 mM	[86]
UiO-66-NH_2@MWCNTs	Electrochemistry	Cd^{2+}	0.50–170 μg/L	[87]
BFMOF-1a	Colorimetric	H_2S	0.60–12 ppm	[88]
ZnO-Co_3O_4 NCs	Colorimetric	Aβ	5–150 nM	[89]
RIgG@Cu-MOF	Colorimetric	mIgG	50–10^5 cells/mL	[90]
Zr-MOF-ssDNA-AuNP	Colorimetric	Semen	90 %	[91]
Ce-MOF	Colorimetric	Hg^+	0.05–6 IM	[92]
Tb0.6Eu0.4-MOF	Fluorescence	malachite green	2–180 μM	[93]
2D Tb-MOF	Fluorescence	Carbendazim	0.06–40 μg/mL	[94]
UiO-66	Fluorescence	PKA	10^{-4}-0.05 U/μL	[95]
Eu-MOF@Fe^{2+}	Fluorescence	bromate	0–0.20 mM	[96]
COOH-Tb MOF	Fluorescence	Pb^{2+}	2–1000 nm	[97]
Fe_3O_4@MOF@Pt	Enzyme linked immunosorbent assay	procalcitonin	0.50 pg/mL-1.26 ng/mL	[98]
Cu-BTC@PQQ	Enzyme linked immunosorbent assay	CEA	0.01–1 ng/mL	[99]
Fe-MIL-88 A	Enzyme linked immunosorbent assay	Thrombin	0–100 ng/mL	[100]
Fe_3O_4@UiO-66/Au@PtNP	Enzyme linked immunosorbent assay	Cardiac troponin I	0.01–100 ng/mL	[101]
AChE/ChOx@MIL-100(Fe)-BA	Multienzyme cascade assay	ACh	6–9600 μM	[102]
AChE/CHO@MPNCs	Multienzyme cascade assay	OPs	0.05–1000 nM	[103]
UsAuNPs/2D MOF	Multienzyme cascade assay	trichlorfon	1.70–42.40 μM	[104]
Eu-MOF	POCT	TC	0–140 μM	[105]
MOF-FeP	POCT	EBV-IgAs	75.56 %-93.30 %	[106]
Au-Zn-Sln-MOF	POCT	hCG	96.20 %	[107]
MOF-818	UV-ECL	H_2S	0.001–2000 μM	[108]
Ru@MOF	ECL-RET	Aβ	10^{-5}-500 ng/mL	[109]
MOF@TB@cDNA Y-junction	SERS	ATP	1–200 nM	[110]
hexaphosphate@MIL-101	Raman	methenamine	3.16×10^{-6}-1×10^{-8} M	[111]

cloth to form Ni/Co(HHTP)MOF/CC. The Ni/Co(HHTP)MOF/CC electrode combines the large surface areas and good conductivities of the MOF and carbon cloth, along with the synergistic catalytic effects of Ni and Co. Additionally, they investigated the effects of variations in the working potential on the sensor current. At the optimal potential of 0.5 V, the relationship between the glucose concentration and current density response of Ni/Co(HHTP)MOF/CC was investigated, and a calibration curve correlating the glucose concentration with the current density response was established. The results revealed an excellent sensor performance, with a low detection limit (100 nM), high sensitivity (3250 μA mM/cm^{-2}), and rapid response time (2 s). In another intriguing study [118], the composite material Ce-MOF(TV)/CNT treated with a NaOH/H_2O_2 solution exhibited two distinct oxidation peaks in the presence of hydroquinone (HQ) and CC. Using the difference between the two oxidation peaks, an electrochemical sensor with the capacity to simultaneously detect and distinguish HQ and CC was developed. Furthermore, changes in the electrochemical signals may reflect redox reactions at electron sites and active regions between the MOF and analytes, potentially leading to energy and electron transfer between the MOF and analytes. A novel strategy for application in detecting pesticide residues using a screen-printed electrode (SPE)-based electrochemical sensor was proposed [119]. This sensor involves the modification of the SPE surface with a synthesized bimetallic manganese-iron MOF (MnFe-MOF). The measured charge transfer resistance (Rct) of the MnFe-MOF-modified SPE is 1.01 kΩ, whereas that of the unmodified pure SPE is 2.31 kΩ. This difference in resistance suggests restricted electron charge transfer between the modified electrode and electrolyte. Cyclic voltammetry (CV) and electrochemical impedance spectroscopy (EIS) reveal that the bimetallic MnFe-MOF effectively modifies the SPE surface, exhibiting enhanced charge transfer kinetics and a superior electrocatalytic performance. Ultimately, the bimetallic MnFe-MOF was developed as a sensor for use in detecting the organophosphate pesticide chlorpyrifos, with a limit of detection (LOD) of 0.85 nM and a measurement range of 1.0×10^{-9}-1.0×10^{-7} M.

4.2. Optical biosensors

Optical sensors based on MOF-based nanozymes are simple, rapid, cost-effective tools for use in detecting analytes. These sensors typically comprise two components: a recognition element that specifically binds to the target analyte, and a transducer that converts the recognition event into a measurable signal [120]. Based on their operating principles and the type of output signal, optical sensors can be categorized as colorimetric, fluorescence, ECL, surface plasmon resonance (SPR), Förster resonance energy transfer (FRET), and Raman spectroscopy sensors, etc [108,118,121–125]. These sensors find wide applications in environmental monitoring, food safety, disease diagnosis, and drug therapy [126–131].

4.2.1. Colorimetric biosensors

Colorimetric biosensors are widely utilized in analyzing various analytes due to their simplicities and ease of operation [132,133]. Their visual signal outputs and capacities for detection using the naked eye or portable low-cost devices endow these sensors with significant application potential. Enzyme-catalyzed chromogenic substrates, such as TMB, OPD, ABTS, PNP, and BPB, are primarily employed in colorimetric biosensors to generate color signals for detection. However, the poor stabilities and high costs of enzymes hinder the further advancement of colorimetric biosensors [134,135]. In the past two decades, nanozymes gradually replaced natural enzymes in the fabrication of colorimetric sensors due to their high catalytic activities, strong stabilities, tunabilities, and low costs. Among them, MOF-based nanozymes stand out prominently, e.g., Shu et al. [136] developed a metalloporphyrin-based MOF nanorod (M-PCN-222 (M = Mn, Fe, Co, Ni)) for use in a colorimetric sensor for application in H_2O_2 detection. By using Fe-PCN-222 nanorods as catalysts and combining them with the colorimetric reaction of TMB, researchers established a standard curve for use in H_2O_2 detection, thus producing a sensitive, highly selective colorimetric sensor (Fig. 6A). This sensor was applied in detecting H_2O_2 in real samples, such as milk and orange juice (Fig. 6B). Based on the principle of colorimetric sensing, Zhang et al. developed a sensor based on an Fe/Mn MOF using a portable cotton pad and smartphone (Fig. 6C) [137].

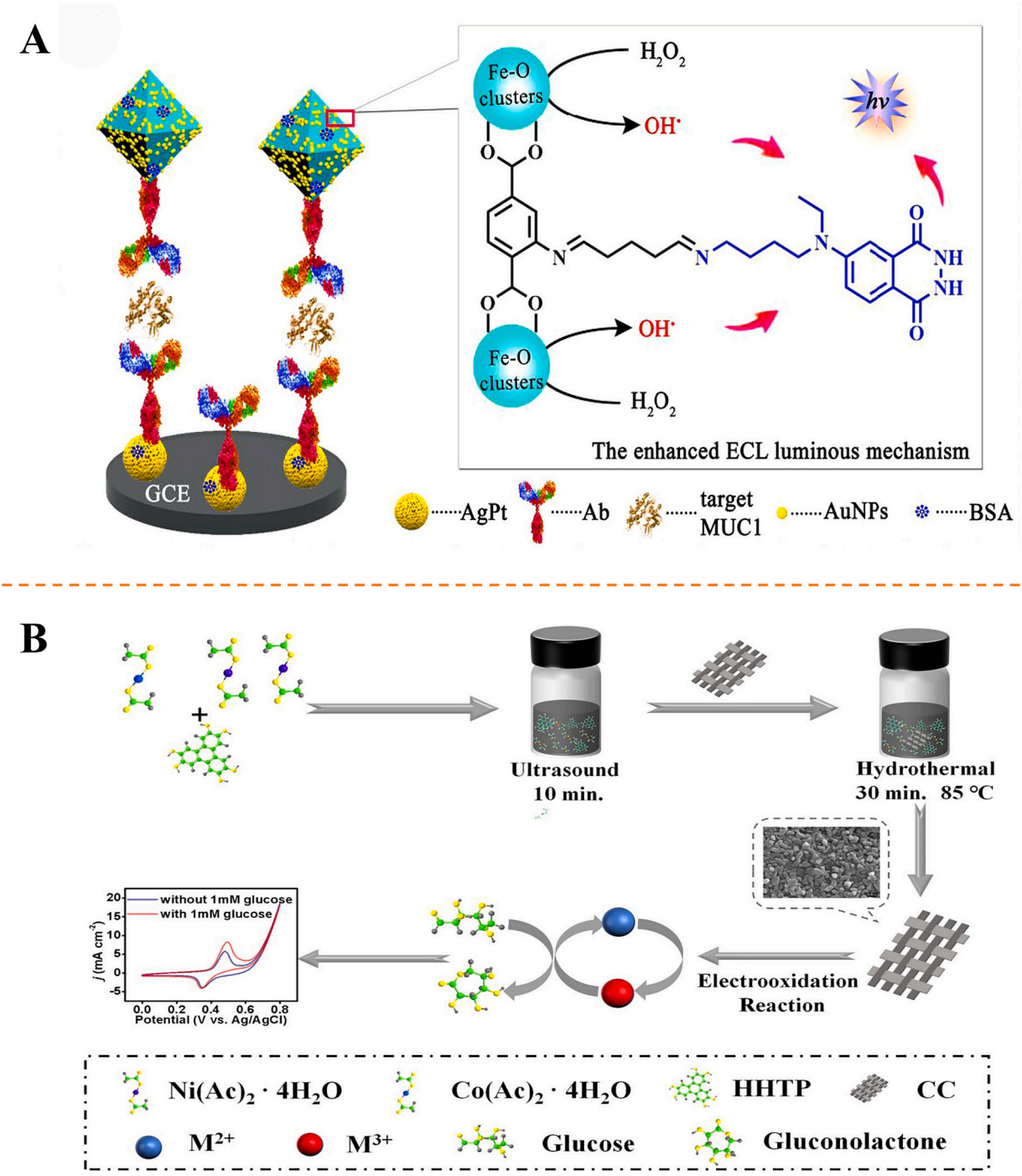

Fig. 5. (A) The fabrication of the ECL immunosensor and possible reaction mechanism. (B) Schematic illustration of the synthetic process of the Ni/Co(HHTP)MOF/CC and their application in glucose determination. Reprinted with permission from Ref. [86].

Dropping a *meta*- (m-AP) or *para*-aminophenol (p-AP) solution onto the pre-prepared Fe/Mn MOF cotton pad results in a color change from light blue-green to pink, with the color intensity directly proportional to the m-AP concentration. Subsequently, the RGB values on the cotton pad are read using a color recognition app on the smartphone, and a linear equation is established, with LODs as low as 0.13 and 0.20 mM, which are suitable for detecting environmental pollutants. However, the reliance on the camera quality and processing capacity of the smartphone limits the on-site analysis of target analytes. Therefore, developing simple, effective recognition sensors based on solid-phase carriers, such as paper-based analytical devices (PADs), is necessary [138]. In addition, researchers developed a dual-mode colorimetric-electrochemical biosensing method, e.g., Wang et al. [20] utilized a MOF (PBA-CP@MOF) wrapped with CuO_2 nanodots modified with phenylboronic acid (PBA) to prepare a dual-mode colorimetric-electrochemical biosensor for use in rapidly and sensitively detecting *Vibrio parahaemolyticus* (VP) (Fig. 6D). PBA, which is known for its specific recognition of polysaccharide binding sites on Gram-negative bacterial surfaces, is commonly used as a recognition element in probes [139]. Under acidic conditions, PBA-CP@MOF decomposes, releasing Cu^{2+} and H_2O_2 to initiate the Fenton reaction, generating ·OH. The ·OH then oxidizes TMB to produce the blue product *o*-TMB, with a characteristic absorption peak at 652 nm. Additionally, Au NPs, which are known for their excellent optical, electrochemical, and magnetic properties, are

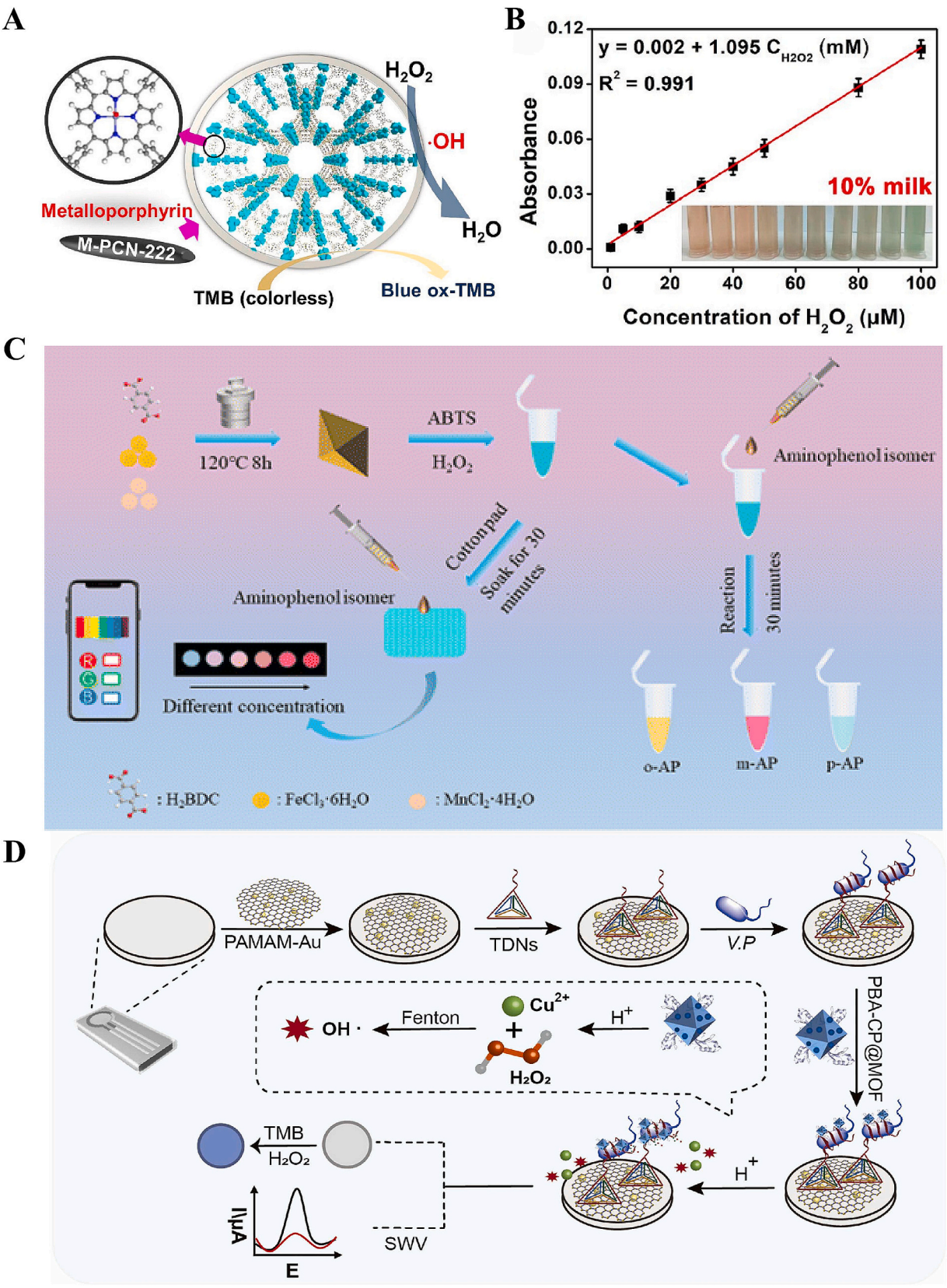

Fig. 6. (A) Construction of the Colorimetric Sensing System. (B) Selectivity of Fe-PCN-222 for H_2O_2 detection and Colorimetric determination of H_2O_2 injection in 10 % milk. Reprinted with permission from Ref. [136]. (C) Schematic diagram of the synthesis and detection principles of Fe/Mn MOFs. Reprinted with permission from Ref. [137]. (D) Schematic diagram of the sensor platform and dual-mode analysis for *VP* detection, along with the corresponding calibration curve. Reprinted with permission from Ref. [20].

well-suited for use in biosensing applications [140]. Electrode interfaces modified with tetrahedral deoxyribonucleic acid (DNA) nanostructures enable the precise control of the distance between capture probes to reduce nonspecific adsorption. Poly(amidoamine) dendrimers, which are commonly used in immobilizing antibodies and aptamers, can specifically recognize VP and effectively bond to the electrode interface. Furthermore, Cu^{2+} ions released during the reaction are utilized in the electrochemical detection of VP. Therefore, the development of a dual-mode colorimetric-electrochemical biosensor realized an accuracy of 88.7 %, which significantly exceeds that of single-mode detection of 81.1 %. This innovation demonstrates the potential for effective on-site pathogen detection in food samples.

4.2.2. *Fluorescence sensors*

Compared to those of colorimetric sensors, fluorescence sensors offer higher sensitivities, stabilities, and lower background interferences [126,141]. The detection mechanism involves measuring the fluorescence signal emitted by a sample under photoexcitation to determine the presence and concentration of the target substance. Based on the nature of the target analyte and electronic properties of MOFs, fluorescence sensors can be broadly classified into three categories: turn-on and -off and ratiometric fluorescent sensors [21,142–144]. Turn-on fluorescent sensors refer to MOF-based nanozymes with weak or no fluorescence under initial dark background or low-emission conditions, exhibiting significantly enhanced fluorescence intensities upon introducing the analyte [144,145]. Li et al. utilized a MOF (PCN-700) as the sensing platform, integrating fluorescent (L1) and recognition groups (L2Hcy) into PCN-700, yielding PCN-700-L1-L2Hcy [146]. The fluorescent and recognition groups are an anthracene fluorophore and a hemicyanine, respectively, with an intramolecular charge transfer (ICT) mechanism between them causing the quenching of the fluorescent group. When exposed to a cyanide solution, PCN-700-L1-L2Hcy reacts with cyanide ions via the hemicyanine recognition group, disrupting ICT and restoring the fluorescence of the fluorescent group, enabling cyanide detection (Fig. 7A). The optimized sensor in terms of the fluorescent group:recognition group ratio displayed a cyanide LOD of 0.05 mM, which is significantly lower than those of traditional cyanide fluorescence sensors. In contrast to turn-on fluorescent sensors, turn-off fluorescent sensors refer to probes with initial fluorescence intensities that decrease or disappear completely in the presence of the analyte [96]. Li et al. [147] employed Cu-MOF and 2,3,5,6-tetrafluorothiophenol as a template and reducing agent, respectively, to synthesize a novel

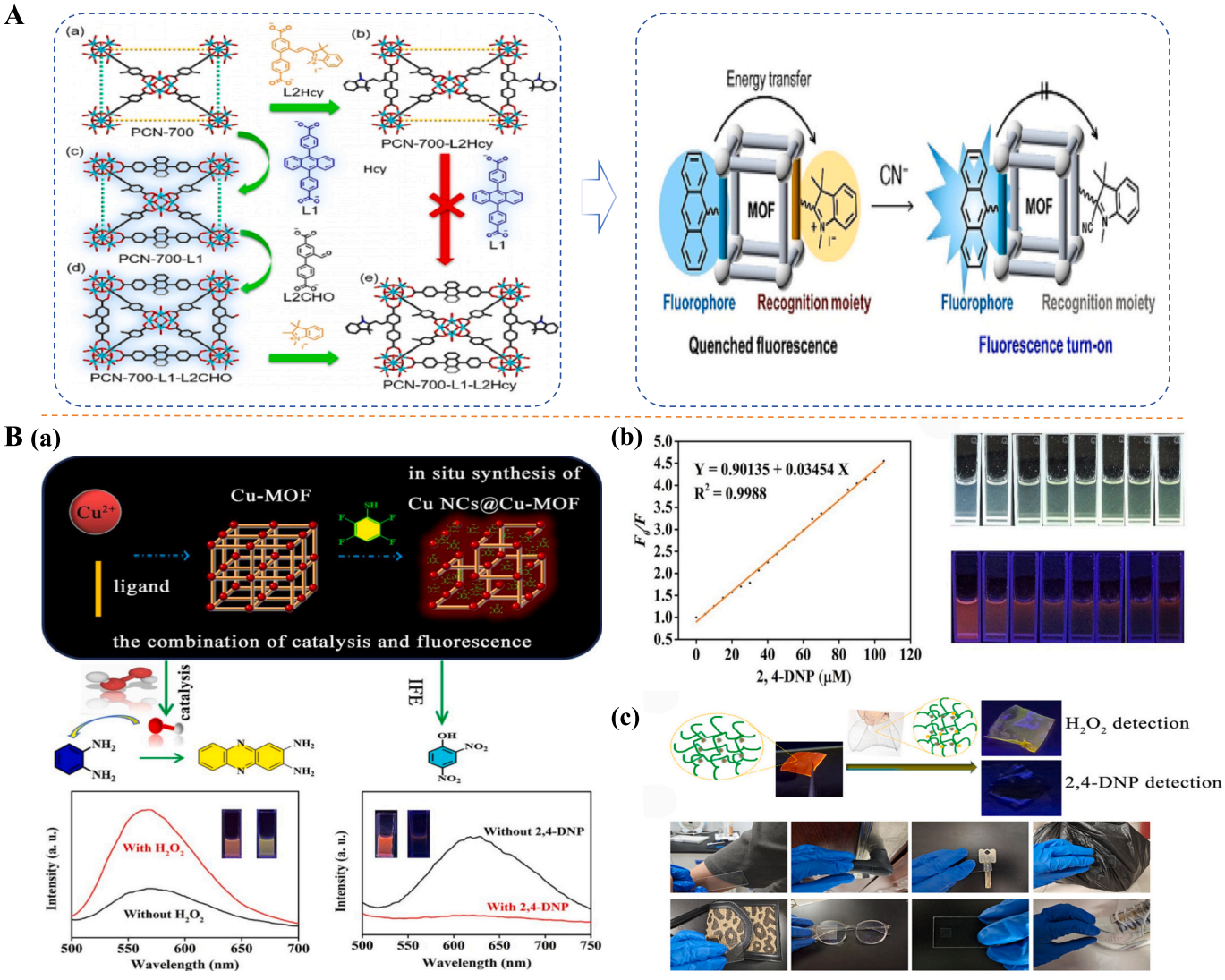

Fig. 7. (A) Schematic representation for the design of a turn-on fluorescence sensor in multicomponent MOFs by integrating a fluorophore and a recognition moiety. Reprinted with permission from Ref. [146]. (B) A schematic diagram of the synthesized probe for H_2O_2 and 2,4-DNP (a); the relation of response values of Cu NCs@Cu-MOFs with concentrations of H_2O_2 and 2,4-DNP (b); The hydrogel portable sensor and the practicality of the hydrogel in wipe sampling microparticulate (c). Reprinted with permission from Ref. [147].

material (Cu NCs@Cu-MOF) with excellent catalytic and fluorescent properties. This material effectively activates H_2O_2 to generate ·OH and oxidize OPD to produce yellow emission. Additionally, the strong red fluorescence of Cu NCs@Cu-MOF is quenched by 2,4-dinitrophenol (2,4-DNP) due to the inner filter effect. The established fluorescence-color dual-mode sensor for H_2O_2 and 2,4-DNP exhibits LODs of 72.5 and 67 nM, respectively (Fig. 7B-a). Furthermore, they developed a portable sensor using polyvinyl alcohol hydrogel for application in the efficient sampling and on-site detection of 2,4-DNP (Fig. 7B-bc).

Various factors, such as analyte concentration, environmental conditions, and excitation light intensity, may lead to monochromatic MOF sensors with decreased detection accuracies during fluorescence intensity measurements [148]. Modifying the fluorophores or ligands of original single-emission MOFs (e.g., Zr-MOF) can alter their fluorescence properties, e.g., by introducing new fluorophores, adjusting their ligand structures, or changing the fluorophore environments. These modifications can result in MOFs with different luminescent characteristics under different conditions, enabling the sensors to detect specific analytes via changes in ratios (e.g., the ratio of the emission peak intensities) [145]. As an illustrative example, Wang et al. [21] synthesized a novel MOF nanozyme (BUC-88) with dual emission signals using 2,6-naphthalenedicarboxylic acid as a bridging ligand. Quinolone antibiotics (ENR, NOR, and CIP) exhibit fluorescence sensitization and quenching effects on BUC-88, offering the potential for the fabrication of quinolone antibiotic ratio sensors. The detection signals are based on the fluorescence intensity ratio of the BUC-88 emissions at 439/615 nm. This method, employing precisely designed ratio sensors, can detect multiple components simultaneously in complex environments owing to its dual-emission capacity. Furthermore, BUC-88 can be utilized to establish a fluorescence sensor for use in TC detection based on the competitive ultraviolet-induced (UV-induced) fluorescence quenching between BUC-88 and TCs.

A novel trimetallic organic framework nanozyme (*apt*-NiCoFe-MOF-74) was developed by our research group for use in detecting TCs [74], significantly enhancing the sensitivity of the fluorescence sensor for use in TC detection (LOD = 0.0013 μmol/L), surpassing the LOD of BUC-88 (0.08 μmol/L). Unlike BUC-88, this detection platform integrates colorimetric and fluorescent dual sensors, significantly improving the accuracies of the detection results. In addition to the common sensing platforms, research indicates the potential of utilizing fluorescence-enhanced detection in live-cell bioimaging applications [149–151].

4.2.3. Other optical sensors

In addition to the optical sensors mentioned above, SPR, FRET, and Raman sensors are also commonly used. Chen et al. [152] engineered a heterostructure on the surface of MXene to grow a 2D MOF with a matching morphology, an excellent stability, and outstanding optoelectronic properties, confirming the photoelectric dual-enhanced MXene@MOF heterostructure. This led to the development of an MXene@MOF/peptide-SPR sensor for use in sensitively and rapidly detecting cancer biomarkers in exosomes. Furthermore, FRET nanoprobes based on MOFs were developed for use in detecting *Staphylococcus aureus* with an LOD of 12 CFU/mL [153]. These nanoprobes exhibited exceptional selectivities and sensitivities in detecting *S. aureus* in real samples, such as lake water, orange juice, and saliva. Additionally, Lai et al. [154] developed an innovative SERS substrate by directly growing gold-silver (Au@Ag) NPs on 2D nickel MOF (Ni-MOF) nanosheets (Ni-MOF-Au@AgNPs). This technique efficiently separated, preconcentrated, and quantitatively detected fipronil, paraquat, and glyphosate in fruit and vegetable samples. Moreover, Wang et al. [155] introduced a novel detection method based on dual-mode signal amplification, which combined fluorescence and SERS signals to monitor Staphylococcal enterotoxin B (SEB) using a MOF with encapsulated gold NPs (AuNPs@MIL-101). This dual detection approach exhibited LODs of 0.5 and 0.2 pg/mL for SEB using fluorescence and SERS, respectively, indicating the exceptional reliability and precision of the AuNPs@MIL-101 platform in SEB detection.

4.3. Enzyme-linked sensors

An enzyme-linked reaction refers to a biochemical experimental method where the activities of enzymes are utilized to catalyze reactions that generate measurable signals for use in detecting target substances. Currently, different types of enzyme-linked sensors (enzyme-linked sensors based on enzyme-signal transduction and enzyme-antibody interactions) can be developed based on the natures of the enzyme and binding molecules involved in the enzyme-linked reaction [156–158]. Enzyme-nanomaterial conjugation involves the combination of natural enzymes with nanomaterials that exhibit enzyme-like activities, such as MOFs and carbon nanomaterials. These nanomaterials, which are characterized by high porosities, large surface areas, and tunable structures, can serve as carriers for natural enzymes, e.g., Mao et al. [159] successfully synthesized an efficient POD-mimic catalyst (HhG-MOF) by immobilizing histidine (H) and hemin-G-quadruplex deoxyribonuclease (hG) on a MOF. Subsequently, they designed a simple, highly sensitive colorimetric sensor for use in detecting acetylcholinesterase (AChE) based on the inhibition effect of thiocholine generated by the reaction between AChE and acetylthiocholine (Fig. 8A). Enzyme-signal transduction cascade sensors utilize the combination of enzyme-catalyzed reactions and signal transduction to convert the concentrations of analytes into corresponding electrical signals, with high sensitivities and rapid responses [160]. Li et al. quantitatively detected target micro ribonucleic acid (miRNA) using a triple-amplification electrochemical biosensor comprising an mCHA circuit and MOF@Au@G-triplex/hemin nanozyme [161]. The sensor circuit comprises three hairpin structures (HpC, HpH1, and HpH2) that maintain stability in the absence of the analyte. In the presence of the target miRNA, HpC unfolds, disrupting the original stem structure. Domain 1 of HpC is then exposed, acting as a primer in initiating amplification. This process results in the generation of a significant amount of a biotin-labeled HpH1-HpH2 complex, which binds to magnetic microspheres via a highly selective interaction with biotin-streptavidin. Subsequently, the complex facilitates the electrocatalytic oxidation of TMB, producing a robust signal for miR-721 detection. Enzyme-linked immunosorbent assay (ELISA) sensors integrate enzymes with antibodies to enable sensitive detection in complex samples by specifically binding target molecules with antibodies and generating signals via enzyme-catalyzed reactions. Karen et al. utilized the fragment crystallizable (Fc) regions of antibodies to induce the crystallization of zinc-based MOFs ($Zn_2(mIM)_2(CO_3)$), generating MOF nanocrystals using solutions of Zn^{2+} and 2-methylimidazole (mIM) [162]. In the resulting composite crystals, a segment of the Fc region of the antibody is incorporated into the MOF surface, while the binding region faces the target, maintaining the target-binding efficacy of the original antibody. These MOF nanocrystals exhibited vast potential for application in sensing, diagnostic imaging, and targeted drug delivery. Expanding on this work, Tian et al. [158] developed a sensor based on the directed assembly of antibodies within a MOF ($Zn_2(mIM)_2(CO_3)$*Cmab), displaying an exceptional performance in on-site sweat cortisol detection, with a detection limit as low as 0.26 pg/mL. Furthermore, the sensor exhibited an excellent durability, with a performance degradation of only 4.1 % after 9 d of storage. Of particular interest, Guo et al. developed a MOF-based nanorobot, i.e., CAT@ZIF-8, with capacities for self-propulsion and biocatalytic buoyancy propulsion (Fig. 8B) [163]. By functionalizing the nanorobot with anti-carcinoembryonic antigen (anti-CEA) antibodies (anti-CEA-CAT-ZIF-8), it was endowed with the capacity for the targeted recognition of specific cells. Subsequently, anti-CEA-CAT-ZIF-8 realized directional vertical motion via CAT-driven oxygen bubble generation to “seek and retrieve” target cells, enabling the simple retrieval of the captured cells with preserved metabolic potentials.

Additionally, ELISA is a typical enzyme-linked immunosorbent test, and effectively coupling a large amount of streptavidin-HRP to the

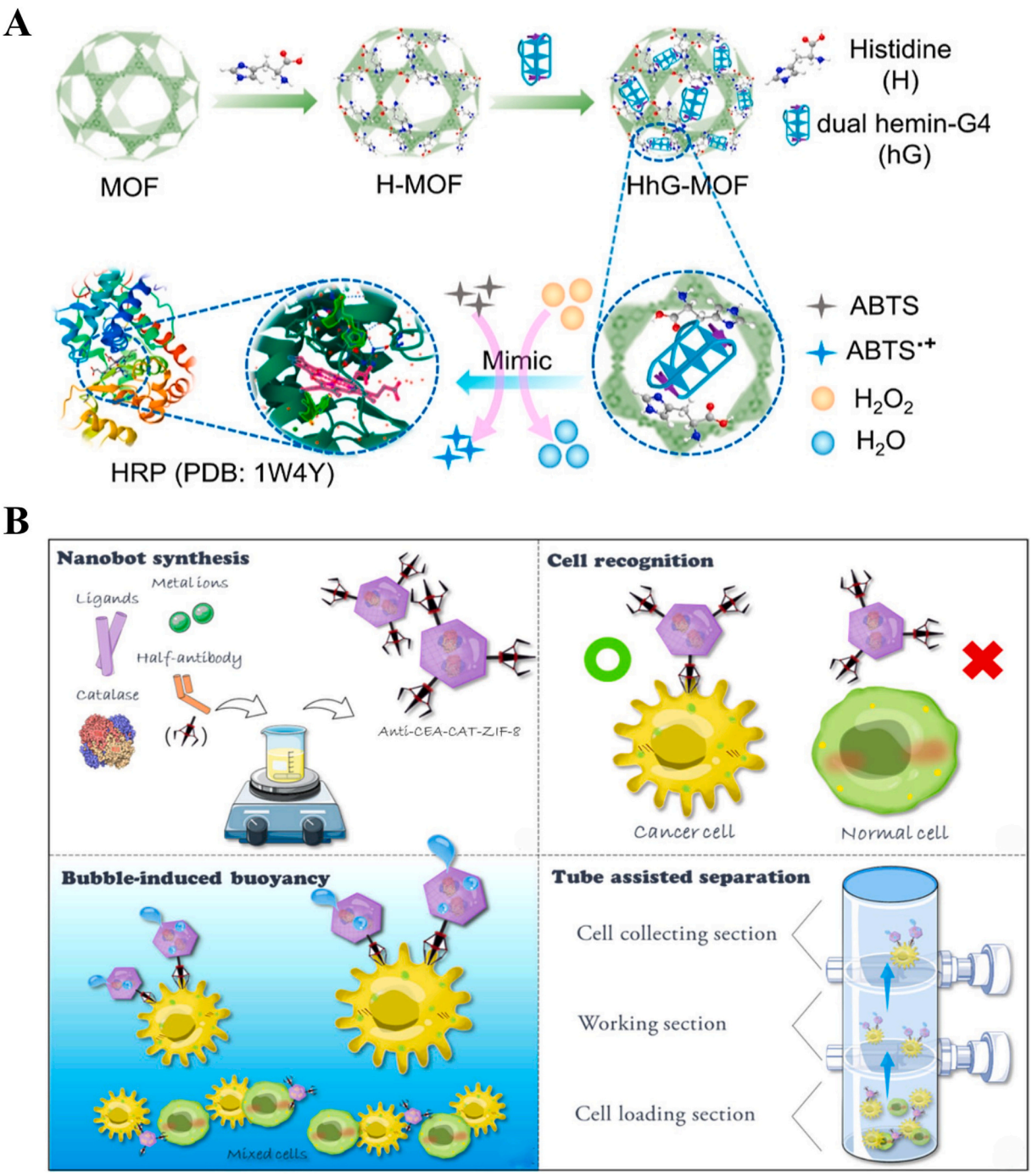

Fig. 8. (A) Construction of a colorimetric sensor for AChE detection. Reprinted with permission from Ref. [159]. (B) Schematic illustration of the anti-CEA-CAT-ZIF-8 nanobot synthesis and its autonomous cell "find-and-fetch" process with a customized glass column. Reprinted with permission from Ref. [163].

interior or surface of metal-nitrogen-doped framework (MAF-7) microparticles can enable a single antibody-antigen sandwich complex to label multiple enzymes, significantly enhancing the signal intensity of the enzyme color reaction and further improving the detection sensitivity of ELISA [164]. Certain MOF-based nanozymes display multiple enzyme activities in the same or different environments. This multifunctionality is due to the unique structural features and tunable properties of a MOF, enabling the introduction of multiple catalytic sites or active centers within its framework. Moreover, MOF-based nanozymes with multiple enzyme activities can prevent interference between different enzymes while amplifying signal transduction, e.g., Wen et al. [165] designed a MOF nanozyme (MOF-808/Pt NPs) with the dual enzyme activities of AChE and POD. This nanozyme catalyzed the hydrolysis of acetylcholine (ACh) to generate acetic acid, thus enhancing the POD-like activity of MOF-808/Pt NPs and amplifying the colorimetric signal.

4.4. *Multi-enzyme cascade analysis sensors*

Inspired by enzyme cascade reactions in biological systems, nanozyme-based biosensors amplify signals via multi-enzyme cascade reactions, significantly enhancing their sensitivities in substrate detection. Similar to enzyme-linked sensors, sensors based on multi-enzyme cascade analysis rely on enzyme binding and catalytic reactions, but

they are distinct because they employ multiple enzymes in cascade reactions to realize more complex analytical processes. As early as 2008, Wei and Wang pioneered a simple system based on multi-enzyme cascade reactions, using nanozymes in glucose detection [166]. They utilized Fe_3O_4 NPs with POD-like activities and GOx in cascade catalysis, converting glucose to gluconic acid. The generated H_2O_2 could then oxidize ABTS to its green oxidized form. Similarly, Yang et al. [104] immobilized ultrasmall gold NPs (UsAuNPs) on 2D MOF nanosheets, forming a POD-like MOF nanozyme (UsAuNPs/2D MOF). In a cascade enzyme reaction mediated by AChE and choline oxidase (ChO_x), the substrate ACh is activated by OPD to generate H_2O_2 (Fig. 9A). The variation in the production of H_2O_2, as a classic POD-like nanozyme substrate, affects the reaction outcome. Organophosphorus pesticides (OPs) can inhibit the AChE activity, reducing H_2O_2 generation and then diminishing the catalytic oxidation capacity of the POD-like nanozyme. To detect this process, TMB is used as the chromogenic substrate for the UsAuNPs/2D MOF composite, establishing a triple-cascade enzyme reaction system comprising AChE, ChO_x, and UsAuNPs/2D MOF. This system displays an LOD as low as 1.7 mM, effectively detecting OPs in tomatoes, cucumbers, and eggplants, with sample recovery rates of 96.6–105.3 % (Fig. 9B). Hassanzadeh et al. [167] integrated sensors based on multi-enzyme cascade analysis with a portable point-of-care monitoring device, designing a sensor with multiple monitoring zones and the capacity for measurement using a smartphone. The sensor was based on a cerium oxide NP-embedded amino-functionalized iron MOF (CeO_2@NH_2-MIL-88B(Fe)), which formed a multifunctional mimetic composite. By maintaining enzyme catalysis on the MOF and combining it with continuous TMB oxidation, a theoretical cascade reaction was realized. This enabled the simultaneous quantitative analyses of various sugars, including glucose, fructose, sucrose, and maltose. Moreover, this method could be directly applied in detecting the sugar levels in samples such as whole blood, urine, semen, honey, and fruit juice, with a relative error of <7.7 %, displaying a superior reliability compared to those of methods based on high-performance liquid chromatography. Furthermore, nanomaterials can be used to package different types of enzymes to fabricate array sensors, e.g., Yuan et al. prepared a nanocomposite encapsulating GOx and HRP, modifying both with polyethylene glycol (mPEG) via Schiff base reactions to prepare an array sensor [22]. mPEG modification within the sensor does not disrupt the secondary structures of the enzymes, while their activities are retained, realizing high sensitivities (LOD: 1.6 μM) and the rapid (30 s) detection of glucose in untreated samples, such as urine, plasma, and saliva.

4.5. MOF-based nanozymes in POCT

The engineering of nanozyme biosensors led to the development of various portable biosensors, such as paper-based or immunochromatographic devices, to satisfy the demands of POCT in real-time settings [168]. MOF-based nanozymes are crucial in fabricating POCT biosensors, owing to their superior catalytic performances and excellent cascading capacities with other substances, rendering them ideal options. Currently, various portable test strips based on MOF-based nanozymes have been developed for use in detecting various analytes. Wang et al. [106] designed a portable sensor based on test strips for use in simultaneously detecting three Epstein-Barr (EB) virus (EBV) IgA antibodies using a nanozyme fabricated based on a heme MOF (MOF-FeP). Fig. 9C shows the design of the MOF-FeP test strip. Researchers enhanced the binding of MOF-FeP to mouse anti-human IgA antibodies via coordination bonds between Zr clusters and the carboxyl groups of COOH-PEG-NHS. Subsequently, the MOF-FeP bound with mouse anti-human IgA antibodies was integrated into the test window of the detection strip. Upon adding the test sample, after lateral flow for 15 min, MOF-FeP binds to the three EBV-IgA antibodies and their corresponding EBV capture antigens, forming a sandwich complex. Due to its excellent POD-like activity, MOF-FeP catalyzes the generation of chemiluminescent signals from a luminol substrate in the presence of H_2O_2, which are then captured by the MiniChemim chemiluminescence imaging system. To demonstrate the practicality of the test strip, a study compared the serum samples of 45 EBV-related nasopharyngeal carcinoma (NPC) patients after dilution (dilution ratio: 1:10–1:10000). The ELISA kit can detect levels of EA-IgA and VCA-IgA at a dilution of 1:100 (Fig. 9D), which significantly exceeds the concentration required by the MOF-FeP test strip (1:10000). Additionally, the MOF-FeP test strip displays higher positivity rates for the three EBV-IgAs compared to those of the ELISA kit (Fig. 9E). Furthermore, whole blood samples from EBV-related NPC patients were utilized to investigate the interference of whole blood with the MOF-FeP test strip, with the corresponding serum diluent as a control. The results reveal no significant background interference in the chromatogram due to the whole blood diluent, indicating the effective removal of endogenous interferents by the blood filter membrane. Based on these findings, Hassanzadehtuand et al. developed a cost-effective, portable POCT device by combining a multi-enzyme cascade system with a paper-based platform [167]. This detection device comprised a multifunctional mimetic composite (CeO_2@NH_2-MIL-88B(Fe)) on a disposable 3D microfluidic PAD (3D μPAD), and it could simultaneously detect glucose, fructose, sucrose, and maltose. This economically efficient and convenient μPAD exhibits significant potential for application in medical diagnostics and food testing, particularly in resource-limited or emergency settings.

5. Clinical diagnostic applications of MOF-based nanozymes

MOF-based nanozymes display considerable potential for use in clinical diagnostic applications for various diseases. Due to their unique structures and catalytic properties, MOF-based nanozymes have been integrated as catalytic labels into existing diagnostic technologies, significantly enhancing their sensitivities, specificities, and accuracies in disease identification based on specific biomarkers. Numerous studies indicate the capacities of MOF-based nanozymes to generate colorimetric or luminescent signals via catalytic reactions for biomarker detection, enabling early disease diagnosis [25,169,170]. Moreover, in disease diagnosis, medical monitoring, and biomedical research, bioimaging techniques play crucial roles by enabling the non-invasive visualization of biological factors at the molecular level [171,172]. MOF-based nanozymes can be utilized in staining pathological tissue sections. With the aid of antibodies, nanozymes can target specific pathological areas, activating the oxidized states of chromogenic substrates (such as 3,3′-diaminobenzidine), thus revealing the statuses of diseases. Furthermore, in in vivo diagnostics, nanozyme systems can respond to elevated levels of ROS and dysfunctional protease levels caused by the microenvironment. This induces degradation into metabolizable fragments that can be excreted via the kidneys. MOFs with tunable structures and compositions exhibit significant potential for use as contrast agents in bioimaging applications. Currently, MOF-based nanozymes generate detectable signals via multiple reaction pathways, enhancing the versatilities of current diagnostic tests and profoundly influencing disease detection and monitoring. Their application in these diagnostic methods not only provides the capacity for rapid, sensitive, specific disease detection but also plays crucial roles in advancing personalized medicine and on-site testing.

5.1. Diagnosis of cancer

Cancer can infiltrate adjacent tissues and spread to other parts of the body via the bloodstream or lymphatic system. Common methods of diagnosing cancer include imaging (such as computed tomography (CT) and X-ray scanning and magnetic resonance imaging (MRI)), pathological, tumor marker, and molecular tests and endoscopic examinations [173–176]. Tumor markers are considered crucial in cost-effective, early, accurate cancer diagnosis. In 2008, a groundbreaking study was published regarding the use of manganese-containing MOFs (Mn NMOFs) in the targeted delivery of molecular probes to cancer cells,

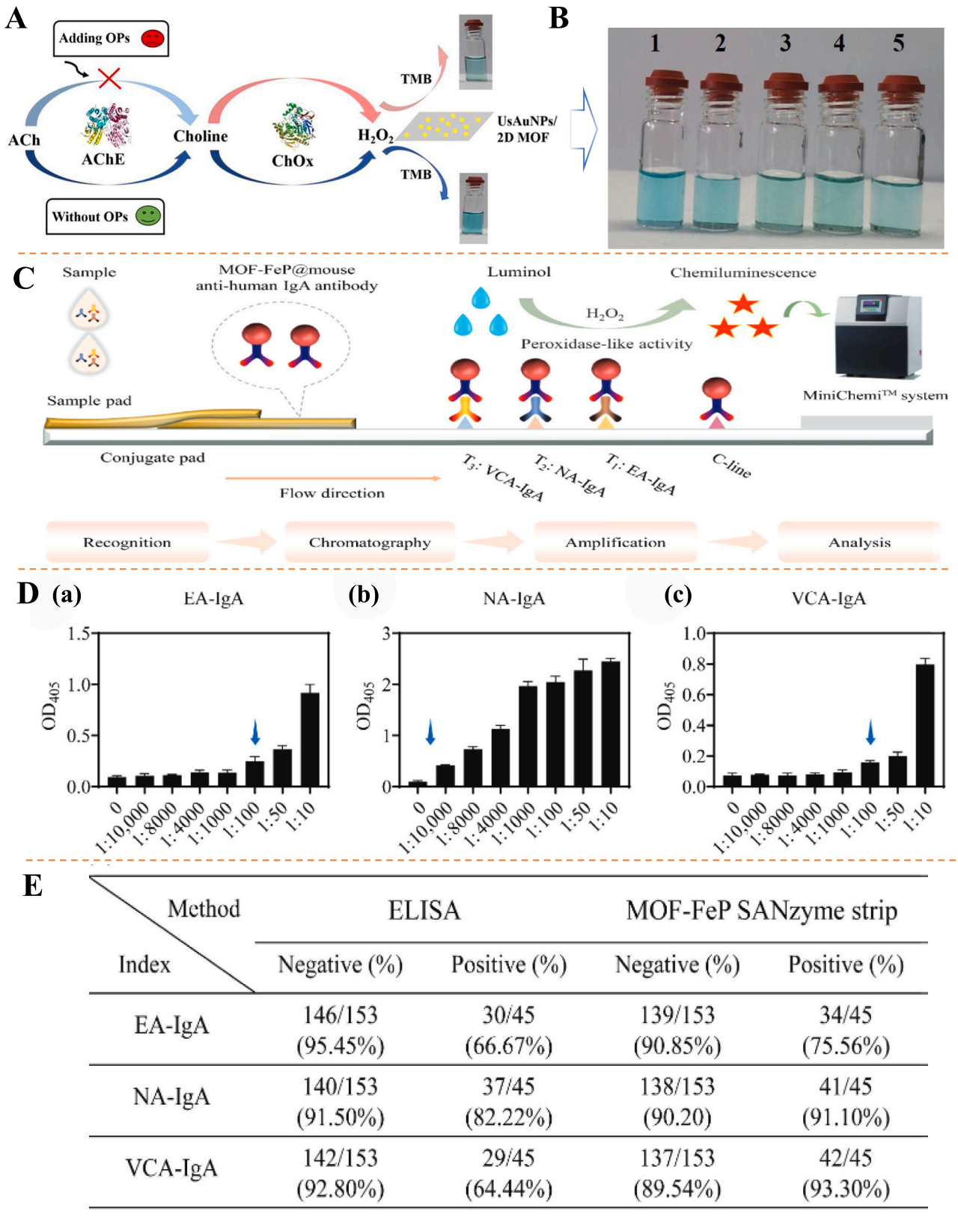

E

Method / Index	ELISA		MOF-FeP SANzyme strip	
	Negative (%)	Positive (%)	Negative (%)	Positive (%)
EA-IgA	146/153 (95.45%)	30/45 (66.67%)	139/153 (90.85%)	34/45 (75.56%)
NA-IgA	140/153 (91.50%)	37/45 (82.22%)	138/153 (90.20)	41/45 (91.10%)
VCA-IgA	142/153 (92.80%)	29/45 (64.44%)	137/153 (89.54%)	42/45 (93.30%)

Fig. 9. (A) Scheme of colorimetric biosensor based on AChE, ChOX and UsAuNPs/2D MOF for Ops detection. (B) Colorimetric diagram of different samples. 1-control sample; 2-tomato; 3-eggplant; 4-cucumber; 5-standard sample. Reprinted with permission from Ref. [104]. (C) Schematic illustration of the MOF-FeP strip tests for EBV-IgAs. Recognition, chromatography, amplification, and analysis. (D) The LOD of the ELISA kits for detecting EBV-IgAs. (E) Comparison of the positive detection rates and the negative coincidence rates of MOF-FeP strip and ELISA kit for detecting EBV-IgAs. Reprinted with permission from Ref. [106].

enabling targeted MRI in vitro [177]. Subsequently, in 2014, Hu et al. [178] introduced a method involving gold NP (AuNP)-embedded MOFs for use in the highly sensitive SERS detection of alpha-fetoprotein (AFP, linear range: 1.0–130.0 ng/mL). This marked the rapid development of MOF-based nanozymes for use in disease diagnosis. Common tumor markers used in clinical cancer diagnosis include CEA, prostate-specific antigen (PSA), AFP, cancer antigen 15–3, cancer antigen 125, and neuron-specific enolase, e.g., Du et al. innovatively developed a multi-functional photoelectrochemical (PEC) biosensor combining copper-based MOFs with clustered regularly interspaced short palindromic repeats-Cas12a (CRISPR-Cas12a) cleavage for use in the sensitive detection of CEA [179]. In contrast, Huang et al. [180] devised a label-free electrochemical immunosensor. This sensor utilized anti-CEA antibodies immobilized on a MOF and a graphene oxide (GO)

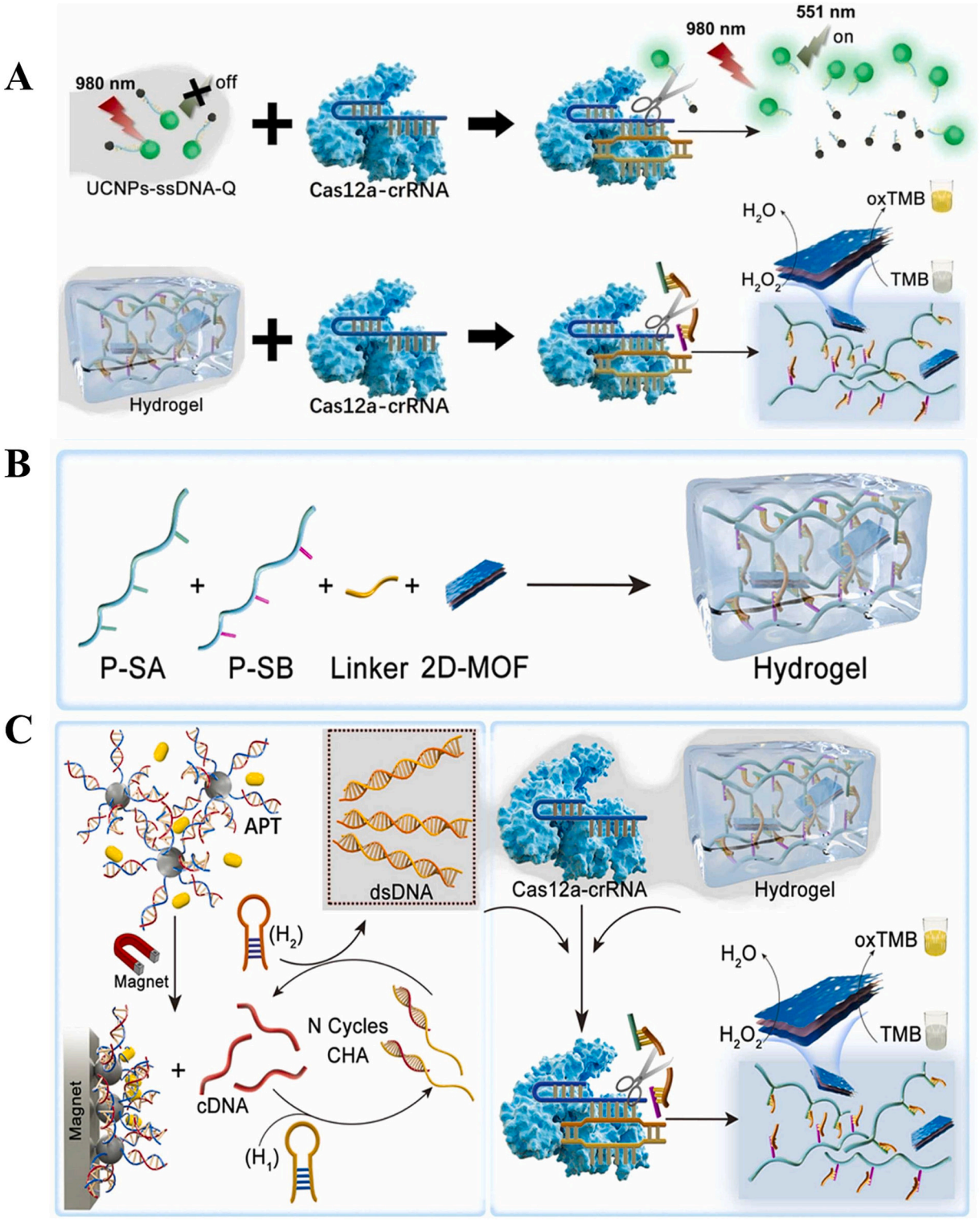

Fig. 10. (A) Principle of UCNPs-Cas12a sensor detection system. (B) Synthesize a responsive hydrogel-MOF. (C) Principle of hydrogel-MOF-Cas12a sensor. Reprinted with permission from Ref. [181].

nanocomposite-modified glassy carbon electrode (Anti-CEA/Ag-MOF/GO/GCE) to realize the highly sensitive detection of CEA in human serum (LOD: 0.005 ng/mL), exhibiting significant consistencies with the results of the ELISA and DPV methods. However, Wang et al. [181] designed a dual-mode fluorescence/colorimetric biosensor for use in detecting non-nucleic acid targets. This sensor integrates the principles of a fluorescence-based CRISPR-Cas12a detection system with the characteristics of MOFs, resulting in a CRISPR-Cas12a colorimetric sensor based on biomimetic DNA hydrogel-coated MOF enzymes (hydrogel-MOF-Cas12a), with a more intuitive signal output mode (Fig. 10A). Signal output is realized using a pre-assembled Cas12a-CRISPR RNA (Cas12a-crRNA) complex and hydrogel-MOF. A responsive hydrogel-MOF is formed by mixing P-SA, P-SB, a linker, and the 2D-MOF (Fig. 10B). Upon adding small target molecules, they activate the cleavage activity of Cas12a, leading to the hydrolysis of the linker within the hydrogel, causing its disintegration and the release of 2D-MOF. The released 2D-MOF catalyzes the generation of oxygen radicals from H_2O_2, which reacts with the TMB substrate, changing the color of the solution from blue to yellow (Fig. 10C). This sensor converts the target into an input DNA signal, amplifies it via catalytic hairpin assembly, and then uses CRISPR-Cas12a to produce a fluorescent or colorimetric output for the detection of small molecules, such as estradiol (E2), and proteins, such as PSA. Different concentrations of small target molecules (PSA and E2) were introduced into the detection system. As the target concentration increases, the absorbance also increases, indicating a linear relationship within a certain range. The viability of the hydrogel-MOF-Cas12a system for use in detecting small target molecules in biological samples was further evaluated. The results revealed good PSA and E2 recovery rates in real sample detection. Khoshfetrat et al. integrated electrochemistry with molecular sensors for use in analyzing DNA methylation [182]. This immuno-DNA sensor could detect methylation levels as low as 0.1 % and successfully identified tumor-specific methylated DNA in the plasma samples of 9 out of 10 thyroid cancer patients. The combination of immunoassays and ECL imaging enables the visualization of the distributions of specific proteins on the cell membrane, which is crucial in monitoring the changes in the target analytes within tumors. After modification, several MOF-based nanozymes can selectively recognize specific biomarkers or receptors on the surfaces of cancer cells, thus facilitating the design of a diagnostic method based on tumor imaging. Unlike contrast agents, this diagnostic method can specifically identify and image cancer cells, e.g., Zhang et al. [183] developed a universal, straightforward strategy for use in fabricating a nanoplatform based on intelligent NMOFs for application in imaging HeLa (cancer) cells. Similarly, leveraging the unique physicochemical properties of MOF materials, various imaging techniques are widely used in in vivo tumor imaging to monitor and diagnose cancer.

Notably, MOF-based nanozymes can also be designed as various anti-tumor catalytic treatment platforms that induce tumor cell apop-, pyrop-, and ferroptosis. Xiong et al. designed a novel nanoplatform (PEG2000-SiNcTI-Ph/CpG-ZIF-8@CM) by combining photosensitizers, immune adjuvants, and tumor cell membranes for use in precisely treating colon cancer in the TME [184]. This platform is activated at a low pH and high ATP concentration, and it can generate ROS under long-wavelength light, inducing immunogenic cell death and anti-tumor immune responses, effectively combatting primary and metastatic colon cancer tumors, and inhibiting recurrence. Additionally, a significant body of research has demonstrated that MOFs can serve as effective platforms for cancer therapy, leveraging their unique structural characteristics and functional potential for targeted drug delivery, diagnostic imaging, and combinatorial treatments [185–190]. For example, Chen et al. [191] synthesized a CaCu-based MOF loaded with artemisinin and GSH-activatable ovalbumin to form a hyaluronic acid-modified multimodal therapy platform linked by lactobionic acid for use in targeted delivery and enhanced synergistic anti-tumor therapy. The results indicate that CDT induced by Ca^{2+}/Cu^{+}/$^{2+}$, Ca^{2+} overload, and ovalbumin combined with chemotherapy significantly enhance the anti-tumor therapeutic effects. The current MOF-based nanozymes for tumor marker detection are as shown in Table 2.

5.2. Cardiovascular diseases (CVDs)

CVDs encompass conditions affecting the heart and vascular system, including myocardial infarction, hypertension, stroke, heart failure, and atherosclerosis (AS) [213–215]. These diseases are typically associated with dysfunction in the circulatory system, leading to severe health problems and complications. The “Chinese Youth Cardiovascular Health White Paper” released by the National Clinical Research Center for Geriatric Diseases (Beijing, China) in 2019 reveals an increase in CVDs affecting younger individuals in China, with a prevalence rate of 15.3 % among those aged 20–29. Improving the methods of preventing and diagnosing CVDs is critical. Cardiac troponin I (cTnI) is one of the most common biomarkers used in clinical practice to diagnose and monitor acute myocardial infarction (AMI). In 2019, Sun et al. developed an electrochemical biosensor based on a magnetic MOF as the gold standard for use in early AMI diagnosis [216]. They immobilized dual

Table 2
The applications of MOF-based nanozymes in Tumor markers.

Tumor maker	Materials	Sensors	LOD	Refs.
PSA	hydrogel-MOF-Cas12a	Fluorescence/Colorimetric	0.648 pg/mL	[181]
	MIL-101-NH_2(Fe)	Sandwichedtype PEC immunosensor	3.000 fg/mL	[192]
	MOF-CLISA	Immunoassay	0.030 pg/mL	[193]
	ZrFe MOF	Fluorescence/Colorimetric	8.500 pg/mL 22.700 pg/mL	[194]
	$Ru(bpy)_3^{2+}$/MOF (Ru-MOF)	Electrochemiluminescence/ Photoelectrochemistry	1.783 pg/mL 0.163 ng/mL	[195]
CEA	Cu-BTC@PQQ	Immunoassay	0.010 ng/mL	[99]
	ZrCo-MOF	Electrochemistry	0.350 fg/mL	[196]
	509-MOF@Apt	Electrochemistry	0.400 pg/mL	[197]
	Pt@SnS_2	Electrochemical Immunosensor	0.060 pg/mL	[198]
	Ni-Co MOF	Electrochemical immunosensor	0.300 ng/mL	[199]
AFP	NiZn MOF	Electrochemistry	0.980 fg/mL	[200]
	MIL-101 (Cr)	Electrochemical Immunosensor	0.054 ng/mL	[201]
	AuNPs@Fe-Zr-MOL	Electrochemistry	0.110 pg/mL	[202]
	Tb-MOF-on-Fe-MOF	Electrochemistry	58 μU/mL	[203]
CA125	MOF-808/CNT	Electrochemical Immunosensor	0.500 pg/mL	[204]
	Ab2-functionalized GOx-Cu-MOF	Cascade Immunosensor	5.060 mu U/mL	[205]
	1 T-MoS_2@dual MOFs	Electrochemical Immunosensor	0.0001 U/mL	[206]
HE4	IRMOF-3	Electrochemistry	9.890 fg/mL	[207]
	TiMOF-KB@AuNPs	Electrochemical Immunosensor	0.020 ng/mL	[208]
	nPCN-224	Electrochemical Immunosensor	0.560 pg/mL	[209]
NSE	NH_2-MIL-88 (Fe)	Electrochemistry	31.600 fg/mL	[210]
	Ru-MOF-5 NFs	Electrochemistry	0.041 pg/mL	[211]
	Zr-TCBPE-PEI	Electrochemistry	52 fg/mL	[212]

aptamers (Tro4 and Tro6) as capture probes on a screen-printed gold electrode to enhance the capturing efficiency of target cTnI, optimizing the interface density and stability. Subsequently, non-enzymatic nanoprobe 1 was employed in specific cTnI recognition, catalyzing the oxidation of HQ to benzoquinone in the presence of H_2O_2 to amplify the current signal. Recently, Ahmadi et al. [217] developed a novel electrochemical immunosensor for use in detecting CTnI. The immunosensor, with a sandwich design, utilizes a nanocomposite of a 2D zinc-based MOF (Zn-MOF), Fe_3O_4-COOH, and methylene blue labeled with monoclonal CTnI antibodies (Ab1) as the signaling molecule. The detection surface is modified with a polymer membrane comprising hexadecyltrimethylammonium bromide containing a choline chloride-urea deep eutectic solvent and coated with polyclonal CTnI antibodies (Ab2) (Fig. 11A). The detection limit for the CTnI concentration can reach as low as 0.0009 ng/mL (Fig. 9A). In contrast, Wang et al. integrated nanozymes into an electrochemiluminescent sensor for use in CTnI detection, combining a Co^{2+}-based zeolitic imidazolate framework (ZIF-67) and luminol-modified silver NPs (luminol-agnps) [218]. This resulted in a significantly enhanced signal 115-fold larger than that of luminol only. Cholesterol serves as a key indicator in evaluating AS [219]. In 2019, studies indicated that stable MOFs could serve as efficient carriers for cholesterol oxidase (ChOx), and they encapsulated HRP [220]. A colorimetric sensor for use in cholesterol detection was established based on such immobilized dual-enzyme cascade catalysis. Recently, Cao et al. [221] designed a molecularly imprinted sensor based on a cascade enzyme system. By embedding gold NPs (AuNPs) on the surface of a UiO-66-NH_2 framework to impart a POD-like activity and immobilizing ChOx on the surface, molecularly imprinted polymers (MIPs) were synthesized using cholesterol as the template molecule. The resulting U_6NH_2@AuNPs-ChOx@MIPs sensor efficiently and selectively detected blood cholesterol, with an LOD of 2.4 mM, which is significantly lower than the normal concentration of blood cholesterol (<5.18 mM). Researchers proposed a novel approach for use in treating cancer by combining ferroptosis and immunotherapy [222]. They developed the novel nanozyme FeMOF/CP, which comprised iron-based MOF (Fe-MOF) NPs loaded with ChOx and mPEG. The strategy, as shown in Scheme 1 of Fig. 11B, enhances iron-induced cell death via three main pathways. Firstly, Fe-MOF exhibits a significant POD-like activity, catalyzing the generation of •OH from H_2O_2 within tumor cells, thus increasing their ROS levels and promoting ferroptosis. Secondly, ChOx is released from Fe-MOF/CP in a pH-responsive manner, depleting the cholesterol and generating H_2O_2, further elevating the intracellular ROS levels. Lastly, Fe-MOF/CP disrupts cell lipid rafts, downregulating the expression of GPX4 and FSP1 to enhance ferroptosis. Additionally, Fe-MOF/CP induces a robust anti-tumor immune response, including dendritic cell maturation, M2 macrophage polarization, and the alleviation of $CD8^+$ T-cell exhaustion and activation of effector memory T cells. Furthermore, ChOx promotes immunogenic cell death, reducing the expression of programmed death-ligand 1 in cancer cells treated with the Fe-MOF NPs, thus inhibiting immune evasion. The in vivo feasibility was demonstrated by co-culturing mouse breast cancer 4 T1 cells with fluorescein isothiocyanate (FITC)-labeled Fe-MOF/P (Fe-MOF/P@FITC) and measuring the cellular fluorescence intensity using flow cytometry. The results (Fig. 11C) reveal a significant increase in the cellular fluorescence intensity after co-culturing the 4 T1 cells with FITC-labeled Fe-MOF/P, indicating the substantial cellular uptake of Fe-MOF/P. The O_2 and H_2O_2 levels of the 4 T1 cells were detected using $Ru(dpp)_3]Cl_2$) and Amplex Red fluorescent probes. Fe-MOF/P exhibits a minimal effect on the intracellular O_2 levels, whereas the cells treated with ChOx and Fe-MOF/CP display decreased and increased levels of O_2 and H_2O_2, respectively. Moreover, the fluorescence intensity of Fe-MOF/CP at the tumor site increases over time, reaching a maximum at 12 h post-injection and remaining detectable at 24 h, indicating its excellent tumor-targeting capacity. Ex vivo imaging confirms the predominant accumulation of Fe-MOF/CP within tumor tissues (Fig. 11D). However, Lv et al. [223] introduced a promising novel option for use in the early diagnosis and treatment of AS, utilizing Cur/MOF@DS nanozymes with excellent MRI performances and anti-AS effects. During the progression of AS, SR-A is overexpressed on activated macrophages. DS-modified NPs can selectively bind to the SR-A receptor, enabling the diagnosis and monitoring of AS via fluorescence localization studies of the interaction between SR-A and Cur/MOF@DS. Conversely, Rejeeth et al. [27] synthesized bimetallic MOF-NPs based on zeolitic imidazolate frameworks and utilized them as matrices in laser desorption/ionization mass spectrometry (LDI-MS) to rapidly analyze serum samples and extract their metabolic profiles. This method effectively distinguished patients with CVDs from those with coronary artery disease with a high sensitivity and specificity.

Notably, MOF-based nanozymes not only hold diagnostic value in terms of CVDs but also display significant therapeutic potential, e.g., Xiang et al. designed a bimetallic MOF nanozyme (Cu-TCPP-Mn) with cascading enzyme activities of SOD and CAT [224]. This nanozyme protected the heart from oxidative stress and inflammation-induced damage by efficiently scavenging ROS, displaying promising results in animal models of myocardial infarction and ischemia-reperfusion injury. Furthermore, utilizing nanozymes as drug delivery vehicles is also a viable approach for use in treating CVDs [225]. Remarkably, the application of nanotechnology exhibits multifaceted potential in the development of cardiac stents [226,227].

5.3. Neurodegenerative diseases

Common neurodegenerative diseases include Alzheimer's disease (AD), Parkinson's disease, Huntington's disease, amyotrophic lateral sclerosis, and multiple sclerosis [228–231]. Oxidative stress is critical in the development of various neurodegenerative diseases, leading to neuronal death and the disruption of neurological functions. Protein oxidation is a common manifestation, with amyloid-β (Aβ) interfering with metal homeostasis in the brain, contributing to the pathogenesis of neurodegenerative diseases (Fig. 12A) [24]. Therefore, measuring the Aβ level in the blood serves as an indicator in diagnosing and monitoring neurodegenerative diseases [232]. Current clinical methods of detecting Aβ mainly involve optical detection, neuroimaging, and immunoassays [233], and each exhibits drawbacks, such as susceptibility to interference from other blood proteins, technical complexity, and high equipment costs. Hence, developing a highly sensitive and accurate method for use in early Aβ detection is crucial. MOFs have emerged as promising nanomaterials in biomedicine due to their exceptional properties, including high surface areas and porosities, mild synthesis conditions, tunable pore sizes and shapes, strong host-guest interactions, versatile functionalization capacities, and excellent biocompatibilities [234].

The fluorescence detection of Aβ is highly attractive in diagnosing and monitoring the progression of AD due to its rapid, sensitive, non-invasive, real-time, simple, cost-effective nature, coupled with its high resolution [235,236], e.g., Wang et al. [26] developed the bioinspired fluorescent probe Zn-FBIFs based on Zn-MOFs for use in the selective enrichment and detection of Aβ. This probe comprises Zn-MOFs, mIM, and the fluorescent molecule *N*-(6-(benzo[*d*]thiazol-2-yl) pyridin-3-yl)-5-(dimethylamino) naphthalene-1-sulfonamide. The hydrophobic nature and size exclusion properties of Zn-FBIFs generate a synergistic effect, enabling the probe to selectively enrich Aβ while effectively excluding the other interfering proteins within serum (Fig. 12B). The fluorescence sensor fabricated using this probe detected Aβ concentrations as low as 3.22 nM in undiluted serum. The results shown in Fig. 12C indicate that Zn-FBIFs exhibits a significantly increased adsorption efficiency for Aβ (87.3 %) compared to those of the major proteins in human serum (human serum albumin, bovine serum albumin, and thyrotropin-releasing factor). Fluorescence measurement and confocal laser scanning microscopy reveal a significant decrease in the fluorescence signal of Aβ with Zn-FBIFs, whereas the effects on the fluorescence signals of the other interfering proteins are minimal (Fig. 12D). Similarly, Wang et al. synthesized an Er-MOF ([Er(L)(DMF)

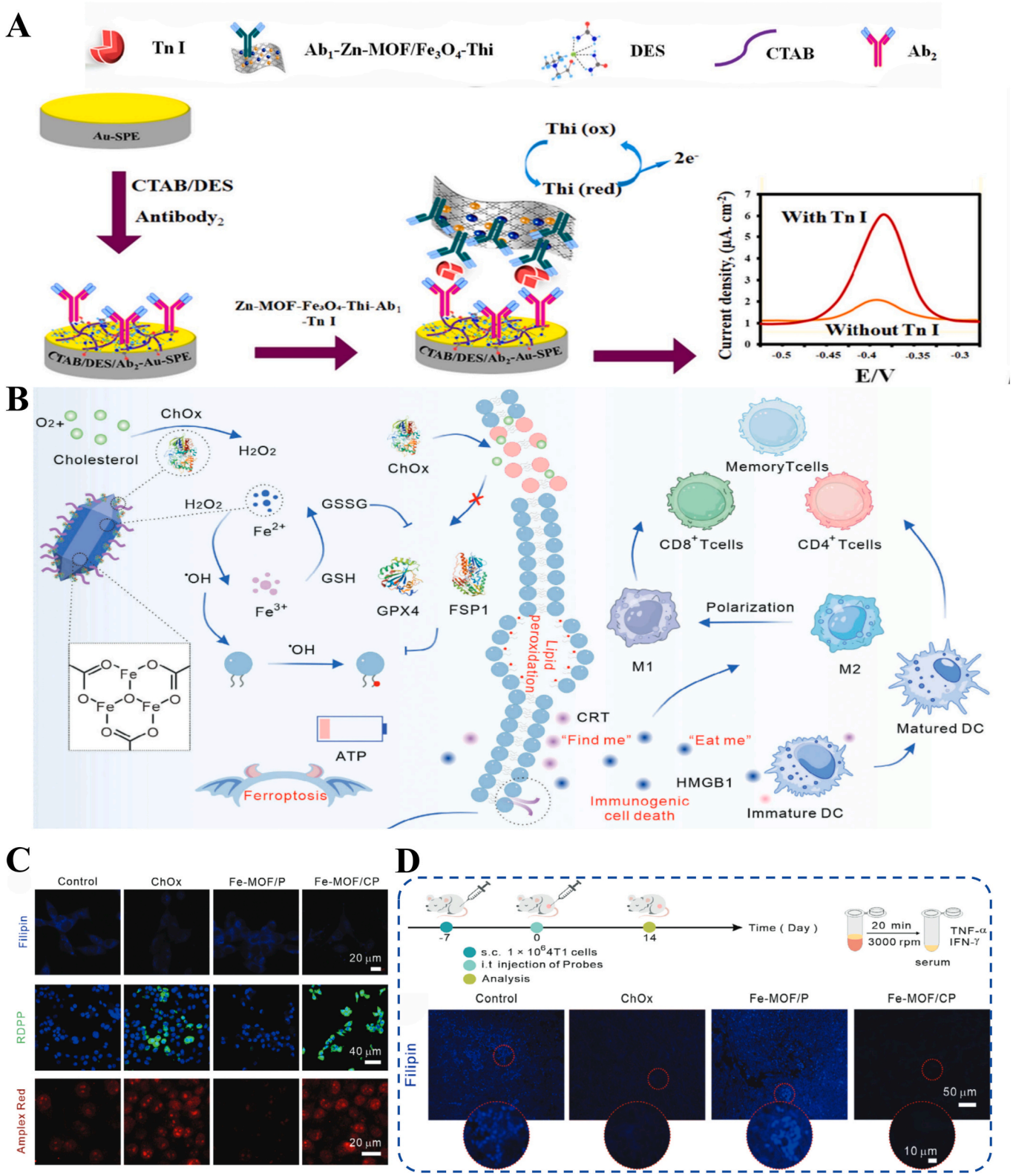

Fig. 11. (A) Schematic diagram of electrochemical determination of CTnI. Reprinted with permission from Ref. [217]. (B) The proposed mechanism of cholesterol-depleting Fe-MOF/CP for tumor synergistic ferroptosis-immune therapy. (C) Cellular fluorescent images of 4 T1 cells under indicated treatments. Filipin: cholesterol; RDPP: oxygen; and Amplex Red: H_2O_2. (D) In vivo cholesterol depletion and immune response of treatment procedure and fluorescent images. Reprinted with permission from Ref. [222]. (For interpretation of the references to color in this figure legend, the reader is referred to the web version of this article.)

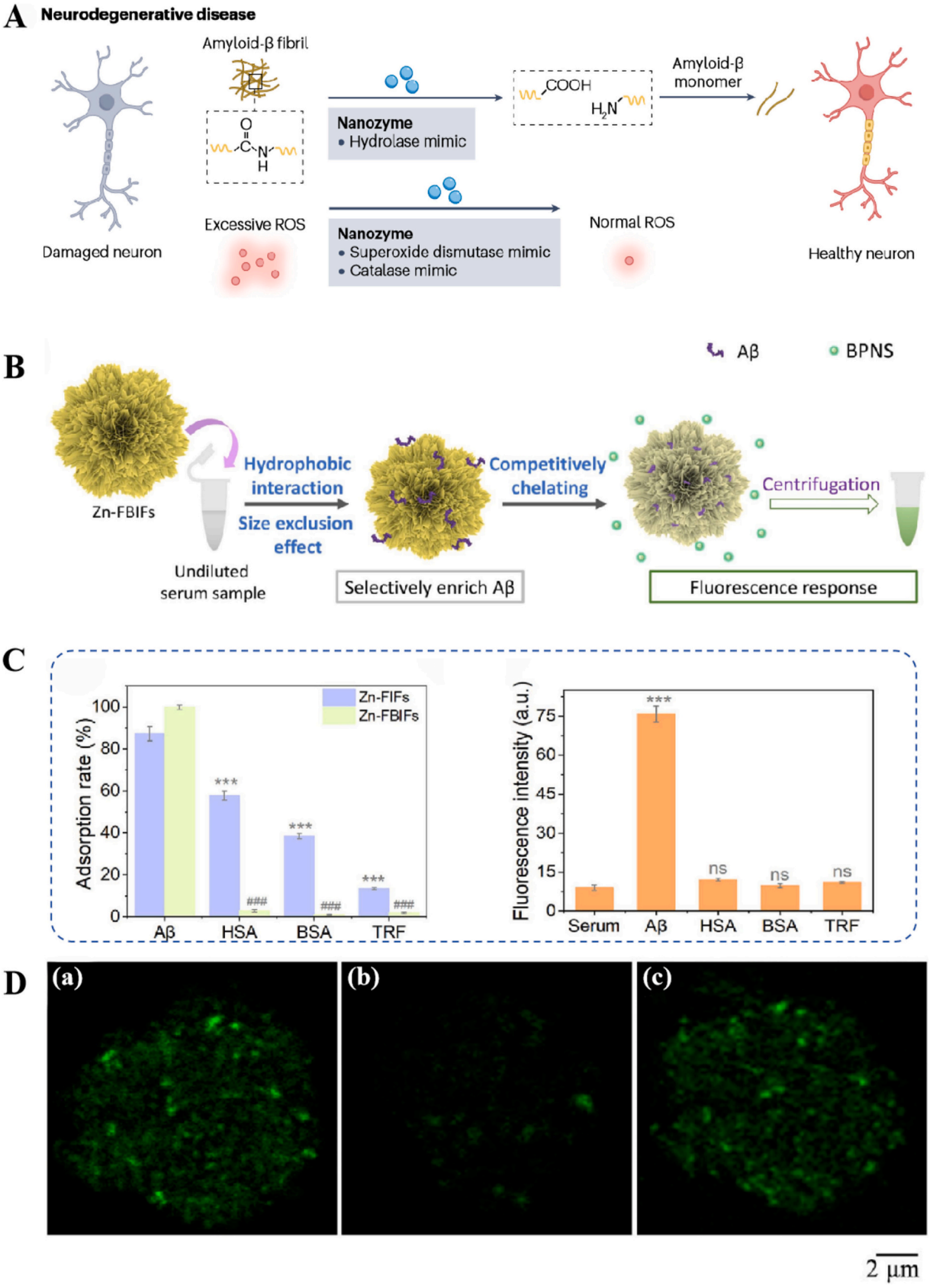

Fig. 12. (A) Pathogenesis of neurodegenerative diseases. Reprinted with permission from Ref. [24]. (B) Mechanism of the probe Zn-FBIFs for accurate Aβ detection in serum. (C) The adsorption capacity of Zn-FIFs or Zn-FBIFs for Aβ, HSA, BSA and TRF, and the fluorescence response of Zn-FBIFs towards Aβ, HSA, BSA and TRF by Zn-FBIFs in undiluted serum. (D) Zoom-in images of (a) Zn-FBIFs, (b) Zn-FBIFs + Aβ, and (c) Zn-FBIFs + HSA by CLSM. Reprinted with permission from Ref. [26].

1.27]) using solvothermal and ultrasonic techniques and incorporated the fluorescent dye thioflavin T (ThT) into the Er-MOF to yield a dual-emission ThT@Er-MOF probe [237]. This probe exhibited high sensitivities in detecting AD-related biomarkers, such as Aβ, amyloid precursor protein 1, and ACh, with a minimum detection limit of 0.142 nM. Conversely, Qin et al. [238] encapsulated ferrocene (Fer) within the porous structure of ZIF-8 for use in the dual detection of AβO. This was due to the tighter interaction between AβO and Zn^{2+} compared to that between mIM and Zn^{2+}. In addition to fluorescence sensors, colorimetric sensors are also commonly used in Aβ detection, e.g., Fan et al. [239] developed a highly sensitive colorimetric sensor based on the POD-like activity of UiO-66-NH_2 and strong affinities of Aβ(1–42) monomers for MOFs. The sensor realized the ultra-low-level detection of Aβ(1–42) monomers in water and cerebrospinal fluid within 5 min, with detection limits of 2.76 and 4.65 nM, respectively, outperforming traditional detection methods in terms of speed and complexity. Dong et al. [240] incorporated $Ru(bpy)^{32+}$ (bpy = 2,2′-bipyridyl) into the pores of NH_2-UiO-66 NPs as a luminescent material, leveraging its smaller molecular diameter (11.5 Å) compared to those of the octahedral cavities of NH_2-UiO-66 (13 Å) to yield a composite with an excellent, stable luminescence efficiency, providing a larger surface area for antibody adsorption. They developed a sandwich-type ECL immunosensor with a signal-off mechanism using a combination of MIL-101 and NH_2-UiO-66. The prepared MIL-101QAu-MoS_2 quantum dots were employed to quench the ECL signal of $Ru(bpy)^{32+}$/NH2-UiO-66, thus labeling the secondary antibody (Ab2). This sensor enabled the precise measurement of the Aβ concentration in solution, as an increase in the Aβ concentration was monitored via the increased binding of the Ab2-MIL-101@Au-MoS_2 quantum dots to the antigen. Conversely, Miao et al. [241] utilized Cu-Al_2O_3-g-C_3N_4-Pd and UiO-66@PANI-MB as the substrate and signal label, respectively, to fabricate a dual-signal (voltammetry and amperometry combined) sandwich-type electrochemical immunosensor for use in quantitative Aβ detection. Similarly, Fang et al. [242] proposed an analytical platform using ECL resonance energy transfer technology for application in highly sensitive Aβ detection. Within this platform, functionalized gold NPs bearing graphene-like carbon nitride nanosheets (g-C_3N_4@Au NPs) and a palladium NP-coated MOF (Pd NPs@NH_2-MIL-53) served as the ECL donor and acceptor, respectively. The gold NPs were utilized not only as accelerators to enhance and stabilize the ECL signal but also as connectors to link β antibodies, enabling the specific recognition of Aβ while enhancing the signal. Aside from Aβ, GSH in plasma is also considered a biomarker in diagnosing AD. Whereas several studies report the application of MOFs in detecting GSH, most research focuses on ROS in cancer treatment, influenced by hypoxia and overexpressed GSH in the TME [243–245]. However, Xu et al. [246] developed an ultrasensitive dual-signal self-calibrating electrochemical platform for use in detecting GSH based on ferrocene-functionalized copper MOFs (Fc-Cu-MOF). The sensor exhibits characteristic stable electrochemical peaks due to the reaction of CuCl with chloride ions in solution. The higher affinity of Cu^{+} for GSH leads to a significant decrease in the current signal of CuCl triggered by the crowding effect in the presence of GSH, whereas the peak current of ferrocene remains constant, serving as an internal reference. The output signal is then calculated as the ratio of the changes in the peak currents. This sensing platform was successfully applied in GSH determination in food and serum samples, with an LOD of 0.025 nM and excellent recovery performance. Recently, our research group developed flower-like artificial nanozymes with POD-like activities (apo-TF-MnO_x NFs) [247]. We utilized these activities to develop a biosensor based on colorimetric GSH detection. Qualitative testing of H_2O_2 and GSH in blood samples from patients with acute coronary syndrome validated the effectiveness of this method. MRI can detect individual Aβ plaques in brain tissue by providing a high spatiotemporal resolution [248]. As early as 2010, studies explored the application of MOFs in MRI. mPEG-modified MIL-88 MOFs exhibited r_2 relaxivities of 50 mM^{-1} s^{-1} at 9.4 T [249]. MRI revealed darker signals in the spleen and liver post-treatment compared to those of normal tissue using spin- and gradient-echo sequences. Notably, no significant toxic reactions were observed in rats following the injection of high doses of iron-based MOFs, indicating the potential of these materials for use in biomedical MRI applications. Furthermore, Zhao et al. developed a multifunctional nanoplatform based on MOFs for use in diagnosing and treating AD [250]. The surfaces of these NPs were modified with NOTA and DMK6240 for use in specific tubulin associated unit (tau) protein detection, with MB encapsulated within as a tau aggregation inhibitor. Ultimately, this functionalized MOF platform could visualize abnormal regions in MRI and inhibit the accumulation of hyperphosphorylated tau via MB release. The current MOF-based nanozyme-constructed sensors are mainly applied to the detection of the following types of neurodegenerative disease biomarkers (Table 3).

5.4. Metabolic diseases

Metabolic diseases, such as hyperglycemia and -lipidemia and diabetes, are commonly encountered in clinical practice [264–266]. These diseases also include thyroid dysfunction, obesity, hypertension, hypercholesterolemia, gout, and phenylketonuria, which are characterized by specific biomarkers. Diabetes, which is a prevalent chronic metabolic disorder, is often associated with fluctuations in blood glucose levels, which are the primary contributors to various diabetes-related complications. Monitoring the blood glucose level in the body is crucial in the

Table 3
Materials for the detection of Neurodegenerative disease biomarkers.

Biomarkers	Materials	Detection method	LOD	Refs.
Aβ	Fc-Zn-MOF	Electrochemistry	0.030 pg/mL.	[84]
	ZnO-Co_3O_4 NCs	Colorimetric	3.500 nM	[89]
	T@Er-MOF	Fluorescence	0.142 nM	[237]
	L-MOF/Apt-Au	Fluorescence	0.300 pM	[251]
	Fe_2O_3@FeS_2	Photoelectrochemical immunosensor	2.100 pg/mL	[252]
	Au@NiFe MOFs	Electrochemiluminescence	13.800 fg/mL	[253]
	Ce-MOF	Colorimetric	129 μM	[254]
	AuNPs/Fe-MIL-88NH_2	Electrochemiluminescence	71 fM	[255]
	Zn-FBIFs	Fluorescence	3.220 nM	[26]
	Fe_2O_3@FeS_2	Photoelectrochemical Immunosensor	7.9 pg/mL	[252]
Tau Protein	2D Nanosheet	Fluorescence	10 pg/mL	[256]
	Pt@ZIF-8	Electrochemistry	1 fg/mL	[257]
	Zr-MOF/MB/Au	Electrochemical Immunosensor	3.340 fg/mL	[258]
	TMBDA-MIL-100(Fe)	Colorimetric	0.036 μM	[259]
	MOF-808/Pt NPs	Colorimetric	5 μM	[165]
ACh	ThT@Er-MOF	Fluorescence	0.032 nM	[237]
	AChE-ChO/PtNPs/MOF	Electrochemistry	0.010 μM	[260]
	ACC-rGO@Cu(BTC)@MnO_2	Electrochemistry	5 nM	[261]
	Ti-MIL125-NH_2	Fluorescence	3×10^{-5} U/μL	[262]
PKA	MOF (Cu-TCPP(Zn))	Electrochemistry	3.7×10^{-3} U/mL	[263]
	UiO-66	Fluorescence	5×10^{-5} U/μL	[95]

timely prevention and diagnosis of diabetes. Zhang et al. [267] developed the trimetallic oxide catalysts with excellent glucose detection performances. Recently, Sun et al. [268] encapsulated 4-mercaptobutyronitrile (4-MBN) as an internal standard within Au@Ag nanorods (NRs, Au@4-MBN@Ag NRs), followed by the encapsulation of Au@4-MBN@Ag NRs, malachite green (LMG), GOx, and HRP within ZIF-8 to prepare a SERS sensor based on the sequential enzyme catalysis ratio, i.e., Au@4-MBN@Ag@LMG@ZIF-8 (GOx, HRP), for use in detecting glucose in saliva. Compared to that of traditional portable fingertip blood glucose meters (LODs: 0.5–5 mM), this sensor realized the sensitive detection of glucose in saliva (LOD: 0.03 μM) without causing wounds. Additionally, researchers developed a skin patch-type electrochemical sensor for use in analyzing the glucose level in sweat [269], but its practical utility is inferior to that of the former method of detecting

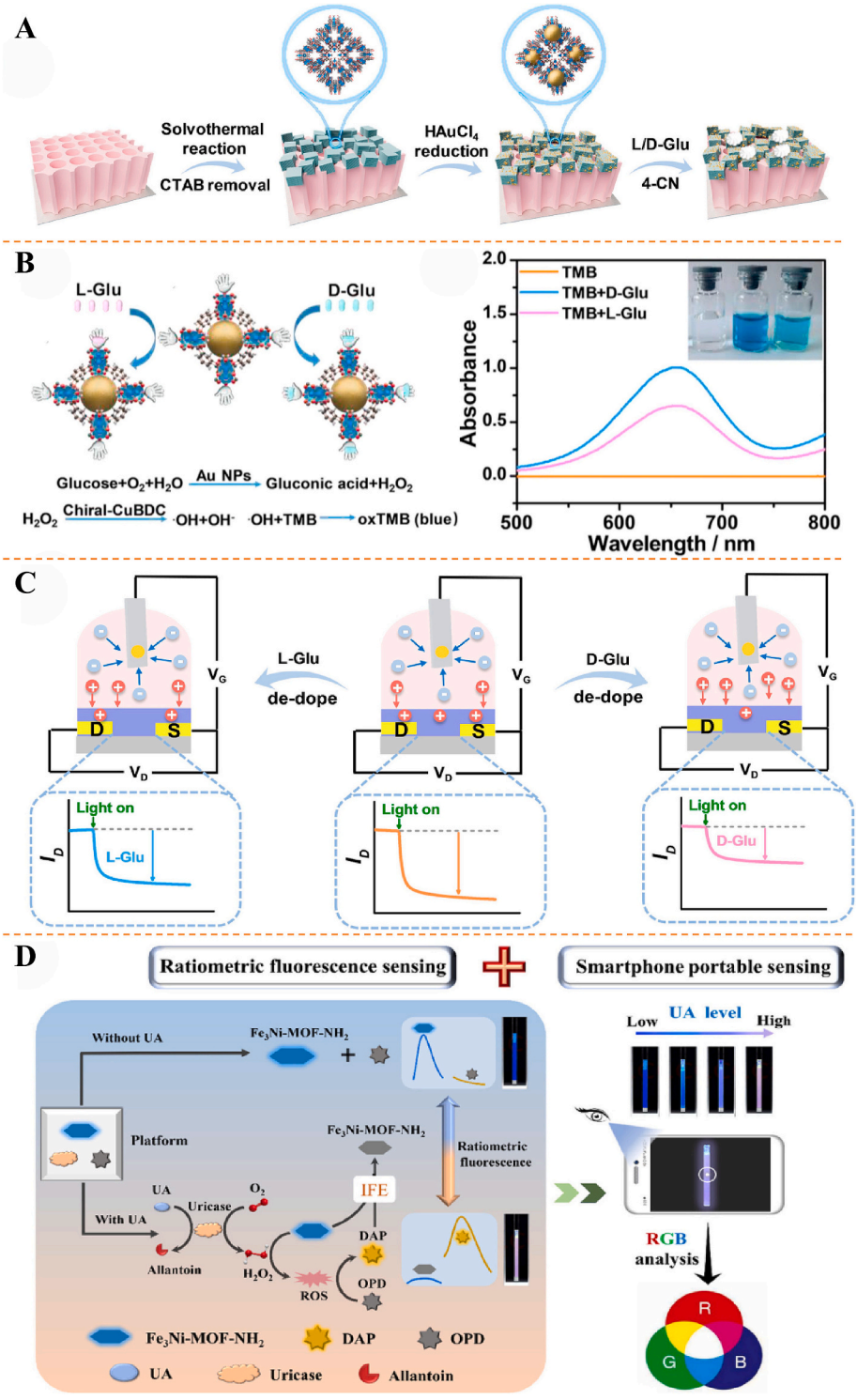

Fig. 13. (A) Synthesis of the Au@*c*-CuBDC/TNT homochiral gate electrode. (B) Schematic illustration of enantioselective Glu detection and colorimetric assay of Au@*c*-CuBDC/TNT. (C) OPECT sensor system for L/D-Glu recognition and quantification and corresponding operation rationale. Reprinted with permission from Ref. [270]. (D) Mechanism of the ratiometric fluorescent biosensor for UA based on the Fe_3Ni-MOF-NH_2 nanozyme and its smartphone-based portable sensing application. Reprinted with permission from Ref. [278].

glucose in saliva. Apart from glucose detection, MOFs can also be utilized in distinguishing glucose enantiomers. Zhu et al. [270] integrated gold NPs (AuNPs) and a chiral Cu(II)-MOF (c-CuMOF) onto TiO_2 nanotube arrays (TNT) to yield a photoelectrochemically active gate electrode. Fig. 13A shows a non-enzyme chiral-driven gate control strategy for use in identifying and quantifying glucose enantiomers. Initially, titanium sodium (TNT) was combined with cCuMOF, the mesoporous pockets of which were loaded with gold NPs (AuNPs). In a chiral environment, L- and D-glucose can be recognized and bound to the Au@c-CuBDC surface. As illustrated in Fig. 13B, the identified glucose is oxidized to gluconic acid and H_2O_2 under catalysis by the AuNPs with GOx activities. Subsequently, CuBDC, acting similarly to POD, activates H_2O_2 to oxidize colorless TMB to blue oxTMB, with a characteristic absorption peak at 652 nm. Under the same conditions, the amount of oxTMB generated from D-Glu is significantly higher than that generated from L-Glu, indicating the pronounced enantiomeric selectivity provided by the chiral environment of c-CuBDC. Furthermore, the effect of Au-LSPR on the precipitation reaction was explored to optimize the chiral sensing performance of Au@c-CuBDC/TNT. The POD-mimicking CuBDC subsequently induced the oxidation of H_2O_2 to 4-CN, resulting in precipitation. As shown in Fig. 13C, this molecular recognition-triggered precipitation strategy modulates Vp, leading to the differentiation of ID via the transfer of cations and anions to the channel and gate regions, respectively, generating distinct IDs. The IDs decrease with increasing Glu concentration, with D-Glu causing larger decreases in the IDs than those caused by L-Glu at the same concentration. The sensor fabricated in this manner exhibits an LOD that is one order of magnitude lower than those of traditional PEC biosensors. Thyroid dysfunction is the most common endocrine disorder in China, with T3 and T4 commonly used as clinical indicators of thyroid function [271]. Kabak et al. [272] synthesized a fluorescent Eu-MOF using a solvothermal method to develop a fluorescence sensor for use in detecting organic molecules (T3 and T4 hormones). In the presence of 500 nM T3 and 800 nM T4 hormones, fluorescence can be deactivated, with the quenching efficiencies reaching 98.7 % and 98.2 %, respectively. In 2017, research indicated the potential of MOF-based nanozymes for use in thyroid tissue imaging, e.g., Chen et al. [273] developed innovative dual-modal fluorescence/CT imaging probes, i.e., iodine-doped gold nanoclusters (AuNCs@BSA-I), for use in visualizing malignant thyroid tumors. The probe exhibited a "fast-in, slow-out" signal background in normal thyroid tissue, whereas in thyroid tumors, the signal displayed partial fluorescence at 1.5 h and rapidly disappeared within 2.5 h, with a "slow-in, fast-out" background ratio. This characteristic enabled significant differentiation between normal and diseased thyroid tissues. Apart from hormone sensing, the use of MOFs in intelligent detection is a method of screening for thyroid dysfunction. Recently, Chen et al. investigated the potential of gold-doped zirconium-based MOF (ZrMOF/Au) nanostructures for application in thyroid disease metabolite analysis [274]. The potential of the ZrMOF/Au-assisted LDI-MS platform for use in rapid thyroid disease screening offers a prospective method of the non-invasive screening of thyroid malignant tumors. Uric acid (UA) is a well-known typical marker used in diagnosing gout [142,275–277]. Numerous nanozymes have been developed for use in UA analysis, as UA can quench the fluorescence of UiO-PSM via coordination, hydrogen bonding, and π-π interactions. Qu et al. [25] designed a post-modified MOF (UiO-PSM) for use in direct UA fluorescence sensing. In contrast, Han et al. [278] established a more efficient ratiometric fluorescence sensor. This sensor utilizes a nanozyme (Fe_3Ni-MOF-NH_2) to drive the cascade catalytic reaction of UA/uricase/OPD (Fig. 13D).

Unlike sensors relying solely on fluorescence properties, Fe_3Ni-MOF-NH_2 exhibits a POD-like activity and fluorescence. In the absence of UA, Fe_3Ni-MOF-NH_2 exhibits fluorescence only at 430 nm (FI430). However, upon UA addition, the POD-like activity of Fe_3Ni-MOF-NH_2 is activated, and the H_2O_2 generated from UA under the catalysis of uricase oxidizes OPD to highly fluorescent 2,3-diaminophenazine (DAP, FI565). DAP quenches the fluorescence of the MOF via an inner filter effect, resulting in a respective decrease and increase in FI430 and FI565. The ratiometric fluorescence sensor fabricated based on this principle exhibits a detection limit of 24 nM, which is significantly lower than those observed in most studies. Remarkably, this sensor can also be combined with the RGB analysis function of a smartphone to realize portable UA detection. Additionally, Chen et al. [275] developed an array sensor based on a 2D layered conductive MOF. This sensor could simultaneously detect UA, ascorbic acid (AA), dopamine, and serotonin in 0.1 M phosphate-buffered saline (pH = 7.4). Recently, Lin et al. [279] designed a multifunctional biosensor that integrated the electrochemical detection of UA and glucose in sweat, electrophysiological signal acquisition, and electrical stimulation therapy. The multiple signals collected by this integrated biosensor could be wirelessly transmitted to mobile devices, indicating significant potential for use in muscle therapy and non-invasive monitoring in daily life.

5.5. Infectious diseases

Infectious diseases, particularly bacterial infections, present significant challenges to global health. Traditional diagnostic techniques are often time-consuming and complex, highlighting the urgent need for the development of efficient diagnostic methods. MOFs, with their high surface areas, tunable porosities, and functionalization capacities, offer an innovative approach for use in enhancing diagnostic capacities. Infectious diseases can be broadly categorized as bacterial, viral, fungal, or parasitic infections, based on the pathogens involved. The reported research regarding MOF-based nanozymes for use in diagnosing infectious diseases is summarized in Table 4.

5.5.1. Bacterial infections

In 2019, research indicated that bacterial infections are the second-leading cause of global mortality [298]. Timely, effective detection and identification of bacteria are crucial in infection prevention and control. Traditional bacterial culture methods are not only time-consuming but also susceptible to environmental contamination. Although advanced technologies, such as the polymerase chain reaction and ELISA, significantly reduced detection times, these methods still rely on complex instruments and skilled personnel, with the risk of false positives. However, the development of sensing platforms based on MOFs facilitated innovation in the diagnosis and monitoring of bacterial infections. Shi et al. [299] developed a luminescent sensor based on Eu-MOF and 2,5-furandicarboxylic acid as a coordinating ligand. This sensor employed a competitive sensing approach to rapidly detect *Pseudomonas aeruginosa* in water. Similarly, Qi et al. fabricated a microfluidic colorimetric biosensor for use in rapidly screening *Salmonella typhimurium* using the POD-like activity of Ab-MOF [280]. Critically, unlike other sensors, colorimetric sensors can be applied to qualitor quantitatively detect analytes using visual observation or low-cost, small-scale equipment. Furthermore, the sensor utilizes an MNB-*Salmonella*-MOF composite to catalyze OPD conversion to yellow DAP in the presence of H_2O_2, enabling the rapid analysis of images via a smartphone for efficient detection. Building on this, Cai et al. [170] developed a multifunctional colorimetric/SERS dual-mode biosensor. As shown in Fig. 14A, the sensor employs a nanozyme (4-MPBA-AuAg@PB MOF) with an excellent POD activity and significantly enhanced SERS properties, in conjunction with a "sandwich" recognition system, realizing a detection limit as low as 6 CFU/mL. This dual-signal sensor provides more accurate detection results compared to those of previously reported sensors that generate single signals. Moreover, via distinctive SERS "fingerprint" spectra, *Escherichia coli* and *S. aureus* can be effectively differentiated. In addition to the detection of pathogenic factors (bacteria), diagnosing infectious diseases by detecting bacterial metabolites is also viable, e.g., Wang et al. used a MOF to synthesize a nanozyme (Au NPs@MIL-101) for use in detecting SEB produced by *S. aureus*, realizing a remarkably low detection limit of only 0.2 pg/mL in milk [155]. Furthermore, bacterial infections trigger the production

Table 4
A typical example of the application of MOF-based sensors in infectious diseases.

Pathogens	MOF-based material	Sensors	Application	Analytes	Refs.
Bacteria	NH_2-MIL-101(Fe)	Colorimetric	Detection of pathogens	Salmonella cells	[280]
	ZIF-8	Colorimetric	Detection of pathogens	*E. coli* O157:H7 cells	[281]
	AuAg@PB MOF	SERS	Detection and discrimination of pathogens	*E. coli* and *S. aureus* cells	[170]
	Au@Ag@mSiO_2	SERS	Detection of metabolites and pH changes	Pyocyanin and pH	[282]
	Au NPs/MOFs	Electrochemistry	Detection of pathogens	*S. aureus* cells and micrococcal nucleases	[283]
	UiO-66-NH_2	Electrochemistry	Identification of MRSA and SA	Nuc and mecA genes	[284]
	ML-Cu_2O@Cu-MOF	Electrochemistry	Detection of pathogens	*S. aureus* cells	[285]
	Mn-MOF	Electrochemistry	Detection of pathogens	*S. aureus*, *E. coli* O157:H7, and *S. enterica* cells	[286]
	Ab_2/AuNPs/MOFs	Electrochemistry	Detection of pathogens	*S. aureus*	[287]
Virus	Zr@MAF@IL-6/PCT Ab	Fluorescence	Detection of biomarkers	IL-6/PCT	[288]
	MOF-FeP	Chemiluminescence	Detection of virus antibodies	EBV-IgA	[106]
	Co/Fe(1:1) MOF	Fluorescence	Nucleic acid detection	T-DNAs	[289]
	P-DNA@1 system	Fluorescence	Nucleic acid detection	Dengue virus and Zika virus RNA	[290]
	MIL-101-NH_2	Fluorescence	Nucleic acid detection	HAC RNA	[291]
	MOF-PC	Fluorescence	Nucleic acid detection	HSV-1 DNA	[292]
	MOF@P1/P2	Fluorescence	Detection of pathogens	SARS-CoV	[293]
	H_2dtoaCu-MOF	Fluorescence	Detection of pathogens H5N1 antibody	FAM-ssDNA- antigen	[294]
	Ni-MOF/AuNPs/CNTs	Electrochemistry	Nucleic acid detection	HIV DNA	[295]
	CdS@Zn-MOF	Electrochemical Immunosensor	Detection of pathogens	FMDV	[296]
Parasite	Cu-(NH_2-BDC)-MOF	Electrochemistry	Detection of Leishmania antibody	anti-gp63	[297]

of specific serum biomarkers in the human body, primarily C-reactive protein, procalcitonin (PCT), and interleukin 6 (IL-6). The combination of IL-6 and PCT serves as an effective indicator in evaluating sepsis. As illustrated in Fig. 14B, Chai et al. [288] developed an instant detection platform for sepsis biomarkers (IL-6/PCT) using fluorescent MOFs (MAFs) and a lateral flow immunoassay (LFA). The MAFs exhibit excellent photostabilities, high quantum efficiencies, and abundant active sites, enhancing the binding affinities of the labeled antibodies (Ab). The optimized composite material (Zr@MAF@IL-6/PCT Ab) displays specific recognition and binding capacities for IL-6 and PCT, realizing an LOD in the range of femtograms per milliliter, which is significantly lower than the physiological concentrations in serum. Furthermore, 29 clinical samples were evaluated, and the results were consistent with the clinical diagnoses. Additionally, the MAFs effectively distinguish between Gram-positive and -negative bacteria, which is attributed to the chemical affinities between the phosphorus-rich bacterial cell walls and Zr^{4+} on the MAFs, enabling specific binding to the cell walls of Gram-positive bacteria and promoting aggregation (Fig. 14C). Therefore, the MAFs not only detect IL-6/PCT but also differentiate between Gram-positive and -negative bacteria, rendering MAFs LFA a promising candidate for use in next-generation LFAs. In addition to the above metabolites, certain bacteria produce volatile organic compounds (VOCs), e.g., *Listeria monocytogenes* generates a microbial VOC (3-hydroxy-2-butanone (3H—2B). Pan et al. innovatively utilized MOFs as templates to successfully synthesize ordered cobalt-doped zinc oxide superparticles (Co_3O_4/ZnO SPs) and developed a highly sensitive and selective gas sensor for 3H—2B [300]. Incorporating cobalt generated more surface lattice defects and oxygen vacancies, significantly enhancing the gas detection performance. Furthermore, the porous structures of MOFs effectively enhance the solid-gas interfacial interactions, facilitating gas diffusion and desorption [301], enabling the rapid and sensitive identification of microbial VOCs. Moreover, antibiotic resistance is a critical factor in the worsening of infectious diseases, underscoring the importance of rapidly and accurately identifying drug-resistant pathogens. Methicillin-resistant *S. aureus* (MRSA) is a strain of *S. aureus* resistant to methicillin, which is identified by detecting the specific nuc gene and mecA gene encoding penicillin-binding protein. To address this, Dai et al. developed an electrochemical DNA sensor using UiO-66-NH_2 as a nanocarrier for electroactive dyes [284]. Upon binding with the nuc and mecA genes, the electroactive dyes were released, enabling the sensitive detection of these genes. The sensor exhibited excellent MRSA recognition capacities in real samples, effectively distinguishing MRSA from common *S. aureus* and providing crucial support in adjusting treatment regimens.

In contrast, Sun et al. [302] integrated diagnostics with resistance testing, producing a portable bandage that indicated drug resistance via color changes. This innovative strategy represents significant progress over the DNA sensor reported by Wang, seamlessly integrating bacterial diagnosis, drug testing, and POCT. Furthermore, incorporating MOFs into in situ imaging and therapeutic methods displays significant potential for use in addressing bacterial infections, e.g., Zhang et al. [303] utilized Zn-TCPP nanorods to visualize in vivo bacterial infections using pH-responsive fluorescence imaging, effectively deactivating bacteria in chronic wounds. This approach provided an innovative comprehensive platform for use in diagnosing and treating infectious diseases. A novel photoacoustic probe was recently developed for use in detecting infections and enhancing antibacterial activity against antibiotic-resistant bacteria. Yuan et al. [304] successfully designed an antibiotic-adjuvant photoacoustic probe targeting bacterially endogenous H_2S based on a bismuth MOF (Bi-MOF) (Fig. 15A). They initially validated the elevated levels of H_2S in MRSA compared to those of wild-type *S. aureus* using an H_2S fluorescent probe and a lead acetate assay (Fig. 15B). Inspired by this, the multifunctionality of MOF nanzymes has become a focal point of research across various fields, encompassing applications such as accelerating wound healing, inhibiting bacterial infections, modulating inflammatory responses, and promoting angiogenesis [305–308]. As shown in the Fig. 15C, the capacity of Bi-MOF as a PAI signal probe was investigated. Co-culturing Bi-MOF with *S. aureus* resulted in a strong PAI signal at approximately 690 nm upon laser irradiation, whereas no signal was detected in groups using Bi-MOF or *S. aureus*. Similarly, no PAI signal was generated under 690 nm laser stimulation of normal *S. aureus* cultures or Bi-MOF solutions, whereas co-cultures of Bi-MOF and *S. aureus* exhibited distinct signals (Fig. 15D). Furthermore, the multifunctionalities of MOF-based nanozymes inspired various applications, including the acceleration of wound healing, eradication of bacteria, reduction of inflammation, and promotion of angiogenesis.

5.5.2. *Viral infections*

Compared to the application of MOF-based nanozymes in bacterial diagnostics, their utilization in viral infection diagnostics has been limited. Nucleic acid testing and immunological assays are the most commonly reported techniques used in viral detection in clinical settings. In nucleic acid testing, MOFs are an ideal option for use in molecular recognition due to their low cytotoxicities, high porosities, tunable structures, and stabilities. Currently, numerous viruses, including human immunodeficiency virus (HIV, ss-HIV, ds-DNA), respiratory syncytial virus, and Ebola (ss-RNA), are targeted [309–311]. Fluorescently labeled DNA probes (P-DNA) are adsorbed onto MOF

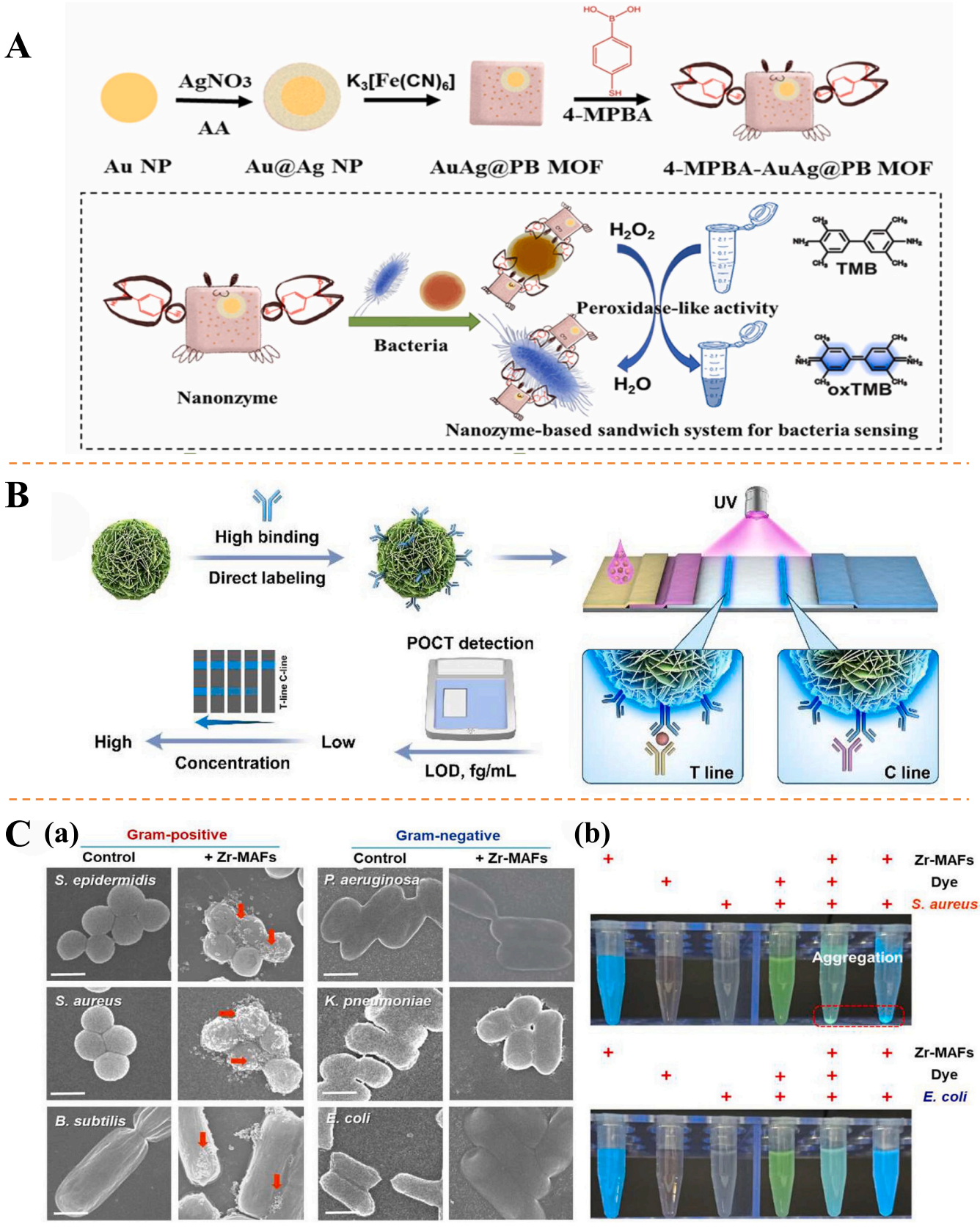

Fig. 14. (A) Schematic illustration of nanozyme-based sandwich system that made of bacteria/4-MPBA/AuAg@PB MOF for dual-mode colorimetric/SERS discrimination and detection of bacteria. Reprinted with permission from Ref. [170]. (B) The Schematic POC Tests of MAFs-Based LFAs for IL-6/PCT detection. (C) SEM images of co-incubation of Gram-positive bacteria/Gram-negative bacteria and MAFs (a). MAF particles are indicated with red arrows. Photographs of the aggregations in *S. a* and *E. coli* induced by MAFs (b). Reprinted with permission from Ref. [288]. (For interpretation of the references to color in this figure legend, the reader is referred to the web version of this article.)

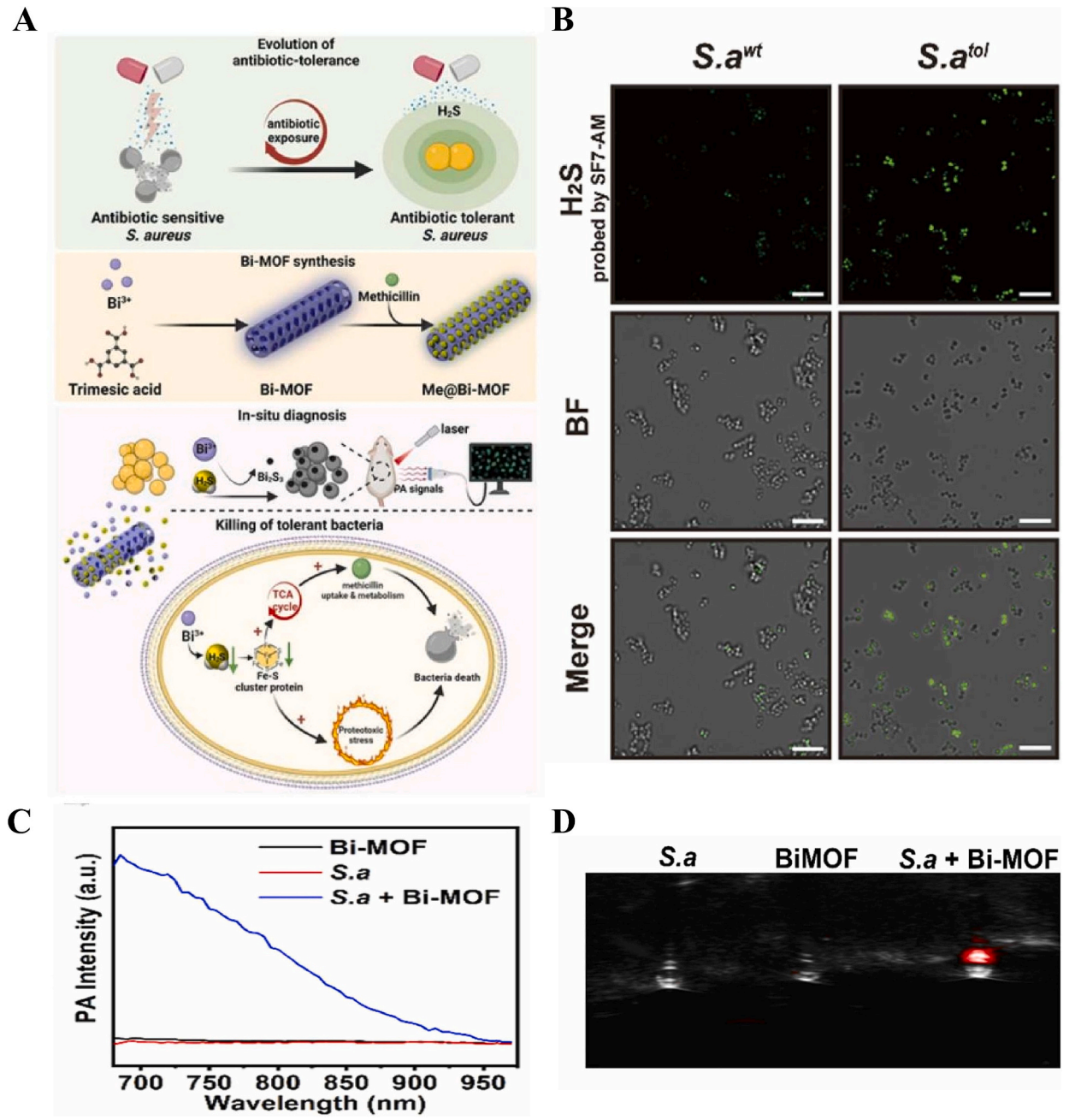

Fig. 15. (A) Synthesis and detection principle of bismuth metal-organic framework (Bi-MOF) as a photoacoustic probe for detecting infections. (B) Representative fluorescence images demonstrated the intracellular H_2S levels of *S. a*^{wt} and *S. a*^{tol} by SF7-AM probing. (C) The wavelength scanning of PA intensity of *S. aureus*, Bi-MOF and their mixture in different groups. (D) Representative image of PA intensity of *S. aureus* treated with Bi-MOF. Reprinted with permission from Ref. [304].

materials via mechanisms such as hydrogen bonding, electrostatic interactions, and π-π stacking via complementary binding to target DNA/RNA. These interactions lead to the fluorescence quenching of the dye on the probe due to photoinduced electron or energy transfer. Upon contact between the target viral DNA/RNA sequence and MOF, specific hybridization with the probe DNA occurs, forming stable double-stranded DNA, hybrid DNA/RNA double strands, or triple-stranded DNA structures. Subsequently, the generated complex is released due to its lower affinity for the MOF, resulting in fluorescence recovery [312]. The extent of fluorescence restoration can be utilized to determine the concentration of a virus in a sample. Viral detection methods can be categorized as single or multiple virus detection. Furthermore, due to the structural complexity of the double-stranded DNA of HIV, which may hinder its interaction with the internal P-DNA of a MOF, numerous studies focusing on HIV detection concentrate on single-stranded DNA detection, e.g., as early as 2014, studies combined SYBR Green I with a single-stranded DNA probe, with a sequence of 5′-atgtggaaaaatctctagcagt-3′, and formed a fluorescence quenching platform with MIL-101 (Cr) for use in detecting single-stranded HIV-1 DNA [313]. The target DNA could hybridize rapidly with the probe, significantly enhancing the recognition capacity for single-base mismatched target DNA. Subsequently, Yang et al. [314] developed two MOFs based on lanthanides (3D-MOF1 and 2D-MOF2) for use in detecting *Sudan ebolavirus*. MOFs 1 and 2 effectively quenched the fluorescence of carboxyfluorescein-labeled (FAM-labeled) P-DNA, with quenching efficiencies of 70.2 % ± 5.3 % and 57.3 % ± 5.3 %, respectively. The difference may be attributed to the positively charged ammonium centers exposed on the surface edges of MOF1, leading to stronger electrostatic

interactions with P-DNA. Upon adding target RNA, the fluorescence of P-DNA was restored. The sensing platform formed by non-disseminating P-DNA@MOF hybrids could identify the conserved linear single-stranded RNA sequence of the *Sudan* virus, with low detection limits of 112 and 67 pM. Moreover, these hybrids exhibited outstanding specificities, effectively distinguishing single-base mismatched RNA sequences.

MOFs are versatile platforms suitable for use in the multiplex detection of analytes. Compared to single-virus nucleic acid detection, multiplex virus nucleic acid detection based on fluorescence biosensing enables the simultaneous detection of multiple nucleic acids, thus enhancing the detection speed and diagnostic accuracy [315]. In 2014, Wang et al. [316] first combined H_2dtoaCu with oligonucleotides for use in detecting multiple sequence-specific DNAs targeting wild-type hepatitis B virus (HBV, T1) and HIV (T2) reverse-transcription RNA segments. The hairpin structures of the oligonucleotides enabled the MOFs to serve not only as nanoscale quenchers for the fluorescently labeled oligonucleotides but also as nanoscaffolds. Subsequently, Xie et al. synthesized a novel water-soluble MOF with a 3D structure and large pores that could exhibit strong affinities for single-stranded DNA probes (P-DNA) labeled with FAM or 5(6)-carboxy-X-rhodamine triethylammonium salt [290]. Via π-π stacking and electrostatic interactions, fluorescence quenching is realized, leading to the simultaneous detection of Dengue virus and Zika virus RNA sequences using the generated P-DNA@1 system. This technology benefits from the different affinities of MOF 1 and P-DNA, in addition to the formation of double-stranded DNA/RNA upon recognition, with sensitivities reaching 184 and 121 pM. In addition, the system employs two types of DNA probes, i.e., P-DNA-1 and P-DNA-2, with cross-reactivity that requires validation. This cross-reactivity is crucial in ensuring detection specificity, directly influencing the accuracies of multiplex assays. As illustrated in Fig. 16A, when only T1 is present in the sample, a significant increase in the fluorescence intensity of P-DNA-1 is observed. Conversely, when only T2 is present, the fluorescence intensity of P-DNA-2 increases independently. In cases where both targets are present simultaneously, the fluorescence intensities of both probes increase, indicating the potential of the system for robust application in multiplex RNA detection. Another study synthesized a 2D bimetallic MOF nanosheet that could selectively detect four hepatitis DNA sequences (hepatitis A, HBV, hepatitis C, and HIV) concurrently [289]. The study also investigated the quenching efficiencies of Co/Fe complexes with different mass ratios, including Co/Fe (1:0.5), Co/Fe (1:1), and Co/Fe (1:2) MOFs. Furthermore, these sensing systems effectively distinguished single-base mismatches in RNA sequences. Although nucleic acid testing is considered the gold standard in diagnosing viral infections, it displays drawbacks, such as extended processing times, sample susceptibility to contamination, and the high levels of expertise required for operators. In contrast, immunological tests based on antigen and -body specific binding significantly improved detection efficiency, which is particularly suitable in initial clinical screening. Viral immunological testing based on MOFs can be further categorized into antigen or -body detection. Electrochemical immunoassays garner widespread attention in antigen detection for viral infections. However, several MOF-based immunosensors are largely constrained via the covalent binding of their biomolecules and inhibited electron transfer due to the weak molecular permeabilities of MOFs. To address these problems, Mehmandoust et al. developed a label-free electrochemical biosensor for use in detecting the SARS-CoV-2 spike protein to provide an effective analytical method of diagnosing the novel coronavirus in real samples [317]. The preparation of this sensor involves synthesizing and modifying SiO_2@UiO-66 on the surface of a screen-printed carbon electrode, followed by angiotensin-converting enzyme 2 (ACE2) modification of the electrode. ACE2, as the primary receptor for viral entry into cells, can specifically bind and interact with the SARS-CoV-2 S protein (Fig. 16B). The fabricated sensor enables the direct analysis of the electrochemical interaction between the electrode-electrolyte interface and viral protein, facilitating the detection of the SARS-CoV-2 S protein in nasal swab samples. Recently, Li et al. [318] developed an electrochemical immunosensor for use in the sensitive detection of HBsAg using bimetallic conductive MOFs (c-MOFs) and cobalt oxide NPs. The sensor functions via the immobilization of HBsAb, which specifically recognizes and binds to HBsAg, on the surface of the sensing electrode (Au@Co_3O_4NPs/NiCo(HITP)/GCE) (Fig. 16C). The binding of HBsAg to the immobilized HBsAb forms an immune complex with a reduced conductivity, leading to an increase in the Rct between the sensor surface and test buffer, resulting in a decreased current intensity, as shown in Fig. 16D. Furthermore, the sensor exhibits a consistent HBsAg detection performance in human serum. Molecular imprinting is another commonly used method in antigen detection, but it faces challenges when capturing large viruses. To address this problem, employing carriers with sufficient surface areas to provide additional imprinting sites is an effective strategy [319,320]. MOF materials are considered ideal for this purpose due to their exceptional surface areas and tunable pore structures. MIL-100 (Cr) and MIL-101 (Cr) display pore sizes of 2.5–2.9 and 2.9–3.4 nm, respectively, with MIL-101 exhibiting a high specific surface area of up to 5900 ± 300 m^2/g [321,322]. This feature offers more imprinting sites for use in virus detection, significantly enhancing sensor sensitivity.

Compared to antigen detection, research regarding the utilization of MOFs in antibody detection during viral infection is limited. However, in 2013, Wei et al. [294] developed an innovative biosensor based on MOFs for use in detecting antibodies against the H5N1 influenza virus. This sensor exhibited a remarkably low detection limit (1.6×10^{-9} mol/L, signal-to-noise ratio = 3) and wide linear range (1.0×10^{-6}-5.0×10^{-9} mol/L).

By ingeniously combining the H5N1 antigen with the fluorescent dye 5′,6-FAM within the MOF structure, the specific binding of the H5N1 antibodies to the H5N1 antigen inhibited the hydrolysis of exonuclease I, resulting in irreversible fluorescence quenching, enabling the efficient, rapid detection of the H5N1 antibodies. Recently, Wang et al. integrated single-atom nanozymes with POD-like activities (MOF-FeP) with mouse anti-human IgA antibodies and incorporated them into conventional test strips, developing a sandwich colorimetric sensor that could specifically recognize and detect EBV-IgA [106]. This sensor could simultaneously detect three types of EBV-IgA, significantly enhancing the accuracy of NPC screening related to EBV. Notably, MOFs can also serve as protective scaffolds for use in encapsulating live viruses and stabilizing vaccines [323]. This is attributed to their effective encapsulation of live viral particles, providing a secure environment to prevent virus inactivation or degradation. Furthermore, the chemical properties of MOFs enable their good compatibilities with vaccine components, ensuring the stabilities of vaccines during storage and transportation.

5.5.3. Other microbial infections

Compared to the widespread application of MOFs in diagnosing bacterial and viral infectious diseases, research regarding diagnostic methods for parasitic and fungal infections is relatively scarce. Currently, the diagnosis of parasitic infections mainly focuses on the stages of the parasites within the tissues, typically their mature or reproductive stages, with weaker capacities in identifying early life or cyst stages. Therefore, parasitic biomarkers are considered crucial indicators in early diagnosis. The *Leishmania* surface proteinase Gp63 is a significant surface molecule in promastigotes, which is often regarded as a virulence factor in parasites and key component in host-parasite interactions. Due to its high conservation across different *Leishmania* species, Gp63 is a preferred target in *Leishmania* detection. Recently, Perk et al. [297] developed an electrochemical immunosensor specifically for use in detecting the major surface proteinase Gp63 of *Leishmania*. Preparing this sensor involves modifying a gold nanoelectrode (AuSPE) with Cu-(NH_2-BDC)-MOF and immobilizing a recombinant *Leishmania* antigen on the electrode surface using a crosslinking agent. Changes in the electrochemical signal are monitored using EIS (Fig. 17A). Furthermore, the sensors were validated via practical sample analysis of *Leishmania* crude antigens and rabbit serum (Fig. 17B). In

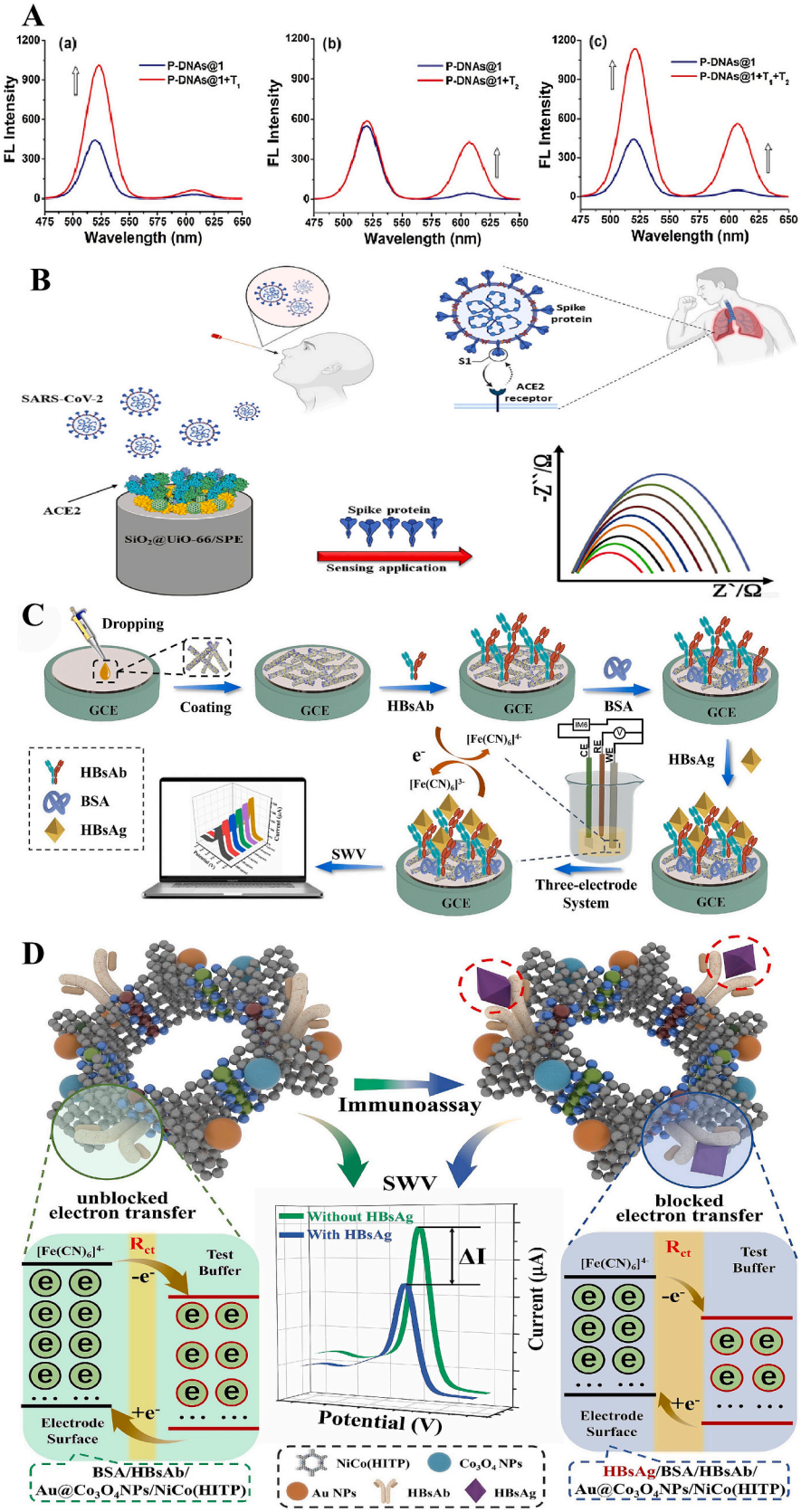

Fig. 16. (A) Fluorescence spectra of both P-DNA@**1** (50 nM/40 μM) with T_1 (a, 60 nM), T_2 (b, 60 nM), T_1 and T_2 (c, 60 nM/60 nM). Reprinted with permission from Ref. [290]. (B) An electrochemical biosensor for detecting SARS-CoV-2 S-protein. Reprinted with permission from Ref. [317]. (C) Schematic illustration of as-prepared Au@Co_3O_4NPs/NiCo(HITP)/GCE electrochemical immunosensor towards HBsAg detection. (D) The principle of as-developed HBsAg electrochemical immunosensor. Reprinted with permission from Ref. [318].

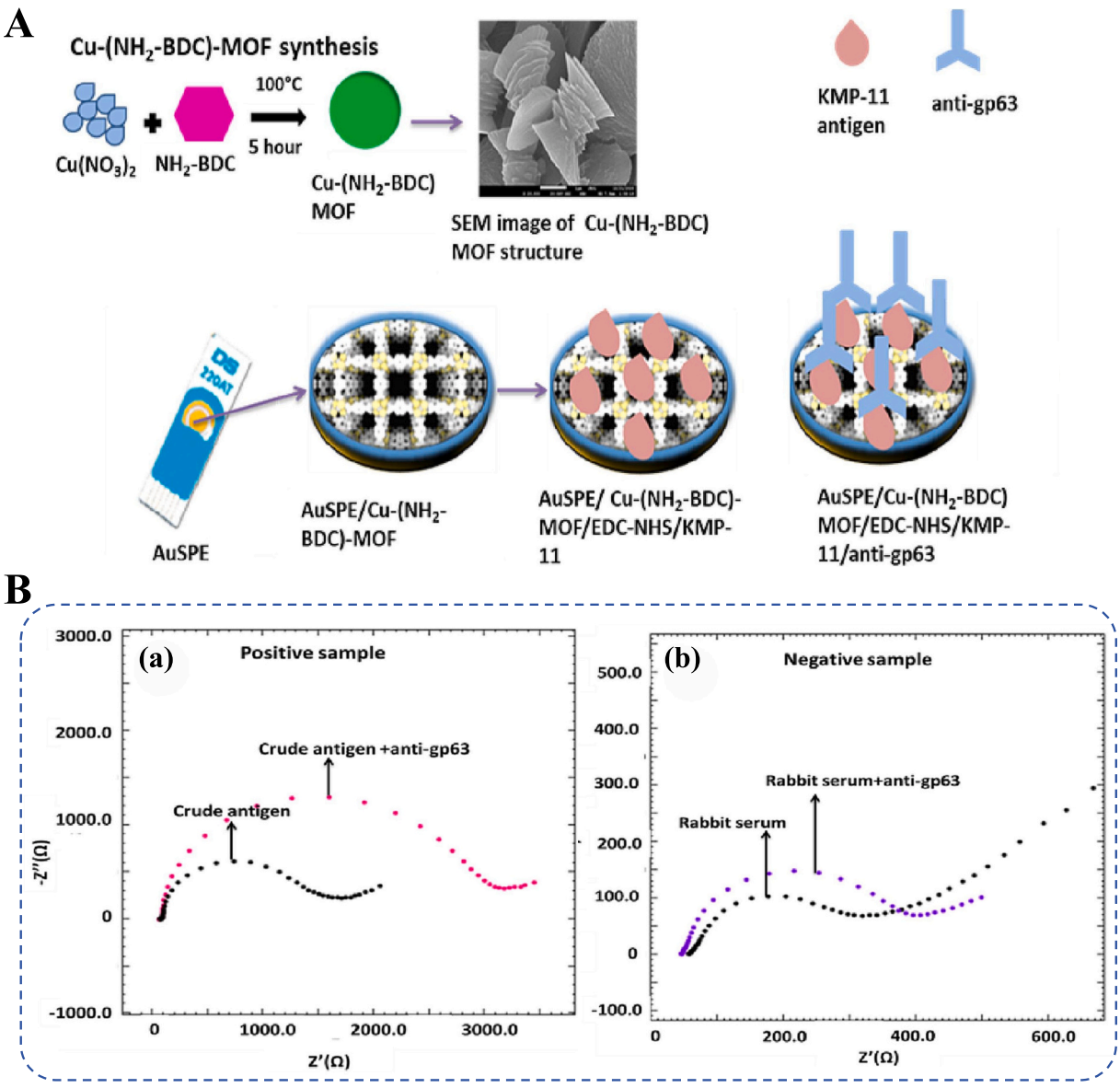

Fig. 17. (A) Schematic representation of synthesis of Cu-(NH_2-BDC) MOF and preparation procedure of *Leishmania* immunosensor. (B) Nyquist diagrams obtained by developed *Leishmania* immunosensor for (a) *Leishmania* parasite crude antigen (positive sample) and (b) rabbit serum (negative sample). Reprinted with permission from Ref. [297].

another study, researchers utilized CV to monitor the antigen-antibody interactions of an electrochemical immunosensor used in diagnosing a *Leishmania* infection [324]. Rispail et al. reported that hydrophilic CdSe/ZnS quantum dots functionalized with 3-mercaptopropionic acid could be internalized by *Fusarium verticillioides*, offering a novel method for use in the rapid and sensitive detection of this plant pathogen [325]. Additionally, Rosamp et al. [326] reported that converting non-luminescent microbes into luminescent forms could endow them with additional functionalities. By integrating Ln-MOFs onto fungal hyphae, they successfully generated luminescent microbes that emitted visible light under UV excitation (i.e., photoluminescence). This technology ultimately found application in the fields of diagnostics and imaging. Compared to diagnostics, MOFs display broader potential for use in the treatment of and anti-infective applications regarding fungal and parasitic infections [327–331].

5.6. Immune diseases

Autoimmune diseases are disorders caused by a malfunction of the immune system, and they are attracting increasing attention from the medical community and general public due to their wide-ranging effects on various physiological systems and potentially far-reaching consequences. Evaluating these diseases primarily involves various inflammatory factors and complement components [332,333]. However, laboratory and clinical applications face numerous challenges. In this context, developing novel, reliable biosensors for use in diagnosing autoimmune diseases is crucial. Fortunately, nanomaterials have emerged as critical candidates for application in fabricating biosensors used in diagnosing these diseases, e.g., Zhao et al. [334] developed a dual-mode PEC and colorimetric sensor for use in the highly sensitive detection of HIgG, based on an Ag_2S/SnO_2 composite material and multifunctional CoOOH nanosheets. In the PEC mode, quantum dots significantly enhanced the PEC activities of the SnO_2 nanofibers and facilitated the effective immobilization of the antibodies. Furthermore, AA could be captured within the pores of Ag_2S/SnO_2, thus enhancing the photocurrent intensity. Additionally, CoOOH, serving as a secondary antibody label, formed a sandwich structure with the electrode. The binding of HigG led to a significant attenuation of the PEC signal. In the

colorimetric mode, CoOOH catalyzed the oxidation of TMB to generate the blue product oxTMB, with varying concentrations of HIgG forming sandwich complexes, causing distinct color changes. Additionally, nanomaterials are commonly employed in immune cell imaging and the enhancement of the accuracy and sensitivity of pathological detection, thus providing robust support for early disease diagnosis and treatment [335–337]. However, the use of MOFs in the field of immune disease diagnosis remains in its nascent stages and requires further research and development. In contrast, the application of MOFs in treating immune-related diseases exhibits broader and more mature prospects. Guo et al. [338] reported an active targeted nanomedicine strategy based on MOFs for use in treating rheumatoid arthritis (RA) by re-educating impaired macrophages. This approach leveraged the proton sponge effects of MOFs to facilitate the rapid escape of small interfering RNA (siRNA) from the endo−/lysosomes, effectively downregulating the expression of inflammation-related cytokines. Furthermore, MOFs display capacities to scavenge free radicals, eliminating a broad spectrum of reactive oxygen and nitrogen species, thus inducing the repolarization of M1 macrophages towards an anti-inflammatory M2 phenotype, further enhancing the therapeutic efficacy against RA in combination with siRNA.

5.7. Other diseases

In addition to the aforementioned diseases, MOFs can also be utilized in diagnosing conditions such as biliary and hematological disorders [337,339], e.g., Chao et al. [340] synthesized a Zr(IV)-based MOF (UiO-66(COOH)$_2$, Zr-MOF: Eu^{3+}), serving as an independent luminescent probe for use in detecting bilirubin in human serum. In this sensor, the red emission of Eu^{3+} was quenched via FRET between bilirubin and its ligands. This sensor exhibited a high sensitivity, rapid response (<1 min), and wide detection range (0–15 μM) and an exceptional selectivity. Building on this, Hou et al. developed a novel fluorescent portable sensor based on a hydrogel for use in detecting neonatal jaundice [341]. Using the UiO-66-NH_2 MOF in an aldimine condensation reaction with 2,3,4-trihydroxybenzaldehyde, they successfully synthesized fluorescent UiO-66-PSM (UP). Subsequently, introducing Fe^{3+} onto the surface of UP led to the formation of UiO-66-PSM-Fe (UPF), where the interaction between Fe^{3+} and UP caused fluorescence quenching. Due to the strong binding affinity between bilirubin and Fe^{3+}, bilirubin could react with UPF, prompting Fe^{3+} release and fluorescence restoration, enabling the highly sensitive detection of free bilirubin in urine (Fig. 18A and B). This approach offers a novel avenue for use in diagnosing neonatal jaundice. Moreover, Lin et al. [342] synthesized a cost-effective MOF-derived binary metal oxide nanomaterial (CoFeNMOF-D) and applied it in the molecular diagnosis of chronic obstructive pulmonary disease (COPD) (Fig. 18C). This study analyzed 202 serum samples, comprising 102 from COPD patients and 100 healthy controls. Each sample contained 75 nL of serum and 1 ng of CoFeNMOF-D. Diagnostic assessments were conducted using various machine learning algorithms, such as support vector machines (SVMs) and neural networks, evaluating the accuracies, specificities, and sensitivities of the models. Four potential

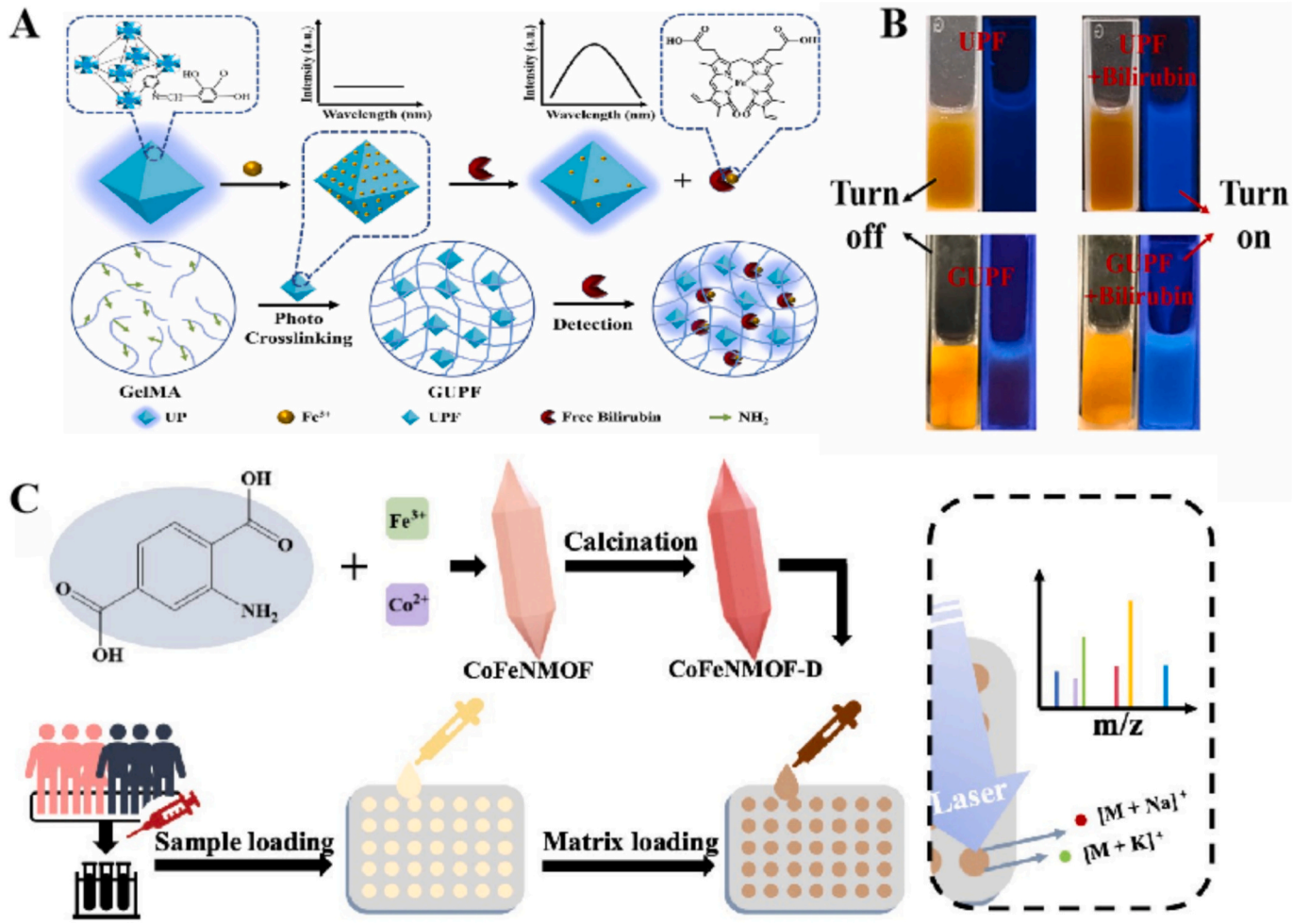

Fig. 18. (A) Fluorescence "turn-on" of GUPF with bilirubin. Reprinted with permission from Ref. [341]. (B) Fluorescence color changes of UPF/GUPF during day light and UV light (365 nm). (C) Synthesis of CoFeNMOF-D and its application in LDI-MS based disease screening. Reprinted with permission from Ref. [342].

COPD biomarkers were identified, demonstrating excellent area-under-the-curve values in the training and validation sets. This research offers an innovative approach to clinical COPD diagnosis. Additionally, Zhang et al. [343] designed and synthesized a fluorescence nanosensor based on MOFs, utilizing Zr(IV) and boronic acid esters as active centers for the simultaneous detection of ROS and protein phosphorylation sites. The dual-photon characteristics of the fluorescence probe effectively reduced background fluorescence, thus enhancing the sensitivity of the imaging of the phosphorus groups. The probe was successfully applied to a pneumonia mouse model, distinguishing pneumonia and healthy mice and providing a novel tool for use in understanding disease pathogenesis.

6. Intelligence assistance

MOFs have emerged as ideal options for use in high-sensitivity sensing materials due to their high surface areas, excellent stabilities, and tunable pore structures, which are suitable for application in detecting gases, liquids, and biomolecules [344]. Integrating MOF-based sensors with machine learning algorithms enables the in-depth analysis and optimization of the collected data, significantly enhancing their detection efficiencies and accuracies. Such an intelligence-assisted detection system displays real-time capacities and convenience in various fields, such as environmental monitoring, food safety, and medical diagnostics, e.g., Huo et al. [345] proposed a flexible, non-contact, multifunctional humidity sensor based on 2D cobalt MOF (Co-MOF) nanosheets. The Co-MOF@PA sensor was developed by coating the Co-MOF surface with a hydrophilic phytic acid (PA) layer. The humidity sensing performance was evaluated by introducing saturated salt solutions to produce different humidity conditions for testing (Fig. 19A). Additionally, the sensor exhibited significant variations in response to different humidity levels, notably reaching a response value as high as 2250 at a relative humidity of 95 %. This indicated the outstanding humidity sensing capacity of the Co-MOF@PA sensor in high- and low-humidity environments. Moreover, minimal changes in current were observed when the sensor was bent at different angles, underscoring its potential advantages in wearable applications. Furthermore, they explored the application of the sensor in fingertip humidity monitoring and the assessment of the moisturizing effects of cosmetics and detection of the surface humidities of fruits (Fig. 19B). The sensor displayed the capacity for non-contact humidity sensing, accurately assessing the moisturizing effects of cosmetics and effectively distinguishing whether an apple was waxed. In another study, Lin et al. developed an integrated paper-based colorimetric sensing system, using in situ encapsulation with ZIF-67 to combine GOx and luminol for use in detecting glucose in saliva [346]. This system utilizes a cascade reaction induced by glucose, where GOx catalyzes the oxidation of glucose to produce gluconic acid and H_2O_2, followed by ZIF-67 catalyzing the oxidation of luminol by H_2O_2, yielding a yellow product. In the presence of purple G&L@ZIF@Paper, the color of the yellow product changes to brown (Fig. 19C), and further validates the selectivity and stability of this sensing system. To enhance the convenience of G & L@ZIF@Paper for use in everyday applications, they embedded it into plastic straws, integrating sample collection and reaction. Users can directly read the R/B of the paper-based chip via the Glucose Sensor smartphone application and calculate the glucose concentration in saliva using this application.

Furthermore, MOF-based sensors can be integrated into smart packaging to monitor the freshness and safety of food in real time, providing feedback via embedded displays or indicator lights [347,348], e.g., Kang et al. combined colorimetric sensing tags with composite film materials to develop smart packaging boxes that not only extend shelf life but also offer real-time monitoring capacities [349]. Microorganisms in food can lead to spoilage, and the Cu^{2+} ions in Cu-MOF within the composite film can replace the natural metal ions utilized by proteins [350], increasing the metal ion concentration for non-toxic sterilization, thus enhancing preservation. Fig. 20A shows the significant antibacterial activities of the SP/Cu-MOF composite film against foodborne pathogens, such as *S. aureus* and *E. coli*, with inhibition zone radii of 9.93 $\pm$ 0.40 and 9.35 $\pm$ 0.33 mm, respectively. As the Cu-MOF content increases, the inhibitory area expands, whereas the pure SP film exhibits minimal antibacterial effects. Additionally, food spoilage releases volatile basic nitrogen (TVB-N), which can be detected as the volatile compounds accumulate at the top of the packaging using an ammonia-sensitive membrane (Fig. 20B). At 4 and 28 °C, the color of shrimp transitions from greenish blue to orange-red, indicating complete spoilage. During this process, the ΔE of the SP0 film remains relatively stable, whereas the color of the Cu-MOF-tagged shrimp visibly changes from the initial blue-green to brown, with a ΔE of >47, indicating the presence of a significant amount of TVB-N in the shrimp, leading to spoilage.

Recently, electronic noses (*E*-noses) based on MOFs emerged as devices that mimic human olfaction, with the capacities to detect and identify gases or volatile compounds, thus becoming a focus of research. An E-nose system typically comprises three modules: a gas sensor array, signal acquisition and preprocessing, and pattern recognition [352]. Via the selection of high-performance sensors to fabricate the sensor array and the preprocessing of the signals, combined with intelligent algorithms, such as principal component analysis, artificial neural networks, and SVMs, the system can effectively identify the types of gases and improve the accuracy of concentration prediction in multicomponent environments [353], e.g., Okur et al. proposed an array sensor comprising thin films coated with different surface-mounted MOFs (SURMOFs) for use in detecting and distinguishing the odors of six volatile plant oils, realizing an accuracy rate of up to 99.97 % [354]. This enabled the development of MOF-based E-noses. Subsequently, they introduced an array comprising six sensors that utilized nanoporous MOF membranes with different chiral and achiral structures, serving as a selective E-nose [355]. The achiral MOF membrane responded similarly to two isomers, whereas the chiral MOF membrane exhibited distinct responses. The stereoselective recognition of five pairs of chiral odor molecules could be realized via machine learning algorithms. Such a chiral MOF E-nose should be a significant tool for use in advanced odor sensing. Additionally, wearable gas sensors and self-powered sensing technologies emerged as crucial intelligent sensors for use in gas monitoring. Recently, Wang et al. [356] developed a self-powered organ-like MXene ammonia sensor, with significant potential for use in wearable devices. The fabricated power supply device could generate a respective short-circuit current and peak open-circuit voltage of 34 μA and up to 810 V. In another study, a wearable sensor was developed to respond via color changes to physiological stimuli, enabling simple visual recognition [351]. The research group loaded various gas-sensitive dyes into porous MOFs and further deposited the composite materials on electrospun nanofiber membranes to realize the specific recognition of various characteristic VOCs and present different color signal tags (Fig. 20C). Subsequently, microfluidic channels consisting of polydimethylsiloxane were combined with different colorimetric components to successfully fabricate a wearable sensor array. This array could be attached to the surfaces of fruits for use in the real-time monitoring of VOCs, effectively assessing the levels of fruit ripeness (Fig. 20D). This innovative approach provides a novel method of monitoring fruit ripeness, further advancing the fields of agriculture and food safety.

7. Commercialization challenges and recommendations

7.1. Commercialization challenges

Despite significant progress in the preparation and biosensing applications of MOF-based nanozymes, overall research is still in the early prototype stage, requiring further efforts to realize commercial production. Several challenges must be addressed in this field:

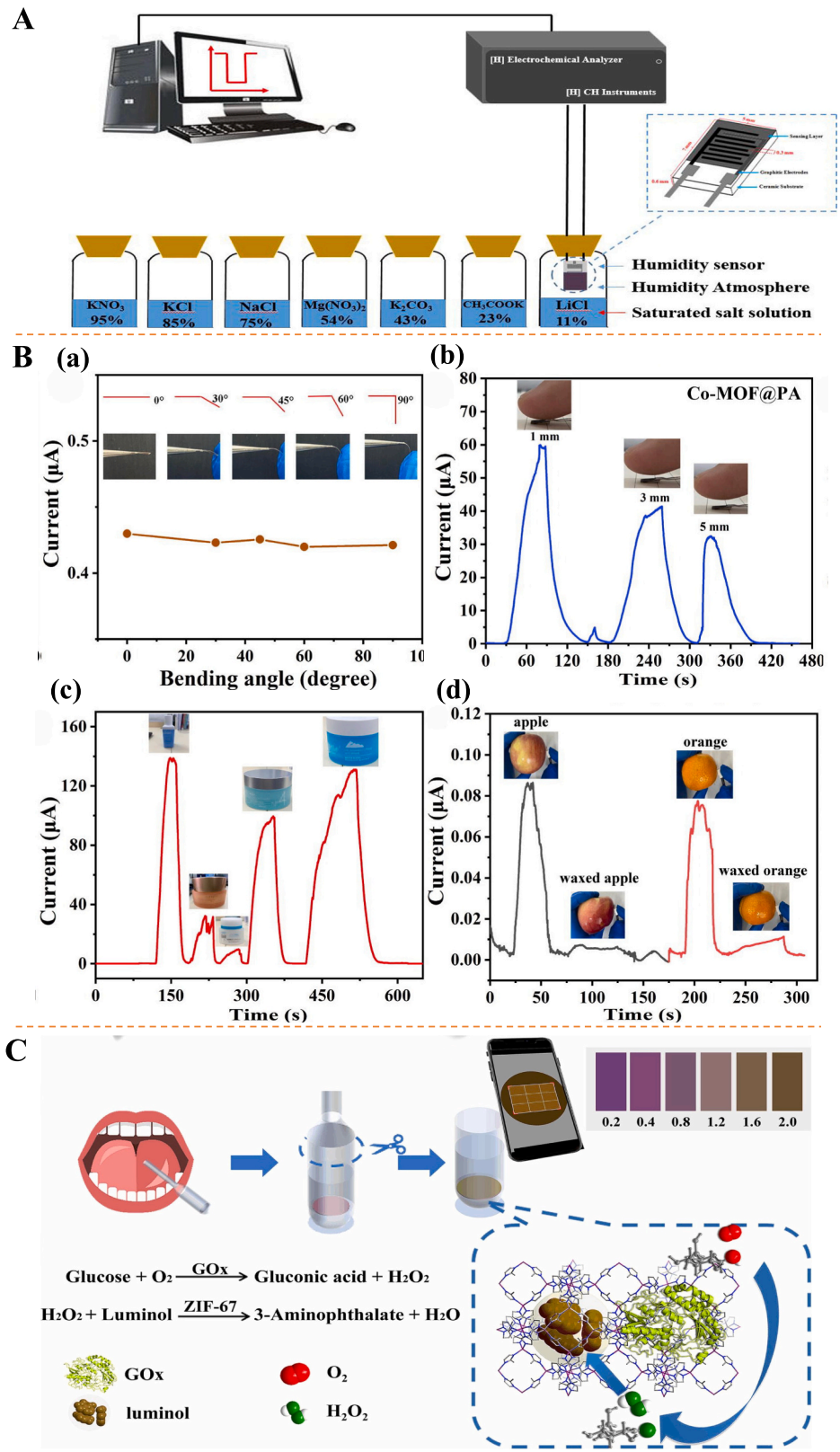

Fig. 19. (A) The schematic diagram of humidity testing process. (B) The stable current value of the flexible 2D Co-MOF@PA sensor at different bending angles (a), the response of the 2D Co-MOF@PA sensor to the moisture on (b) the bare finger with different distances, (c) the surface of the skin coated with different brands of cosmetics and (d) the surface of waxed and unwaxed apples and oranges. Reprinted with permission from Ref. [345]. (C) The principle of detecting glucose in saliva by G&L@ZIF paper. Reprinted with permission from Ref. [346].

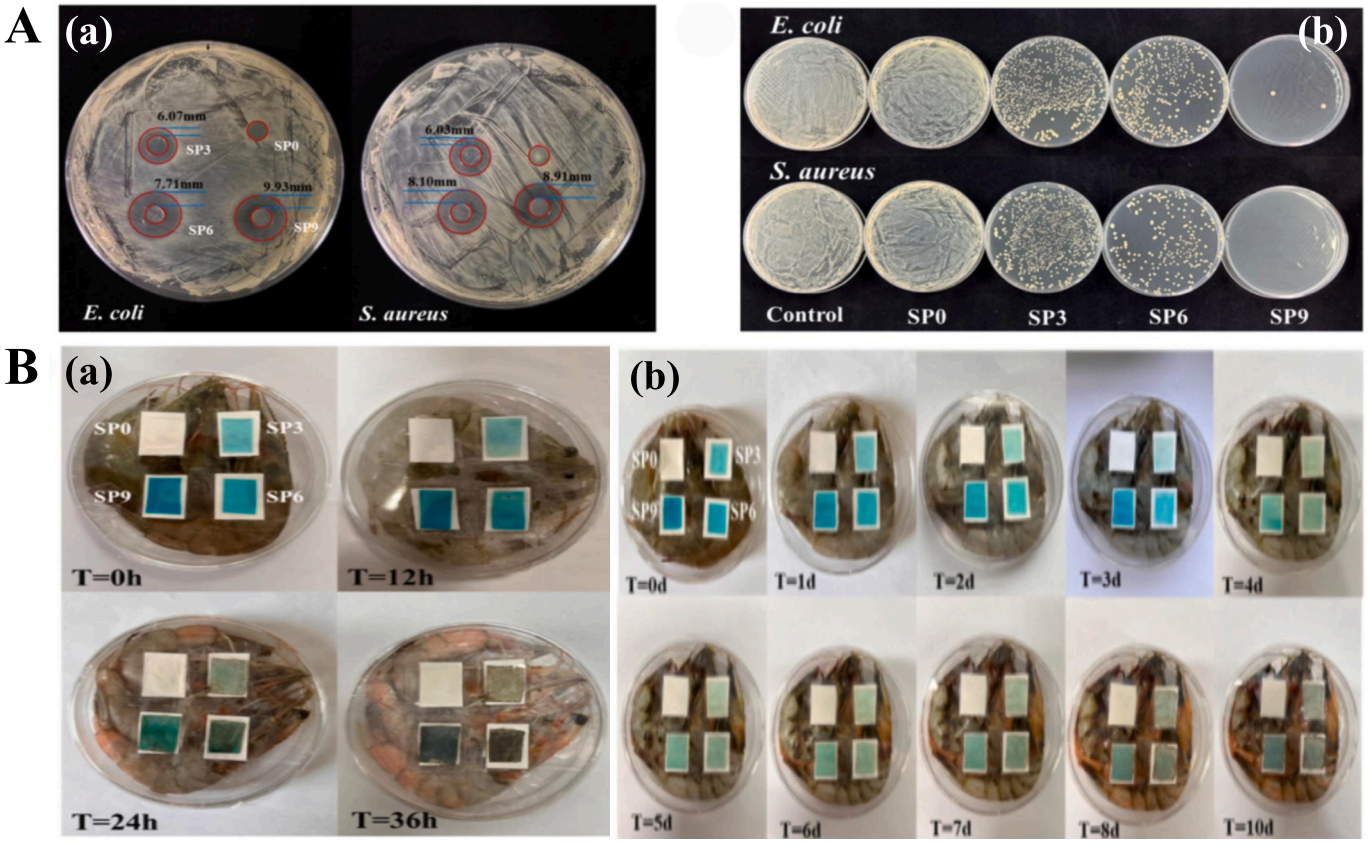

(caption on next page)

Fig. 20. (A) Antimicrobial activities (a); photographs of the *E. coli* and *S. aureus* inhibition rate (b). (B) Smart labels made of SP/Cu-MOF composite films were utilized to track the freshness of shrimp stored at two different temperatures, 28 °C and 4 °C. (a) real-time picture at 28 °C, (b) real-time picture at 4 °C. Reprinted with permission from Ref. [349]. (C) Photograph of 10 dye/MOF/PAN and Pd^{2+}/dye/MOF/PAN NFM (a); Preparation of the colorimetric elements using laser etching technology (b); Photograph of the sensor based on dye/MOF/PAN and Pd^{2+}/dye/MOF/PAN NFM (c). (D) Sensor arrays for detecting fruit ripening; (a) Schematic illustration of a wearable colorimetric sensor array device and the data acquisition methods; (b) RGB difference values of the sensor for detecting VOCs emitted by bananas during storage. Reprinted with permission from Ref. [351].

(i) While various methods of preparing MOF nanoshells are reported, significant challenges remain in precisely controlling their morphologies, sizes, shell thicknesses, compositions, spatial distributions, and sizes of the internal cores. Therefore, developing a viable universal strategy for use in the controlled synthesis and assembly of MOF nanoshell structures according to the application requirements is urgent and crucial.

(ii) Standardized large-scale production remains impossible. Currently, most MOF nanomaterials are still in the laboratory research stage. Due to the lack of uniform standards and specifications, the comparability between different research results is poor, thus limiting market acceptance. Furthermore, controlling the morphologies and structures of MOFs is often challenging when scaling up production. Therefore, developing novel technologies with simplified preparation processes and low costs to realize the large-scale production of MOF-based nanozymes remains a pressing challenge.

(iii) The relationships between the composition of a MOF and its biomedical properties remain unclear, particularly in terms of synergistic effects between different components or structures. Numerous studies attribute the diagnostic and therapeutic effects against certain diseases to synergy, yet the specific mechanisms are not fully elucidated. Furthermore, animal model studies currently lack clear indicators to support the application of existing MOF-based sensors in disease monitoring in the human body.

(iv) The category of MOFs suitable for use in diagnosing internal diseases is very limited. Several MOF-based nanozymes containing heavy metals lack biocompatibility, rendering them ineffective for metabolism in the human body. This leads to their long-term accumulation and potential toxicity, rendering them unsuitable for use in monitoring internal diseases. Consequently, the variety of MOFs that can be used in diagnosis is restricted.

(v) Inadequate targeting specificities are challenges in the application of MOFs. The high surface areas and porosities of MOFs render them prone to nonspecific adsorption. While surface modifications can enhance the targeting specificities of MOFs, current functionalization methods require further optimization to increase the affinities towards target molecules. Moreover, various interfering substances in the monitoring environment limit the capacities of MOFs to effectively recognize and bind to target molecules in complex biological media.

(vi) Limited clinical research regarding MOF-based nanozymes has been reported. Currently, most studies regarding the application of MOF-based nanozymes in disease diagnosis predominantly focus on basic experiments, without sufficient preclinical and clinical trial data to support practical implementation. The challenge of translating fundamental research findings into clinical applications remains significant.

(vii) Low market acceptance poses a barrier. Currently, conventional methods of disease diagnosis and monitoring in clinical settings are relatively well-established. Consequently, the integration of MOF-based nanozymes into current technologies is met with low acceptance levels from clinical practitioners and healthcare institutions, serving as a significant obstacle to their widespread adoption.

7.2. Recommendations

(i) Establish a standardized process for use in preparing MOF-based nanozymes to simplify the production steps, reduce costs, and increase their yields. Additionally, develop innovative synthetic strategies to precisely control key parameters, such as the morphologies, sizes, wall thicknesses, porosities, and compositions of MOF-based nanozymes based on the application requirements.

(ii) Utilize advanced characterization techniques to systematically evaluate the structures, compositions, and other key parameters of MOF nanomaterials. In addition to conventional characterization methods, employ cutting-edge in situ techniques to monitor key indicators in real time during processing. This shall aid in a deeper understanding of the relationships between their structures, compositions, and performances, elucidating the mechanisms of action and reliabilities of MOF-based nanozymes in disease diagnosis.

(iii) Fabricate novel sensors for use in biomedical applications. Develop sensors with superior performances for use in the underexplored areas of disease diagnosis, such as hematological disorders, by leveraging MOF-based nanozymes with diverse structures and compositions. Furthermore, integrate chemotherapy drugs, immunotherapies, gene therapies, and biologics with MOF-based nanozymes to realize synergistic effects between diagnosis and treatment, enhancing the overall therapeutic outcomes.

(iv) Address the biocompatibilities of MOF-based nanozymes. Develop MOF materials with enhanced biocompatibilities by prioritizing naturally occurring or biodegradable metals and organic ligands. Additionally, employ surface modification techniques to reduce material toxicity and improve its compatibilities with biological environments, ensuring safety in biomedical applications.

(v) Select more stable combinations of metals and organic ligands in preparing MOFs or enhance their structural stabilities via cross-linking, encapsulation, and other methods to ensure their prolonged use within biological systems.

(vi) Conduct thorough validation in animal models and clinical trials to confirm the safeties and efficacies of MOF-based nanozymes. Establish standardized operational procedures and data analysis methods, systematically comparing the experimental results with those of established clinical techniques to facilitate the translation of MOF-based nanozymes into clinical practice.

8. Conclusion

The present review article explores the emerging field of MOF-based nanozymes in analytical and sensing applications, particularly placed on its utilization in the domain of clinical medical detection. MOF-based nanozymes exhibit catalytic properties that offer synthetic utility and potential as prebiotic catalysts, driving chemical transformations. These properties also enhance sensing platforms by serving as versatile amplifying transducing labels for detecting various target analytes. The diverse compositions, porosity, size and shape-dependent functionality, chemical stability, and selectivity of nanozymes make them appealing components for analytical tools. Our recent research efforts have focused on utilizing MOF-based nanozymes as amplifying labels in sensing platforms, with applications in clinical diagnostics. Some

nanozyme materials, such as Prussian Blue and superparamagnetic iron oxide nanoparticles have already obtained approval from the US Food and Drug Administration (FDA) for therapeutic purposes, indicating the potential for these MOF-based nanozymes to be used for in vivo sensing applications. However, how to mitigate toxicity of MOF-based nanozyme for future biomedical applications are still a vast challenge. Before their clinical implementation, it is imperative to thoroughly assess the biocompatibility and toxicity of MOF-based nanozyme. Such as establishing the standardized toxicity testing protocols, determining suitable animal models for preclinical investigations, developing cost-effective and scalable techniques for MOF-based green synthesis and functionalization, and evaluating their long-term biocompatibility and stability in vivo.

Declaration of competing interest

The authors declare that they have no known competing financial interests or personal relationships that could have appeared to influence the work reported in this paper.

Acknowledgements

The authors appreciate financial supports from the Shenyang Science and Technology Talent Special Project (RC230022), Basic Research Projects of Liaoning Provincial Department of Education (LJ222410164024), Natural Science Foundation of Liaoning Province (2023-MSLH-288), Science Research Foundation of Education Department for Liaoning Province (LJKMZ20221790).

Data availability

Data will be made available on request.

References

[1] K. Beyzavi, S. Hampton, P. Kwasowski, S. Fickling, V. Marks, R. Clift, Comparison of horseradish peroxidase and alkaline phosphatase-labelled antibodies in enzyme immunoassays, Ann. Clin. Biochem. 24 (1987) 145–152, https://doi.org/10.1177/000456328702400204.

[2] F.W. Krainer, A. Glieder, An updated view on horseradish peroxidases: recombinant production and biotechnological applications, Appl. Microbiol. Biotechnol. 99 (2015) 1611–1625, https://doi.org/10.1007/s00253-014-6346-7.

[3] S.U. Pathan, A. Kharwar, M.A. Ibrahim, S.B. Singh, P. Bajaj, Enzymes as indispensable markers in disease diagnosis, Bioanalysis 16 (2024) 485–497, https://doi.org/10.4155/bio-2023-0207.

[4] N. Stasyuk, O. Smutok, O. Demkiv, T. Prokopiv, G. Gayda, M. Nisnevitch, M. Gonchar, Synthesis, catalytic properties and application in biosensorics of nanozymes and electronanocatalysts: a review, Sensors 20 (2020) 4509, https://doi.org/10.3390/s20164509.

[5] X. Cai, L. Jiao, H. Yan, Y. Wu, W. Gu, D. Du, Y. Lin, C. Zhu, Nanozyme-involved biomimetic cascade catalysis for biomedical applications, Mater. Today 44 (2021) 211–228, https://doi.org/10.1016/j.mattod.2020.12.005.

[6] P. Giri, A.D. Pagar, M.D. Patil, H. Yun, Chemical modification of enzymes to improve biocatalytic performance, Biotechnol. Adv. 53 (2021) 107868, https://doi.org/10.1016/j.biotechadv.2021.107868.

[7] L. Ma, F. Jiang, X. Fan, L. Wang, C. He, M. Zhou, S. Li, H. Luo, C. Cheng, L. Qiu, Metal–organic-framework-engineered enzyme-mimetic catalysts, Adv. Mater. 32 (2020) 2003065, https://doi.org/10.1002/adma.202003065.

[8] D. Jiang, D. Ni, Z.T. Rosenkrans, P. Huang, X. Yan, W. Cai, Nanozyme: new horizons for responsive biomedical applications, Chem. Soc. Rev. 48 (2019) 3683–3704, https://doi.org/10.1039/C8CS00718G.

[9] L. Gao, J. Zhuang, L. Nie, J. Zhang, Y. Zhang, N. Gu, T. Wang, J. Feng, D. Yang, S. Perrett, X. Yan, Intrinsic peroxidase-like activity of ferromagnetic nanoparticles, Nat. Nanotechnol. 2 (2007) 577–583, https://doi.org/10.1038/nnano.2007.260.

[10] H. Dong, Y. Fan, W. Zhang, N. Gu, Y. Zhang, Catalytic mechanisms of nanozymes and their applications in biomedicine, Bioconjug. Chem. 30 (2019) 1273–1296, https://doi.org/10.1021/acs.bioconjchem.9b00171.

[11] Y. Sun, C. Zhao, N. Gao, J. Ren, X. Qu, Stereoselective nanozyme based on ceria nanoparticles engineered with amino acids, Chem. Eur. J. 23 (2017) 18146–18150, https://doi.org/10.1002/chem.201704579.

[12] Y. Zhu, Z. Wang, R. Zhao, Y. Zhou, L. Feng, S. Gai, P. Yang, Pt decorated $Ti_3C_2T_x$ MXene with NIR-II light amplified Nanozyme catalytic activity for efficient Phototheranostics, ACS Nano 16 (2022) 3105–3118, https://doi.org/10.1021/acsnano.1c10732.

[13] Y. Du, X. Jia, L. Zhong, Y. Jiao, Z. Zhang, Z. Wang, Y. Feng, M. Bilal, J. Cui, S. Jia, Metal-organic frameworks with different dimensionalities: An ideal host platform for enzyme@MOF composites, Coord. Chem. Rev. 454 (2022) 214327, https://doi.org/10.1016/j.ccr.2021.214327.

[14] J.E. Cun, X. Fan, Q.Q. Pan, W.X. Gao, K. Luo, B. He, Y.J. Pu, Copper-based metal-organic frameworks for biomedical applications, Adv. Colloid Interf. Sci. 305 (2022) 102686, https://doi.org/10.1016/j.cis.2022.102686.

[15] I. Chandio, Y. Ai, L. Wu, Q. Liang, Recent progress in MOFs-based nanozymes for biosensing, Nano Res. 17 (2024) 39–64, https://doi.org/10.1007/s12274-023-5770-3.

[16] J. Yan, Y. Zhao, M. Du, C. Cui, Z. Bai, Y. Liu, L. Sun, D. Qin, J. Zhou, X. Wu, B. Li, Stimuli-responsive new horizons for biomedical applications: metal-organic framework-based nanozymes, Small Struct. (2024) 2400029, https://doi.org/10.1002/sstr.202400029.

[17] X. Shen, W. Liu, X. Gao, Z. Lu, X. Wu, X. Gao, Mechanisms of oxidase and superoxide dismutation-like activities of gold, silver, platinum, and palladium, and their alloys: ag eneral way to the activation of molecular oxygen, J. Am. Chem. Soc. 137 (2015) 15882–15891, https://doi.org/10.1021/jacs.5b10346.

[18] Z. Xu, L.L. Long, Y.Q. Chen, M.L. Chen, Y.H. Cheng, A nanozyme-linked immunosorbent assay based on metal-organic frameworks (MOFs) for sensitive detection of aflatoxin B1, Food Chem. 338 (2021) 128039, https://doi.org/10.1016/j.foodchem.2020.128039.

[19] D. Song, X. Jiang, Y. Li, X. Lu, S. Luan, Y. Wang, Y. Li, F. Gao, Metal-organic frameworks-derived MnO2/Mn3O4 microcuboids with hierarchically ordered nanosheets and Ti3C2 MXene/au NPs composites for electrochemical pesticide detection, J. Hazard. Mater. 373 (2019) 367–376, https://doi.org/10.1016/j.jhazmat.2019.03.083.

[20] W.H. Wang, S. Xiao, M.L. Zeng, H.Z. Xie, N. Gan, Dual-mode colorimetric-electrochemical biosensor for vibrio parahaemolyticus detection based on CuO2 nanodot-encapsulated metal-organic framework nanozymes, Sens. Actuators B. Chem. 387 (2023) 133835, https://doi.org/10.1016/j.snb.2023.133835.

[21] C.Y. Wang, C.C. Wang, X.W. Zhang, X.Y. Ren, B. Yu, P. Wang, Z.X. Zhao, H. Fu, A new Eu-MOF for ratiometrically fluorescent detection toward quinolone antibiotics and selective detection toward tetracycline antibiotics, Chin. Chem. Lett. 33 (2022) 1353–1357, https://doi.org/10.1016/j.cclet.2021.08.095.

[22] H. Yuan, S. Yi, L. Jia, S. Chen, T. Guo, T. Meng, Biomimetic multienzyme nanocomplex for efficient cascade reactions, Chem. Eng. J. 454 (2023) 140276, https://doi.org/10.1016/j.cej.2022.140276.

[23] K. Wang, X. Meng, X. Yan, K. Fan, Nanozyme-based point-of-care testing: revolutionizing environmental pollutant detection with high efficiency and low cost, Nano Today 54 (2024) 102145, https://doi.org/10.1016/j.nantod.2023.102145.

[24] Y. Zhang, G. Wei, W. Liu, T. Li, Y. Wang, M. Zhou, Y. Liu, X. Wang, H. Wei, Nanozymes for nanohealthcare, Nat. Rev. Methods Primers 4 (2024) 36, https://doi.org/10.1038/s43586-024-00315-5.

[25] S. Qu, Z. Li, Q. Jia, Detection of purine metabolite uric acid with picolinic-acid-functionalized metal-organic frameworks, ACS Appl. Mater. Interfaces 11 (2019) 34196–34202, https://doi.org/10.1021/acsami.9b07442.

[26] Z. Wang, Y. Jiao, Q. Ding, Y. Song, Q. Ma, H. Ren, K. Lu, S. Jia, J. Cui, A bioinspired fluorescent probe based on metal-organic frameworks to selectively enrich and detect amyloid-β peptide, Chem. Eng. J. 470 (2023) 144124, https://doi.org/10.1016/j.cej.2023.144124.

[27] C. Rejeeth, A. Sharma, R.S. Kumar, A.I. Almansour, N. Arumugam, N. B. Varukattu, S. Afewerki, Bimetallic metal-organic framework nanoparticles for monitoring metabolic changes in cardiovascular disorders, ACS Appl. Nano Mater. 6 (2023) 8071–8081, https://doi.org/10.1021/acsanm.3c01512.

[28] J. Du, F. Shi, K. Wang, Q. Han, Y. Shi, W. Zhang, Y. Gao, B. Dong, L. Wang, L. Xu, Metal-organic framework-based biosensing platforms for diagnosis of bacteria-induced infectious diseases, Trends Anal. Chem. 175 (2024) 117707, https://doi.org/10.1016/j.trac.2024.117707.

[29] X. Liu, Y. Zhang, N. Li, Z. Yang, S. Yang, J. Li, J. Chen, D. Huo, C. Hou, Cu-MOF/aptamer/magnetic bead sensor for detection of breast cancer biomarkers HER_2 and ER, ACS Appl. Nano Mater. 7 (2024) 9768–9776, https://doi.org/10.1021/acsanm.4c01671.

[30] X. Liu, X. Li, W. Li, L. Liu, H. Ren, H. Jing, L. Zhang, J. Yin, L. Fan, Eu(III) encapsulation strategy to construct intelligent ratiometric luminescent sensor for efficient detection of phenylglyoxylic acid biomarker in bodily fluids, Microchem. J. 207 (2024) 112127, https://doi.org/10.1016/j.microc.2024.112127.

[31] W. Li, X. Liu, N. Lei, L. Liu, X. Li, H. Ren, J. Yin, L. Zhang, T. Yu, L. Fan, Zinc(II) organic framework based bifunctional biomarker sensor for efficient detection of urinary 5-Hydroxyindoleacetic acid and serum 3-Nitrotyrosine, Spectrochimica Acta part a, Spectrochim. Acta A 329 (2025) 125610, https://doi.org/10.1016/j.saa.2024.125610.

[32] R. Wen, C. Zhou, J. Tian, J. Lu, Confined catalysis of MOF-818 nanozyme and colorimetric aptasensing for cardiac troponin I, Talanta 252 (2023) 123830, https://doi.org/10.1016/j.talanta.2022.123830.

[33] H. Lim, H. Kwon, H. Kang, J.E. Jang, H.J. Kwon, Semiconducting MOFs on ultraviolet laser-induced graphene with a hierarchical pore architecture for NO_2 monitoring, Nat. Commun. 14 (2023) 3114, https://doi.org/10.1038/s41467-023-38918-3.

[34] Z. Han, K. Wang, H. Min, J. Xu, W. Shi, P. Cheng, Bifunctionalized metal-organic frameworks for pore-size-dependent enantioselective sensing, Angew. Chem. Int. Ed. 61 (2022) e202204066, https://doi.org/10.1002/anie.202204066.

[35] T. Feng, Q. Hao, B. Sun, D. Wang, Metal-covalent organic frameworks linked by Fe-iminopyridine for single-atom peroxidase-mimetic nanoenzymes, J. Phys. Chem. C 127 (2023) 3228–3234, https://doi.org/10.1021/acs.jpcc.2c07887.

[36] T. Jin, Y. Li, W. Jing, Y. Li, L. Fan, X. Li, Cobalt-based metal organic frameworks: a highly active oxidase-mimicking nanozyme for fluorescence "turn-on" assays of biothiol, Chem. Commun. 56 (2020) 659–662, https://doi.org/10.1039/c9cc06840f.
[37] D. Feng, Z. Gu, J. Li, H. Jiang, Z. Wei, H. Zhou, Zirconium-metalloporphyrin PCN-222: mesoporous metal-organic frameworks with ultrahigh stability as biomimetic catalysts, Angew. Chem. Int. Ed. 51 (2012) 10307–10310, https://doi.org/10.1002/anie.201204475.
[38] Y. Wang, M. Zhao, J. Ping, B. Chen, X. Cao, Y. Huang, C. Tan, Q. Ma, S. Wu, Y. Yu, Q. Lu, J. Chen, W. Zhao, Y. Ying, H. Zhang, Bioinspired design of ultrathin 2D bimetallic metal-organic-framework nanosheets used as biomimetic enzymes, Adv. Mater. 28 (2016) 4149–4155, https://doi.org/10.1002/adma.201600108.
[39] J. Wang, Y. Zhou, M. Zeng, Y. Zhao, X. Zuo, F. Meng, F. Lv, Y. Lu, Zr(IV)-based metal-organic framework nanocomposites with enhanced peroxidase-like activity as a colorimetric sensing platform for sensitive detection of hydrogen peroxide and phenol, Environ. Res. 203 (2022) 111818, https://doi.org/10.1016/j.envres.2021.111818.
[40] P. Ling, J. Lei, H. Ju, Nanoscaled porphyrinic metal-organic frameworks for electrochemical detection of telomerase activity via telomerase triggered conformation switch, Anal. Chem. 88 (2016) 10680–10686, https://doi.org/10.1021/acs.analchem.6b03131.
[41] K.M.D. Sisican, K.A.S. Usman, C.J.O. Bacal, Y.D.G. Edañol, M.T. Conato, Benzoic acid modulation of MIL-88B(Fe) nanocrystals toward tunable synthesis of MOF-based Fenton-like degradation catalysts, Cryst. Growth Des. 23 (2023) 8509–8517, https://doi.org/10.1021/acs.cgd.3c00266.
[42] H.E. Ahmed, M.K. Albolkany, M.E. El-Khouly, A.A. El-Moneim, Tailoring MIL-100 (Fe)-derived catalyst for controlled carbon dioxide conversion and product selectivity, RSC Adv. 14 (2024) 13946–13956, https://doi.org/10.1039/D4RA01772B.
[43] S. Ghosh, P. Roy, N. Karmodak, E.D. Jemmis, G. Mugesh, Inside back cover: nanoisozymes: crystal-facet-dependent enzyme-mimetic activity of V_2O_5 nanomaterials, Angew. Chem. Int. Ed. 57 (2018) 4803, https://doi.org/10.1002/anie.201802324.
[44] P. Ni, H. Dai, Y. Wang, Y. Sun, Y. Shi, J. Hu, Z. Li, Visual detection of melamine based on the peroxidase-like activity enhancement of bare gold nanoparticles, Biosens. Bioelectron. 60 (2014) 286–291, https://doi.org/10.1016/j.bios.2014.04.029.
[45] Z. Xu, A. Qu, W. Wang, M. Lu, B. Shi, C. Chen, C. Hao, L. Xu, M. Sun, C. Xu, H. Kuang, Facet-dependent biodegradable Mn_3O_4 nanoparticles for ameliorating parkinson's disease, Adv. Healthc. Mater. 10 (2021) 2101316, https://doi.org/10.1002/adhm.202101316.
[46] N. Singh, M.A. Savanur, S. Srivastava, P. D'Silva, G. Mugesh, A redox modulatory Mn_3O_4 nanozyme with multi-enzyme activity provides efficient cytoprotection to human cells in a Parkinson's disease model, Angew. Chem. Int. Ed. 129 (2017) 14455–14459, https://doi.org/10.1002/ange.201708573.
[47] N. Logan, J. Lou Franco, C. Elliott, C. Cao, Catalytic gold nanostars for SERS-based detection of mercury ions (Hg^{2+}) with inverse sensitivity, Environ. Sci. Nano 8 (2021) 2718–2730, https://doi.org/10.1039/D1EN00548K.
[48] L. Huang, W. Zhang, K. Chen, W. Zhu, X. Liu, R. Wang, X. Zhang, N. Hu, Y. Suo, J. Wang, Facet-selective response of trigger molecule to CeO_2 {110} for up-regulating oxidase-like activity, Chem. Eng. J. 330 (2017) 746–752, https://doi.org/10.1016/j.cej.2017.08.026.
[49] Y. Huang, J. Ren, X. Qu, Nanozymes: classification, catalytic mechanisms, activity regulation, and applications, Chem. Rev. 119 (2019) 4357–4412, https://doi.org/10.1021/acs.chemrev.8b00672.
[50] P. Yang, J. Tao, F. Chen, Y. Chen, J. He, K. Shen, P. Zhao, Y. Li, Multienzyme-mimic ultrafine alloyed nanoparticles in metal organic frameworks for enhanced chemodynamic therapy, Small 17 (2021) 2005865, https://doi.org/10.1002/smll.202005865.
[51] L. Cui, X. Zhao, J. Zhang, Z. Zhou, D. Lin, Y. Qin, Aluminum-decorated MIL-100 (Fe) nanozyme for the detection of glutathione, ACS Appl. Nano Mater. 7 (2024) 4764–4771, https://doi.org/10.1021/acsanm.3c05262.
[52] N. Zhu, C. Liu, R. Liu, X. Niu, D. Xiong, K. Wang, D. Yin, Z. Zhang, Biomimic nanozymes with tunable peroxidase-like activity based on the confinement effect of metal-organic frameworks (MOFs) for biosensing, Anal. Chem. 94 (2022) 4821–4830, https://doi.org/10.1021/acs.analchem.2c00058.
[53] K. Fan, H. Wang, J. Xi, Q. Liu, X. Meng, D. Duan, L. Gao, X. Yan, Optimization of Fe_3O_4 nanozyme activity via single amino acid modification mimicking an enzyme active site, Chem. Commun. 53 (2017) 424–427, https://doi.org/10.1039/C6CC08542C.
[54] D. Yu, M. Ma, Z. Liu, Z. Pi, X. Du, J. Ren, X. Qu, MOF-encapsulated nanozyme enhanced siRNA combo: control neural stem cell differentiation and ameliorate cognitive impairments in Alzheimer's disease model, Biomaterials 255 (2020) 120160, https://doi.org/10.1016/j.biomaterials.2020.120160.
[55] S. Maddheshiya, S. Nara, Recent trends in composite nanozymes and their pro-oxidative role in therapeutics, Front. Bioeng. Biotechnol. 10 (2022) 880214, https://doi.org/10.3389/fbioe.2022.880214.
[56] X. Xu, P. Luo, H. Yang, S. Pan, H. Liu, X. Hu, Regulating the enzymatic activities of metal-ATP nanoparticles by metal doping and their application for H_2O_2 detection, Sensors Actuators B Chem. 335 (2021) 129671, https://doi.org/10.1016/j.snb.2021.129671.
[57] M. Li, J. Chen, W. Wu, Y. Fang, S. Dong, Oxidase-like MOF-818 nanozyme with high specificity for catalysis of catechol oxidation, J. Am. Chem. Soc. 142 (2020) 15569–15574, https://doi.org/10.1021/jacs.0c07273.
[58] Y. Liu, Y. Cheng, H. Zhang, M. Zhou, Y. Yu, S. Lin, B. Jiang, X. Zhao, L. Miao, C. W. Wei, Q. Liu, Y.W. Lin, Y. Du, C.J. Butch, H. Wei, Integrated cascade nanozyme catalyzes in vivo ROS scavenging for anti-inflammatory therapy, Sci. Adv. 6 (2020) eabb2695, https://doi.org/10.1126/sciadv.abb2695.
[59] C. Song, H. Liu, L. Zhang, J. Wang, C. Zhao, Q. Xu, C. Yao, FeS nanoparticles embedded in 2D carbon nanosheets as novel nanozymes with peroxidase-like activity for colorimetric and fluorescence assay of H_2O_2 and antioxidant capacity, Sensors Actuators B Chem. 353 (2022) 131131, https://doi.org/10.1016/j.snb.2021.131131.
[60] J. Zhang, J. Liu, Light-activated nanozymes: catalytic mechanisms and applications, Nanoscale 12 (2020) 2914–2923, https://doi.org/10.1039/C9NR10822J.
[61] Z. Chen, J. Shan, Q. Niu, H. Chen, W. Zhang, D. Cao, X. Wang, pH-responsive double-enzyme active metal-organic framework for promoting the healing of infected wounds, J. Colloid Interface Sci. 657 (2024) 250–262, https://doi.org/10.1016/j.jcis.2023.11.143.
[62] X. Liu, Z. Yan, Y. Zhang, Z. Liu, Y. Sun, J. Ren, X. Qu, Two-dimensional metal-organic framework/enzyme hybrid nanocatalyst as a benign and self-activated aascade reagent for in vivo wound healing, ACS Nano 13 (2019) 5222–5230, https://doi.org/10.1021/acsnano.8b09501.
[63] R. Cao Milán, S. Gopalakrishnan, L.D. He, R. Huang, L.S. Wang, L. Castellanos, D. C. Luther, R.F. Landis, J.M.V. Makabenta, C.H. Li, X. Zhang, F. Scaletti, R. W. Vachet, V.M. Rotello, Thermally gated bio-orthogonal nanozymes with supramolecularly confined porphyrin catalysts for antimicrobial uses, Chem 6 (2020) 1113–1124, https://doi.org/10.1016/j.chempr.2020.01.015.
[64] L. Luo, L. Huang, X. Liu, W. Zhang, X. Yao, L. Dou, X. Zhang, Y. Nian, J. Sun, J. Wang, Mixed-valence Ce-BPyDC metal-organic framework with dual enzyme-like activities for colorimetric biosensing, Inorg. Chem. 58 (2019) 11382–11388, https://doi.org/10.1021/acs.inorgchem.9b00661.
[65] J. Qiao, C. Cheng, D. Li, L. Qi, Thermo-responsive polymer-modified metal-organic frameworks as soft-rigid enzyme-reactors for enhancement of enzymolysis efficiency using a controllable embedding protocol, J. Mater. Chem. B 11 (2023) 6428–6434, https://doi.org/10.1039/d3tb00844d.
[66] X. Zhang, C. Liu, J. Li, R. Chu, Y. Lyu, Z. Lan, Dual source-powered multifunctional Pt/FePc@Mn-MOF spindle-like Janus nanomotors for active CT imaging-guided synergistic photothermal/chemodynamic therapy, J. Colloid Interface Sci. 657 (2024) 799–810, https://doi.org/10.1016/j.jcis.2023.12.018.
[67] C. Gu, Y. She, X.C. Chen, B.Y. Zhou, Y.X. Zhu, X.Q. Ding, P. Tan, X.Q. Liu, L. B. Sun, Modulating the activity of enzyme in metal-organic frameworks using the photothermal effect of Ti_3C_2 nanosheets, ACS Appl. Mater. Interfaces 14 (2022) 30090–30098, https://doi.org/10.1021/acsami.2c06375.
[68] W. Guo, Y. Wang, K. Zhang, X. Dai, Z. Qiao, Z. Liu, B. Yu, N. Zhao, F.J. Xu, Near-infrared light-propelled MOF@au nanomotors for enhanced penetration and sonodynamic therapy of bacterial biofilms, Chem. Mater. 35 (2023) 6853–6864, https://doi.org/10.1021/acs.chemmater.3c01140.
[69] J. Zhao, J. Gong, J. Wei, Q. Yang, G. Li, Y. Tong, W. He, Metal organic framework loaded fluorescent nitrogen-doped carbon nanozyme with light regulating redox ability for detection of ferric ion and glutathione, J. Colloid Interface Sci. 618 (2022) 11–21, https://doi.org/10.1016/j.jcis.2022.03.028.
[70] Y. Liu, M. Zhou, W. Cao, X. Wang, Q. Wang, S. Li, H. Wei, Light-responsive metal-organic framework as an oxidase mimic for cellular glutathione detection, Anal. Chem. 91 (2019) 8170–8175, https://doi.org/10.1021/acs.analchem.9b00512.
[71] M. Furuhashi, New insights into purine metabolism in metabolic diseases: role of xanthine oxidoreductase activity, Am. J. Phys. 319 (2020) E827–E834, https://doi.org/10.1152/ajpendo.00378.2020.
[72] E. Verdin, NAD+ in aging, metabolism, and neurodegeneration, Science 350 (2015) 1208–1213, https://doi.org/10.1126/science.aac4854.
[73] M. Sha, L. Rao, W. Xu, Y. Qin, R. Su, Y. Wu, Q. Fang, H. Wang, X. Cui, L. Zheng, W. Gu, C. Zhu, Amino-ligand-coordinated dicopper active sites enable catechol oxidase-like activity for chiral recognition and catalysis, Nano Lett. 23 (2023) 701–709, https://doi.org/10.1021/acs.nanolett.2c04697.
[74] Q. Chen, H.J. Zhang, H. Sun, Y.Z. Yang, D.D. Zhang, X. Li, L. Han, G.N. Wang, Y. Zhang, Sensitive dual-signal detection and effective removal of tetracycline antibiotics in honey based on a hollow triple-metal organic framework nanozymes, Food Chem. 442 (2024) 138383, https://doi.org/10.1016/j.foodchem.2024.138383.
[75] Z. Mu, S. Wu, J. Guo, M. Zhao, Y. Wang, Dual mechanism enhanced peroxidase-like activity of iron–nickel bimetal–organic framework nanozyme and its application for biosensing, ACS Sustain. Chem. Eng. 10 (2022) 2984–2993, https://doi.org/10.1021/acssuschemeng.1c07975.
[76] L. Zhang, X. Wang, R. Cueto, C. Effi, Y. Zhang, H. Tan, X. Qin, Y. Ji, X. Yang, H. Wang, Biochemical basis and metabolic interplay of redox regulation, Redox Biol. 26 (2019) 101284, https://doi.org/10.1016/j.redox.2019.101284.
[77] Y. Zhang, F. Wang, C. Liu, Z. Wang, L. Kang, Y. Huang, K. Dong, J. Ren, X. Qu, Nanozyme decorated metal-organic frameworks for enhanced photodynamic therapy, ACS Nano 12 (2018) 651–661, https://doi.org/10.1021/acsnano.7b07746.
[78] B. Yang, H. Yao, J. Yang, C. Chen, J. Shi, Construction of a two-dimensional artificial antioxidase for nanocatalytic rheumatoid arthritis treatment, Nat. Commun. 13 (2022) 1988, https://doi.org/10.1038/s41467-022-29735-1.
[79] S. Bhattacharjee, T. Chakraborty, A. Bhaumik, A Ce-MOF as an alkaline phosphatase mimic: Ce-OH_2 sites in catalytic dephosphorylation, Inorg. Chem. Front. 9 (2022) 5735–5744, https://doi.org/10.1039/d2qi01443b.
[80] S. Liu, Y. He, W. Zhang, T. Fu, L. Wang, Y. Zhang, Y. Xu, H. Sun, H. Zhao, Self-cascade Ce-MOF-818 nanozyme for sequential hydrolysis and oxidation, Small 20 (2024), https://doi.org/10.1002/smll.202306522.
[81] H.G.T. Ly, G. Fu, F. de Azambuja, D. De Vos, T.N. Parac-Vogt, Nanozymatic activity of UiO-66 metal-organic frameworks: tuning the nanopore environment

enhances hydrolytic activity toward peptide bonds, ACS Appl. Nano Mater. 3 (2020) 8931–8938, https://doi.org/10.1021/acsanm.0c01688.
[82] M.C. de Koning, C.V. Soares, M. van Grol, R.P.T. Bross, G. Maurin, Effective degradation of Novichok nerve agents by the zirconium metal-organic framework MOF-808, ACS Appl. Mater. Interfaces 14 (2022) 9222–9230, https://doi.org/10.1021/acsami.1c24295.
[83] X. Li, X. Li, D. Li, M. Zhao, H. Wu, B. Shen, P. Liu, S. Ding, Electrochemical biosensor for ultrasensitive exosomal miRNA analysis by cascade primer exchange reaction and MOF@Pt@MOF nanozyme, Biosens. Bioelectron. 168 (2020) 112554, https://doi.org/10.1016/j.bios.2020.112554.
[84] J. Han, M. Zhang, G. Chen, Y. Zhang, Q. Wei, Y. Zhuo, G. Xie, R. Yuan, S. Chen, Ferrocene covalently confined in porous MOF as signal tag for highly sensitive electrochemical immunoassay of amyloid-β, J. Mater. Chem. B 5 (2017) 8330–8336, https://doi.org/10.1039/c7tb02240a.
[85] D. Cheng, P. Li, Z. Xu, X. Liu, Y. Zhang, M. Liu, S. Yao, Signal on-off electrochemical sensor for glutathione based on a AuCu-decorated Zr-containing metal-organic framework via solid-state electrochemistry of cuprous chloride, ACS Sens. 7 (2022) 2465–2474, https://doi.org/10.1021/acssensors.2c01221.
[86] Z. Xu, Q. Wang, H. Zhangsun, S. Zhao, Y. Zhao, L. Wang, Carbon cloth-supported nanorod-like conductive Ni/co bimetal MOF: a stable and high-performance enzyme-free electrochemical sensor for determination of glucose in serum and beverage, Food Chem. 349 (2021) 129202, https://doi.org/10.1016/j.foodchem.2021.129202.
[87] X. Wang, Y. Xu, Y. Li, Y. Li, Z. Li, W. Zhang, X. Zou, J. Shi, X. Huang, C. Liu, W. Li, Rapid detection of cadmium ions in meat by a multi-walled carbon nanotubes enhanced metal-organic framework modified electrochemical sensor, Food Chem. 357 (2021) 129762, https://doi.org/10.1016/j.foodchem.2021.129762.
[88] J. Cui, Y.-L. Wong, M. Zeller, A.D. Hunter, Z. Xu, Pd uptake and H_2S sensing by an amphoteric metal-organic framework with a soft core and rigid side arms, Angew. Chem. Int. Ed. 53 (2014) 14438–14442, https://doi.org/10.1002/anie.201408453.
[89] X. Zhou, S. Wang, C. Zhang, Y. Lin, J. Lv, S. Hu, S. Zhang, M. Li, Colorimetric determination of amyloid-β peptide using MOF-derived nanozyme based on porous ZnO-Co_3O_4 nanocages, Microchim. Acta 188 (2021) 56, https://doi.org/10.1007/s00604-021-04705-4.
[90] N. Alizadeh, A. Salimi, R. Hallaj, F. Fathi, F. Soleimani, Ni-hemin metal-organic framework with highly efficient peroxidase catalytic activity: toward colorimetric cancer cell detection and targeted therapeutics, J. Nanobiotechnol. 16 (2018) 93, https://doi.org/10.1186/s12951-018-0421-7.
[91] Z. Sun, S. Wu, J. Ma, H. Shi, L. Wang, A. Sheng, T. Yin, L. Sun, G. Li, Colorimetric sensor array for human semen identification designed by coupling zirconium metal-organic frameworks with DNA-modified gold nanoparticles, ACS Appl. Mater. Interfaces 11 (2019) 36316–36323, https://doi.org/10.1021/acsami.9b10729.
[92] C. Wang, G. Tang, H. Tan, Colorimetric determination of mercury(II) via the inhibition by ssDNA of the oxidase-like activity of a mixed valence state cerium-based metal-organic framework, Microchim. Acta 185 (2018), https://doi.org/10.1007/s00604-018-3011-3.
[93] X. Yue, L. Fu, Y. Li, S. Xu, X. Lin, Y. Bai, Lanthanide bimetallic MOF-based fluorescent sensor for sensitive and visual detection of sulfamerazine and malachite, Food Chem. 410 (2023) 135390, https://doi.org/10.1016/j.foodchem.2023.135390.
[94] T. Wang, L. Zhang, J. Zhang, G. Guo, X. Jiang, Z. Zhang, S. Li, Highly sensitive fluorescent quantification of carbendazim by two-dimensional Tb-MOF nanosheets for food safety, Food Chem. 416 (2023) 135853, https://doi.org/10.1016/j.foodchem.2023.135853.
[95] J. Bai, L. Liu, C. Jia, Z. Liu, S. Gao, Y. Han, H. Yan, Fluorescence method for the detection of protein kinase activity by using a zirconium-based metal-organic framework as an affinity probe, ACS Appl. Bio Mater. 2 (2019) 6021–6028, https://doi.org/10.1021/acsabm.9b00978.
[96] X. Zhang, Q. Ma, X. Liu, H. Niu, L. Luo, R. Li, X. Feng, A turn-off Eu-MOF@Fe^{2+} sensor for the selective and sensitive fluorescence detection of bromate in wheat flour, Food Chem. 382 (2022) 132379, https://doi.org/10.1016/j.foodchem.2022.132379.
[97] S. Jain, N. Dilbaghi, N.K. Singhal, A. Kaushik, K.H. Kim, S. Kumar, Carbon quantum dots@metal-organic framework based catalytic nucleic acid fluorescent system for highly sensitive and selective detection of Pb^{2+} in aqueous solutions, Chem. Eng. J. 457 (2023) 141375, https://doi.org/10.1016/j.cej.2023.141375.
[98] R. Chen, X. Chen, Y. Zhou, T. Lin, Y. Leng, X. Huang, Y. Xiong, "Three-in-one" multifunctional nanohybrids with colorimetric magnetic catalytic activities to enhance immunochromatographic diagnosis, ACS Nano 16 (2022) 3351–3361, https://doi.org/10.1021/acsnano.2c00008.
[99] Z.J. Yu, T.T. Yang, G. Liu, D.H. Deng, L. Liu, Gold nanoparticles-based colorimetric immunoassay of carcinoembryonic antigen with metal-organic framework to load quinones for catalytic oxidation of cysteine, Sensors 24 (2024) 6701, https://doi.org/10.3390/s24206701.
[100] C. Wang, J. Gao, H. Tan, Integrated antibody with catalytic metal-organic framework for colorimetric immunoassay, ACS Appl. Mater. Interfaces 10 (2018) 25113–25120, https://doi.org/10.1021/acsami.8b07225.
[101] Z. Luo, D. Sun, Y. Tong, Y. Zhong, Z. Chen, DNA nanotetrahedron linked dual-aptamer based voltammetric aptasensor for cardiac troponin I using a magnetic metal-organic framework as a label, Microchim. Acta 186 (2019), https://doi.org/10.1007/s00604-019-3470-1.
[102] H. Shen, H. Shi, B. Feng, C. Ding, S. Yu, A versatile biomimetic multienzyme cascade nanoplatform based on boronic acid-modified metal-organic framework for colorimetric biosensing, J. Mater. Chem. B 10 (2022) 3444–3451, https://doi.org/10.1039/d2tb00158f.
[103] C. Gong, B. Chen, Y. Xing, H. Zhao, Metal-pyrimidine nanocubes immobilized enzymes with pH-switchable multienzyme-like activity for broad-pH-responsive sensing assay for organophosphorus pesticides, J. Hazard. Mater. 463 (2024) 132849, https://doi.org/10.1016/j.jhazmat.2023.132849.
[104] H.Y. Yang, Z.P. Sun, X.G. Qin, H.Y. Wu, H.Z. Zhang, G. Liu, Ultrasmall au nanoparticles modified 2D metalloporphyrinic metal-organic framework nanosheets with high peroxidase-like activity for colorimetric detection of organophosphorus pesticides, Food Chem. 376 (2022) 131906, https://doi.org/10.1016/j.foodchem.2021.131906.
[105] Z. Gan, X. Hu, X. Xu, W. Zhang, X. Zou, J. Shi, K. Zheng, M. Arslan, A portable test strip based on fluorescent europium-based metal-organic framework for rapid and visual detection of tetracycline in food samples, Food Chem. 354 (2021) 129501, https://doi.org/10.1016/j.foodchem.2021.129501.
[106] D. Wang, J. Wang, D. Liu, J. He, M. Wang, H. Huang, G. Nie, H. Ding, X. Yan, Rapid and sensitive detection of Epstein-Barr virus antibodies in nasopharyngeal carcinoma by chemiluminescence strips based on iron-porphyrin single atom nanozyme, Nano Res. 17 (2023) 1827–1836, https://doi.org/10.1007/s12274-023-5915-4.
[107] R.M. Mohamed, S.M. Sheikh, M.W. Kadi, A.A. Labib, S.M. Sheta, A novel test device and quantitative colorimetric method for the detection of human chorionic gonadotropin (hCG) based on Au@Zn-salen MOF for POCT applications, RSC Adv. 13 (2023) 11751–11761, https://doi.org/10.1039/d2ra07854f.
[108] K. Yu, M. Li, H. Chai, Q. Liu, X. Hai, M. Tian, L. Qu, T. Xu, G. Zhang, X. Zhang, MOF-818 nanozyme-based colorimetric and electrochemical dual-mode smartphone sensing platform for in situ detection of H_2O_2 and H_2S released from living cells, Chem. Eng. J. 451 (2023) 138321, https://doi.org/10.1016/j.cej.2022.138321.
[109] Y. Wang, Y. Zhang, H. Sha, X. Xiong, N. Jia, Design and biosensing of a ratiometric electrochemiluminescence resonance energy transfer aptasensor between a g-C_3N_4 nanosheet and Ru@MOF for amyloid-β protein, ACS Appl. Mater. Interfaces 11 (2019) 36299–36306, https://doi.org/10.1021/acsami.9b09492.
[110] C. Wu, S. Wang, X. Luo, R. Yuan, X. Yang, Adenosine triphosphate responsive metal-organic frameworks equipped with a DNA structure lock for construction of a ratiometric SERS biosensor, Chem. Commun. 56 (2020) 1413–1416, https://doi.org/10.1039/c9cc08440a.
[111] Y. Cai, Y. Wu, T. Xuan, X. Guo, Y. Wen, H. Yang, Core-shell Au@metal-organic frameworks for promoting Raman detection sensitivity of methenamine, ACS Appl. Mater. Interfaces 10 (2018) 15412–15417, https://doi.org/10.1021/acsami.8b01765.
[112] L. Jiao, Y. Wang, H.-L. Jiang, Q. Xu, Metal-organic frameworks as platforms for catalytic applications, Adv. Mater. 30 (2018) 1703663, https://doi.org/10.1002/adma.201703663.
[113] G. Chen, Y. Qin, L. Jiao, J. Huang, Y. Wu, L. Hu, W. Gu, D. Xu, C. Zhu, Nanozyme-activated synergistic amplification for ultrasensitive photoelectrochemical immunoassay, Anal. Chem. 93 (2021) 6881–6888, https://doi.org/10.1021/acs.analchem.1c01217.
[114] L. Cao, C. Wang, Metal-organic layers for electrocatalysis and photocatalysis, ACS Central Sci. 6 (2020) 2149–2158, https://doi.org/10.1021/acscentsci.0c01150.
[115] Q. Yang, Q. Xu, H.L. Jiang, Metal-organic frameworks meet metal nanoparticles: synergistic effect for enhanced catalysis, Chem. Soc. Rev. 46 (2017) 4774–4808, https://doi.org/10.1039/c6cs00724d.
[116] L. Jiao, J.Y.R. Seow, W.S. Skinner, Z.U. Wang, H.L. Jiang, Metal-organic frameworks: structures and functional applications, Mater. Today 27 (2019) 43–68, https://doi.org/10.1016/j.mattod.2018.10.038.
[117] Z.L. Wang, X.Y. Jiang, R. Yuan, Y.Q. Chai, N-(aminobutyl)-N-(ethylisoluminol) functionalized Fe-based metal-organic frameworks with intrinsic mimic peroxidase activity for sensitive electrochemiluminescence mucin1 determination, Biosens. Bioelectron. 121 (2018) 250–256, https://doi.org/10.1016/j.bios.2018.09.022.
[118] H. Huang, Y. Chen, Z. Chen, J. Chen, Y. Hu, J.J. Zhu, Electrochemical sensor based on Ce-MOF/carbon nanotube composite for the simultaneous discrimination of hydroquinone and catechol, J. Hazard. Mater. 416 (2021) 125895, https://doi.org/10.1016/j.jhazmat.2021.125895.
[119] P. Janjani, U. Bhardwaj, R. Gupta, H.S. Kushwaha, Bimetallic Mn/Fe MOF modified screen-printed electrodes for non-enzymatic electrochemical sensing of organophosphate, Anal. Chim. Acta 1202 (2022) 339676.
[120] X. Yan, H. Li, X. Su, Review of optical sensors for pesticides, Trac, Trends Anal. Chem. 103 (2018) 1–20, https://doi.org/10.1016/j.trac.2018.03.004.
[121] S. Wu, H. Min, W. Shi, P. Cheng, Multicenter metal-organic framework-based ratiometric fluorescent sensors, Adv. Mater. 32 (2020) 1805871, https://doi.org/10.1002/adma.201805871.
[122] Y. Wang, Z. Mao, Q. Chen, K. Koh, X. Hu, H. Chen, Rapid and sensitive detection of PD-L1 exosomes using cu-TCPP 2D MOF as a SPR sensitizer, Biosens. Bioelectron. 201 (2022) 113954, https://doi.org/10.1016/j.bios.2021.113954.
[123] J. Gao, W. Yang, R. Liu, J. Feng, Y. Li, M. Jiang, S. Jiang, A reliable gold nanoparticle/cu-TCPP 2D MOF/gold/D-shaped fiber sensor based on SPR and LSPR coupling for dopamine detection, Appl. Surf. Sci. 655 (2024) 159523, https://doi.org/10.1016/j.apsusc.2024.159523.
[124] J. Xu, X. Zhang, J. Zhong, S. Huang, S. Wang, H. Zhai, Surface-active agent enhanced FRET effect cu-doped NH 2-MIL-88(Fe) for highly sensitive detection of 3-nitro-L-tyrosine, Spectroc. Acta Pt. A-Molec. Biomolec. Spectr. 316 (2024) 124315, https://doi.org/10.1016/j.saa.2024.124315.

[125] Q. Ding, J. Wang, X. Chen, H. Liu, Q. Li, Y. Wang, S. Yang, Quantitative and sensitive SERS platform with analyte enrichment and filtration function, Nano Lett. 20 (2020) 7304–7312, https://doi.org/10.1021/acs.nanolett.0c02683.
[126] F. Zhao, L. Wang, M. Li, M. Wang, G. Liu, J. Ping, Nanozyme-based biosensor for organophosphorus pesticide monitoring: functional design, biosensing strategy, and detection application, TrAC, Trends Anal. Chem. 165 (2023) 117152, https://doi.org/10.1016/j.trac.2023.117152.
[127] W. Cheng, X. Tang, Y. Zhang, D. Wu, W. Yang, Applications of metal-organic framework (MOF)-based sensors for food safety: nhancing mechanisms and recent advances, Trends Food Sci. Technol. 112 (2021) 268–282, https://doi.org/10.1016/j.tifs.2021.04.004.
[128] L. Su, S. Qin, Z. Xie, L. Wang, K. Khan, A.K. Tareen, D. Li, H. Zhang, Multi-enzyme activity nanozymes for biosensing and disease treatment, Coord. Chem. Rev. 473 (2022) 214784, https://doi.org/10.1016/j.ccr.2022.214784.
[129] G. Fang, R. Kang, S. Cai, C. Ge, Insight into nanozymes for their environmental applications as antimicrobial and antifouling agents: progress, challenges and prospects, Nano Today 48 (2023) 101755, https://doi.org/10.1016/j.nantod.2023.101755.
[130] B. Mohan, R. Kumar Virender, A.J.L. Gupta, P. Ren Pombeiro, Advanced luminescent metal–organic framework (MOF) sensors engineered for urine analysis applications, Coord. Chem. Rev. 519 (2024) 216090, https://doi.org/10.1016/j.ccr.2024.216090.
[131] B. Mohanty, S. Kumari, P. Yadav, P. Kanoo, A. Chakraborty, Metal-organic frameworks (MOFs) and MOF composites based biosensors, Coord. Chem. Rev. 519 (2024) 216102, https://doi.org/10.1016/j.ccr.2024.216102.
[132] D. Zhu, B. Liu, G. Wei, Two-dimensional material-based colorimetric biosensors: a review, Biosensors Basel 11 (2021) 259, https://doi.org/10.3390/bios11080259.
[133] G. Zhang, H. Hu, S. Deng, X. Xiao, Y. Xiong, J. Peng, W. Lai, An integrated colorimetric and photothermal lateral flow immunoassay based on bimetallic Ag-Au urchin-like hollow structures for the sensitive detection of *E. coli* O157:H7, Biosens. Bioelectron. 225 (2023) 115090, https://doi.org/10.1016/j.bios.2023.115090.
[134] J.I. Reyes, H.E. Olstad, R. Garcia, Stability and stabilization of enzyme biosensors: the key to successful application and commercialization, Annu. Rev. Food Sci. Technol. 9 (2018) 293–322, https://doi.org/10.1146/annurev- food-030216-025713.
[135] Y.-F. Fan, Z.-B. Guo, G.-B. Ge, Enzyme-based biosensors and their applications, Biosensors-Basel 13 (2023) 476, https://doi.org/10.3390/bios13040476.
[136] Y. Shu, Q. Ye, J. Tan, H. Lv, Z. Liu, Q. Mo, Metalloporphyrin-based metal-organic framework nanorods for peroxidase-like catalysis, ACS Appl. Nano Mater. 5 (2022) 17909–17918, https://doi.org/10.1021/acsanm.2c03871.
[137] Y. Zhang, Y. Wang, Z. Li, L. Qu, L. Yu, Highly selective detection and differentiation of aminophenol isomers based on a bimetallic metal-organic-framework with peroxidase-like activity, New J. Chem. 48 (2024) 1152–1163, https://doi.org/10.1039/D3NJ04369J.
[138] H. Li, S. Zhao, Z. Wang, F. Li, Controllable preparation of 2D V2O5 peroxidase-mimetic nanozyme to develop portable paper-based analytical device for intelligent pesticide assay, Small 19 (2023) 2206465, https://doi.org/10.1002/smll.202206465.
[139] J. Wang, J. Gao, D. Liu, D. Han, Z. Wang, Phenylboronic acid functionalized gold nanoparticles for highly sensitive detection of Staphylococcus aureus, Nanoscale 4 (2012) 451–454, https://doi.org/10.1039/c2nr11657j.
[140] X. Chen, Y. Wang, Y. Zhang, Z. Chen, Y. Liu, Z. Li, J. Li, Sensitive electrochemical aptamer biosensor for dynamic cell surface N-glycan evaluation featuring multivalent recognition and signal amplification on a dendrimer-graphene electrode interface, Anal. Chem. 86 (2014) 4278–4286, https://doi.org/10.1021/ac404070m.
[141] A.C.M. Rodrigues, M.V. Barbieri, M. Chino, G. Manco, F. Febbraio, A FRET approach to detect paraoxon among organophosphate pesticides using a fluorescent biosensor, Sensors 22 (2022) 561, https://doi.org/10.3390/s22020561.
[142] S.M. Pirot, K.M. Omer, A.H. Alshatteri, G.K. Ali, O.B.A. Shatery, Dual-template molecularly surface imprinted polymer on fluorescent metal-organic frameworks functionalized with carbon dots for ascorbic acid and uric acid detection, Spectroc. Acta Pt. A Molec. Biomolec. Spectr. 291 (2023) 122340, https://doi.org/10.1016/j.saa.2023.122340.
[143] D. Zhao, W. Li, R. Wen, N. Lei, W. Li, X. Liu, X. Zhang, L. Fan, Eu(III)-functionalized MOF-based dual-emission ratiometric sensor integrated with logic gate operation for efficient detection of hippuric acid in urine and serum, Inorg. Chem. (2023), https://doi.org/10.1021/acs.inorgchem.2c03828.
[144] S. Nandi, S. Banesh, V. Trivedi, S. Biswas, A dinitro-functionalized metal-organic framework featuring visual and fluorogenic sensing of H_2S in living cells, human blood plasma and environmental samples, Analyst 143 (2018) 1482–1491, https://doi.org/10.1039/c7an01964e.
[145] H. Zhang, P. Xiong, G.L. Li, C.Y. Liao, G.B. Jiang, Applications of multifunctional zirconium-based metal-organic frameworks in analytical chemistry: overview and perspectives, TrAC Trends Anal. Chem. 131 (2020) 116015, https://doi.org/10.1016/j.trac.2020.116015.
[146] J. Li, S. Yuan, J. Qin, J. Pang, P. Zhang, Y. Zhang, Y. Huang, H.F. Drake, W.R. Liu, H. Zhou, Stepwise assembly of turn-on fluorescence sensors in multicomponent metal–organic frameworks for in vitro cyanide detection, Angew. Chem. Int. Ed. 59 (2020) 9319–9323, https://doi.org/10.1002/anie.202000702.
[147] H. Li, Y. Wu, Z. Xu, Y. Wang, In situ anchoring cu nanoclusters on cu-MOF: a new strategy for a combination of catalysis and fluorescence toward the detection of H_2O_2 and 2,4-DNP, Chem. Eng. J. 479 (2024) 147508, https://doi.org/10.1016/j.cej.2023.147508.
[148] A. Bigdeli, F. Ghasemi, S. Abbasi Moayed, M. Shahrajabian, N. Fahimi Kashani, S. Jafarinejad, M.A.F. Nejad, M.R. Hormozi Nezhad, Ratiometric fluorescent nanoprobes for visual detection: design principles and recent advances-a review, Anal. Chim. Acta 1079 (2019) 30–58, https://doi.org/10.1016/j.aca.2019.06.035.
[149] J. Li, Y. Zhu, H. Xu, T.F. Zheng, S.J. Liu, Y. Wu, J.L. Chen, Y.Q. Chen, H.R. Wen, A benzothiadiazole-based Eu^{3+} metal-organic framework as the turn-on luminescent sensor toward Al^{3+} and Ga^{3+} with potential bioimaging application, Inorg. Chem. 61 (2022) 3607–3615, https://doi.org/10.1021/acs.inorgchem.1c03661.
[150] Q.X. Wang, Y.F. Yang, X.F. Yang, Y. Pan, L.D. Sun, W.Y. Zhang, Y. Shao, J. Shen, J. Lin, L. Li, C.H. Yan, Upconverted/downshifted $NaLnF_4$ and metal-organic framework heterostructures boosting NIR-II imaging-guided photodynamic immunotherapy toward tumors, Nano Today 43 (2022) 101439, https://doi.org/10.1016/j.nantod.2022.101439.
[151] D.K. Gupta, S. Kumar, M.Y. Wani, MOF magic: zirconium-based frameworks in theranostic and bio-imaging applications, J. Mater. Chem. B 12 (2024) 2691–2710, https://doi.org/10.1039/d3tb02562d.
[152] Y. Wang, C. Xu, Y. Zhou, J. Lee, Q. Chen, H. Chen, Interface-engineered 2D heterojunction with photoelectric dual gain: Mxene@MOF-enhanced SPR spectroscopy for direct sensing of exosomes, Small 20 (2024), https://doi.org/10.1002/smll.202308897.
[153] J. Qiao, X. Chen, X. Xu, B. Fan, Y.S. Guan, H. Yang, Q. Li, A metal-organic framework-based fluorescence resonance energy transfer nanoprobe for highly selective detection of staphylococcus aureus, J. Mater. Chem. B 11 (2023) 8519–8527, https://doi.org/10.1039/d3tb01428b.
[154] H. Lai, H. Dai, G. Li, Z. Zhang, Rapid determination of pesticide residues in fruit and vegetable using Au@AgNPs decorated 2D Ni-MOF nanosheets as efficient surface-enhanced Raman scattering substrate, Sensors Actuators B Chem. 369 (2022) 132360, https://doi.org/10.1016/j.snb.2022.132360.
[155] Y. Wang, D. He, Z. Du, E. Xu, Z. Jin, Z. Wu, B. Cui, Ultrasensitive detection of staphylococcal enterotoxin B with an AuNPs@MIL-101 nanohybrid-based dual-modal aptasensor, Food Anal. Methods 15 (2022) 1368–1376, https://doi.org/10.1007/s12161-021-02204-z.
[156] R. Sakthivel, S.B. Prasanna, C. Tseng, L. Lin, Y. Duann, J. He, R. Chung, A sandwich-type electrochemical immunosensor for insulin detection based on au-adhered Cu_5Zn_8 hollow porous carbon nanocubes and AuNP deposited nitrogen-doped holey graphene, Small 18 (2022) 2202516, https://doi.org/10.1002/smll.202202516.
[157] S. Li, H. Xie, F. Xie, Q. Yi, H. Tan, Immunoassay based on urease-encapsulated metal-organic framework for sensitive detection of foodborne pathogen with pH meter as a readout, Microchim. Acta 189 (2022) 358, https://doi.org/10.1007/s00604-022-05462-8.
[158] G. Tian, Z. Zhou, M. Li, X. Li, T. Xu, X. Zhang, Oriented antibody-assembled metal-organic frameworks for persistent wearable sweat cortisol detection, Anal. Chem. (2023), https://doi.org/10.1021/acs.analchem.3c02392.
[159] X. Mao, Q. Chen, S. Wei, D. Qiu, X. Zhang, J. Lei, J.L. Mergny, H. Ju, J. Zhou, Bioinspired dual hemin-bonded G-quadruplex and histidine-functionalized metal-organic framework for sensitive biosensing, Anal. Chem. 96 (2024) 13371–13378, https://doi.org/10.1021/acs.analchem.4c00010.
[160] M. Wang, Y. Yang, J. Min, Y. Song, J. Tu, D. Mukasa, C. Ye, C. Xu, N. Heflin, J. S. McCune, T.K. Hsiai, Z. Li, W. Gao, A wearable electrochemical biosensor for the monitoring of metabolites and nutrients, Nat. Biomed. Eng. 6 (2022) 1225–1235, https://doi.org/10.1038/s41551-022-00916-z.
[161] Y. Li, C. Zhang, Y. He, J. Gao, W. Li, L. Cheng, F. Sun, P. Xia, Q. Wang, A generic and non-enzymatic electrochemical biosensor integrated molecular beacon-like catalyzed hairpin assembly circuit with MOF@Au@G-triplex/hemin nanozyme for ultrasensitive detection of miR-721, Biosens. Bioelectron. 203 (2022) 114051, https://doi.org/10.1016/j.bios.2022.114051.
[162] K. Alt, F. Carraro, E. Jap, M. Linares Moreau, R. Riccò, M. Righetto, M. Bogar, H. Amenitsch, R.A. Hashad, C. Doonan, C.E. Hagemeyer, P. Falcaro, Self-assembly of oriented antibody-decorated metal-organic framework nanocrystals for active-targeting applications, Adv. Mater. 34 (2022) 2106607, https://doi.org/10.1002/adma.202106607.
[163] Z.Y. Guo, C.C. Zhuang, Y.H. Song, J.L. Yong, Y. Li, Z. Guo, B. Kong, J. M. Whitelock, J. Wang, K. Liang, Biocatalytic buoyancy-driven nanobots for autonomous cell recognition and enrichment, Nano Micro Lett. 15 (2023) 236, https://doi.org/10.1007/s40820-023-01207-1.
[164] J. Shi, S.C. Barman, S. Cheng, Y. Zeng, Metal-organic framework-interfaced ELISA probe enables ultrasensitive detection of extracellular vesicle biomarkers, J. Mater. Chem. B 12 (2024) 6342–6350, https://doi.org/10.1039/D4TB00585F.
[165] Y. Wen, W. Xu, Y. Wu, Y. Tang, M. Liu, M. Sha, J. Li, R. Xiao, L. Hu, Y. Lin, C. Zhu, W. Gu, Bifunctional enzyme-mimicking metal-organic frameworks for sensitive acetylcholine analysis, Talanta 275 (2024) 126112, https://doi.org/10.1016/j.talanta.2024.126112.
[166] H. Wei, E. Wang, Fe_3O_4 magnetic nanoparticles as peroxidase mimetics and their applications in H_2O_2 and glucose detection, Anal. Chem. 80 (2008) 2250–2254, https://doi.org/10.1021/ac702203f.
[167] J. Hassanzadeh, H.A.J. Al Lawati, N. Bagheri, On paper synthesis of multifunctional CeO_2 nanoparticles@Fe-MOF composite as a multi-enzyme cascade platform for multiplex colorimetric detection of glucose, fructose, sucrose, and maltose, Biosens. Bioelectron. 207 (2022) 114184, https://doi.org/10.1016/j.bios.2022.114184.
[168] Z. Wang, Y. Shao, Z. Zhu, J. Wang, X. Gao, J. Xie, Y. Wang, Q. Wu, Y. Shen, Y. Ding, Novel gold nanozyme regulation strategies facilitate analytes detection,

Coord. Chem. Rev. 495 (2023) 215369, https://doi.org/10.1016/j.ccr.2023.215369.
[169] L. Zhang, H. Wang, X. Qu, Biosystem-inspired engineering of nanozymes for biomedical applications, Adv. Mater. 36 (2024) 2211147, https://doi.org/10.1002/adma.202211147.
[170] J. Cai, Y. Lin, X. Yu, Y. Yang, Y. Hu, L. Gao, H. Xiao, J. Du, H. Wang, X. Zhong, P. Sun, X. Liang, H. Zhou, H. Cai, Multifunctional AuAg-doping prussian blue-based MOF: enhanced colorimetric catalytic activities and amplified SERS signals for bacteria discrimination and detection, Sensors Actuators B Chem. 394 (2023) 134279, https://doi.org/10.1016/j.snb.2023.134279.
[171] J. Tang, C. Huang, Y. Liu, T. Wang, M. Yu, H. Hao, W. Zeng, W. Huang, J. Wang, M. Wu, Metal-organic framework nanoshell structures: preparation and biomedical applications, Coord. Chem. Rev. 490 (2023) 215211, https://doi.org/10.1016/j.ccr.2023.215211.
[172] Q. Liu, B. Wu, M. Li, Y. Huang, L. Li, Heterostructures made of upconversion nanoparticles and metal-organic frameworks for biomedical applications, Adv. Sci. 9 (2022) 2103911, https://doi.org/10.1002/advs.202103911.
[173] L. Fabris, Y. Ceder, A.M. Chinnaiyan, G.W. Jenster, K.D. Sorensen, S. Tomlins, T. Visakorpi, G.A. Calin, The potential of microRNAs as prostate cancer biomarkers, Eur. Urol. 70 (2016) 312–322, https://doi.org/10.1016/j.eururo.2015.12.054.
[174] W. Li, J.B. Liu, L.K. Hou, F. Yu, J. Zhang, W. Wu, X.M. Tang, F. Sun, H.M. Lu, J. Deng, J. Bai, J. Li, C.Y. Wu, Q.L. Lin, Z.W. Lv, G.R. Wang, G.X. Jiang, Y.S. Ma, D. Fu, Liquid biopsy in lung cancer: significance in diagnostics, prediction, and treatment monitoring, Mol. Cancer 21 (2022) 25, https://doi.org/10.1186/s12943-022-01505-z.
[175] J. Cuzick, M.A. Thorat, G. Andriole, O.W. Brawley, P.H. Brown, Z. Culig, R. A. Eeles, L.G. Ford, F.C. Hamdy, L. Holmberg, D. Ilic, T.J. Key, C. La Vecchia, H. Lilja, M. Marberger, F.L. Meyskens, L.M. Minasian, C. Parker, H.L. Parnes, S. Perner, H. Rittenhouse, J. Schalken, H.P. Schmid, B.J. Schmitz Draeger, F. H. Schroder, A. Stenzl, B. Tombal, T.J. Wilt, A. Wolk, Prevention and early detection of prostate cancer, Lancet Oncol. 15 (2014) E484–E492, https://doi.org/10.1016/S1470-2045(14)70211-6.
[176] M. Ashrafizadeh, S. Aghamiri, S.C. Tan, A. Zarrabi, E. Sharifi, N. Rabiee, F. B. Kadumudi, A.D. Pirouz, M. Delfi, K. Byrappa, V.K. Thakur, K.S.S. Kumar, Y. R. Girish, F. Zandsalimi, E.N. Zare, G. Orive, F. Tay, K. Hushmandi, A.P. Kumar, C. Karaman, H. Karimi-Maleh, E. Mostafavi, P. Makvandi, Y. Wang, Nanotechnological approaches in prostate cancer therapy: integration of engineering and biology, Nano Today 45 (2022) 101532, https://doi.org/10.1016/j.nantod.2022.101532.
[177] K.M.L. Taylor, W.J. Rieter, W. Lin, Manganese-based nanoscale metal-organic frameworks for magnetic resonance imaging, J. Am. Chem. Soc. 130 (2008) 14358, https://doi.org/10.1021/ja803777x.
[178] Y. Hu, J. Liao, D. Wang, G. Li, Fabrication of gold nanoparticle-embedded metal-organic framework for highly sensitive surface-enhanced Raman scattering detection, Anal. Chem. 86 (2014) 3955–3963, https://doi.org/10.1021/ac5002355.
[179] H. Du, T. Yin, J. Wang, G. Jie, Multifunctional photoelectrochemical biosensor based on $ZnIn_2S_4$/ZnS QDs@au-ag-reversed photocurrent of Cu-metal-organic framework coupled with CRISPR/Cas-12a-shearing for assay of dual targets, Anal. Chem. 95 (2023) 7053–7061, https://doi.org/10.1021/acs.analchem.3c00846.
[180] P. Huang, L. Meng, J. Pang, H. Huang, J. Ma, L. He, P. Amani, Development of a high-performance label-free electrochemical immunosensor for early cancer diagnosis using anti-CEA/ag-MOF/GO/GCE nanocomposite, Environ. Res. 238 (2023) 117178, https://doi.org/10.1016/j.envres.2023.117178.
[181] Y. Wang, Y. Peng, S. Li, D. Han, S. Ren, K. Qin, H. Zhou, T. Han, Z. Gao, The development of a fluorescence/colorimetric biosensor based on the cleavage activity of CRISPR-Cas12a for the detection of non-nucleic acid targets, J. Hazard. Mater. 449 (2023) 131044, https://doi.org/10.1016/j.jhazmat.2023.131044.
[182] S.M. Khoshfetrat, P.S. Dorraji, L. Fotouhi, M. Hosseini, F. Khatami, H.R. Moazami, K. Omidfar, Enhanced electrochemiluminescence biosensing of gene-specific methylation in thyroid cancer patients' plasma based integrated graphitic carbon nitride-encapsulated metal-organic framework nanozyme optimized by central composite design, Sensors Actuators B Chem. 364 (2022) 131895, https://doi.org/10.1016/j.snb.2022.131895.
[183] H. Zhang, Y. Shang, Y.H. Li, S.K. Sun, X.B. Yin, Smart metal–organic framework-based nanoplatforms for imaging-guided precise chemotherapy, ACS Appl. Mater. Interfaces 13 (2021) 20917–20918, https://doi.org/10.1021/acsami.1c05207.
[184] M. Xiong, Y. Zhang, H. Zhang, Q. Shao, Q. Hu, J. Ma, Y. Wan, L. Guo, X. Wan, H. Sun, Z. Yuan, H. Wan, A tumor environment-activated photosensitized biomimetic nanoplatform for precise photodynamic immunotherapy of colon cancer, Adv. Sci. 11 (2024), https://doi.org/10.1002/advs.202402465.
[185] P.H. Tong, J.J. Yang, Y.F. Zhou, Y.F. Tang, M.T. Tang, Y. Zang, Y.F. Pan, L. W. Dong, Y.X. Tan, K.T. Nam, X.L. Hu, H. Huang, J. Li, H.Y. Wang, T.D. James, J. Yoon, X.P. He, Metal-organic frameworks (MOFs) for phototherapy and synergistic phototherapy of cancer, Coord. Chem. Rev. 526 (2025) 216381, https://doi.org/10.1016/j.ccr.2024.216381.
[186] J. Han, J. Yoon, Supramolecular nanozyme-based cancer catalytic therapy, ACS Appl. Bio. Mater. 3 (2020) 7344–7351, https://doi.org/10.1021/acsabm.0c01127.
[187] X. Cao, N. Feng, Q. Huang, Y. Liu, Nanoscale metal-organic frameworks and nanoscale coordination polymers: from synthesis to cancer therapy and biomedical imaging, ACS Appl. Bio Mater. 7 (2024) 7965–7986, https://doi.org/10.1021/acsabm.3c01300.
[188] Z. Zhou, X. Wang, H. Zhang, H. Huang, L. Sun, L. Ma, Y. Du, C. Pei, Q. Zhang, H. Li, L. Ma, L. Gu, Z. Liu, L. Cheng, C. Tan, Activating layered metal oxide nanomaterials via structural engineering as biodegradable nanoagents for photothermal cancer therapy, Small 17 (2021) e2007486, https://doi.org/10.1002/smll.202007486.
[189] Z. Zhou, B. Li, C. Shen, D. Wu, H. Fan, J. Zhao, H. Li, Z. Zeng, Z. Luo, L. Ma, C. Tan, Metallic 1T phase enabling MoS_2 nanodots as an efficient agent for photoacoustic imaging guided photothermal therapy in the near-infrared-II window, Small 16 (2020) e2004173, https://doi.org/10.1002/smll.202004173.
[190] J. Zhang, Y. Yang, F. Qin, T. Hu, X. Zhao, S. Zhao, Y. Cao, Z. Gao, Z. Zhou, R. Liang, C. Tan, Y. Qin, Catalyzing generation and stabilization of oxygen vacancies on CeO_2-x nanorods by Pt nanoclusters as nanozymes for catalytic therapy, Adv. Healthc. Mater. 12 (2023) e2302056, https://doi.org/10.1002/adhm.202302056.
[191] W. Chen, M. Yang, H. Wang, J. Song, C. Mei, L. Qiu, J. Chen, A novel CaCu-metal-organic-framework based multimodal treatment platform for enhanced synergistic therapy of hepatocellular carcinoma, Adv. Healthc. Mater. 13 (2024), https://doi.org/10.1002/adhm.202304000.
[192] Z. Cheng, G. He, R. Liao, Y. Tan, W. Deng, A sensitive immunosensing platform based on the high cathodic photoelectrochemical activity of Zr-MOF and dual-signal amplification of peroxidase-mimetic Fe-MOF, Bioelectrochemistry 157 (2024) 108677, https://doi.org/10.1016/j.bioelechem.2024.108677.
[193] W. Long, J. Yang, Q. Zhao, Y. Pan, X. Luan, B. He, X. Han, Y. Wang, Y. Song, Metal-organic framework-DNA bio-barcodes amplified CRISPR/ Cas12a assay for ultrasensitive detection of protein biomarkers, Anal. Chem. (2022), https://doi.org/10.1021/acs.analchem.2c04737.
[194] L. Wang, Y. Ji, L. Wang, S. Zheng, Y. Chen, X. Xu, F. Wang, C. Li, Ratio fluorescence/colorimetric dual mode aptasensor and smartphones-assisted miniaturized device for early diagnosis of prostate cancer, Chem. Eng. J. 485 (2024) 150152, https://doi.org/10.1016/j.cej.2024.150152.
[195] L. Zheng, Q. Guo, C. Yang, J. Wang, X. Xu, G. Nie, Electrochemiluminescence and photoelectrochemistry dual-signal immunosensor based on $Ru(bpy)_3^{2+}$-functionalized MOF for prostate-specific antigen sensitive detection, Sensors Actuators B Chem. 379 (2023) 133269, https://doi.org/10.1016/j.snb.2022.133269.
[196] Y. Song, K. Chen, S. Li, L. He, M. Wang, N. Zhou, M. Du, Impedimetric aptasensor based on zirconium-cobalt metal-organic framework for detection of carcinoembryonic antigen, Microchim. Acta 189 (2022) 338, https://doi.org/10.1007/s00604-022-05427-x.
[197] Z.H. Zhang, F.H. Duan, J.Y. Tian, J.Y. He, L.Y. Yang, H. Zhao, S. Zhang, C.S. Liu, L.H. He, M. Chen, D.M. Chen, M. Du, Aptamer-embedded zirconium-based metal-organic framework composites prepared by de novo bio-inspired approach with enhanced biosensing for detecting trace analytes, ACS Sens. 2 (2017) 982–989, https://doi.org/10.1021/acssensors.7b00236.
[198] J. Li, H. Yang, R. Cai, W. Tan, Ultrahighly sensitive sandwich-type electrochemical Immunosensor for selective detection of tumor biomarkers, ACS Appl. Mater. Interfaces 14 (2022) 44222–44227, https://doi.org/10.1021/acsami.2c13891.
[199] Y. Shu, T. Su, Q. Lu, Z. Shang, J. Feng, D. Jin, A. Zhu, Q. Xu, X. Hu, Paper-based electrochemical immunosensor device via Ni-co MOF nanosheet as a peroxidase mimic for the label-free detection of alpha-fetoprotein, Sensors Actuators B 373 (2022) 132736, https://doi.org/10.1016/j.snb.2022.132736.
[200] C. Zhao, C. Ma, F. Zhang, W. Li, C. Hong, Y. Qi, Two-dimensional metal-organic framework nanosheets: an efficient two-electron oxygen reduction reaction electrocatalyst for boosting cathodic luminol electrochemiluminescence, Chem. Eng. J. 466 (2023) 143156, https://doi.org/10.1016/j.cej.2023.143156.
[201] X. Zhong, M. Zhang, L. Guo, Y. Xie, R. Luo, W. Chen, F. Cheng, L. Wang, A dual-signal self-checking photoelectrochemical immunosensor based on the sole composite of MIL-101(Cr) and CdSe quantum dots for the detection of α-fetoprotein, Biosens. Bioelectron. 189 (2021) 113389, https://doi.org/10.1016/j.bios.2021.113389.
[202] W. Zhang, D. Han, Z. Wu, K. Yang, S. Sun, J. Wen, Metal-organic layers-catalyzed amplification of electrochemiluminescence signal and its application for immunosensor construction, Sensors Actuators B 376 (2023) 133004, https://doi.org/10.1016/j.snb.2022.133004.
[203] M. Wang, M. Hu, Z. Li, L. He, Y. Song, Q. Jia, Z. Zhang, M. Du, Construction of Tb-MOF-on-Fe-MOF conjugate as a novel platform for ultrasensitive detection of carbohydrate antigen 125 and living cancer cells, Biosens. Bioelectron. 142 (2019) 111536, https://doi.org/10.1016/j.bios.2019.111536.
[204] S. Biswas, Q. Lan, Y. Xie, X. Sun, Y. Wang, Label-free electrochemical immunosensor for ultrasensitive detection of carbohydrate antigen 125 based on antibody-immobilized biocompatible MOF-808/CNT, ACS Appl. Mater. Interfaces 13 (2021) 3295–3302, https://doi.org/10.1021/acsami.0c14946.
[205] C. Zhang, D. Zhang, Z. Ma, H. Han, Cascade catalysis-initiated radical polymerization amplified impedimetric immunosensor for ultrasensitive detection of carbohydrate antigen 15-3, Biosens. Bioelectron. 137 (2019) 1–7, https://doi.org/10.1016/j.bios.2019.04.049.
[206] L. Qu, W. Zhao, J. Liu, J. Wang, J. Li, H. Pan, A sandwich electrochemiluminescence immunoassay based on 1T-MoS_2@dual MOFs for detecting CA153, Talanta 269 (2024) 125412, https://doi.org/10.1016/j.talanta.2023.125412.
[207] X. Liu, D. Han, F. Jiang, S. Liu, Y. Li, Z. Xu, Q. Liu, Y. Li, Q. Wei, Enhanced electrochemiluminescence of CdS QDs encapsulated in IRMOF-3 for sensitive detection of human epithelial protein 4, Talanta 282 (2025) 127052, https://doi.org/10.1016/j.talanta.2024.127052.
[208] X. Xu, L. Tang, Y. Yu, J. Zhang, X. Zhou, T. Zhou, C. Xuan, Q. Tian, D. Pan, Cooperative amplification of Prussian blue as a signal indicator and functionalized metal-organic framework-based electrochemical biosensor for an

ultrasensitive HE4 assay, Biosens. Bioelectron. 262 (2024) 116541, https://doi.org/10.1016/j.bios.2024.116541.
[209] K. Chen, J. Xue, Q. Zhou, Y. Zhang, M. Zhang, Y. Zhang, H. Zhang, Y. Shen, Coupling metal-organic framework nanosphere and nanobody for boosted photoelectrochemical immunoassay of human epididymis protein 4, Anal. Chim. Acta 1107 (2020) 145–154, https://doi.org/10.1016/j.aca.2020.02.011.
[210] C. Li, Y. Li, Y. Zhang, G. Zhao, Y. Wang, H. Wang, H. Wang, R. Xu, Q. Wei, Signal-enhanced electrochemiluminescence strategy using iron-based metal-organic frameworks modified with carboxylated Ru(II) complexes for neuron-specific enolase detection, Biosens. Bioelectron. 215 (2022) 114605, https://doi.org/10.1016/j.bios.2022.114605.
[211] X. Dong, Y. Du, G. Zhao, W. Cao, D. Fan, X. Kuang, Q. Wei, H. Ju, Dual-signal electrochemiluminescence immunosensor for neuron-specific enolase detection based on "dual-potential" emitter $Ru(bpy)_3^{2+}$functionalized zinc-based metal-organic frameworks, Biosens. Bioelectron. 192 (2021) 113505, https://doi.org/10.1016/j.bios.2021.113505.
[212] J. Li, H. Jia, X. Ren, Y. Li, L. Liu, R. Feng, H. Ma, Q. Wei, Dumbbell plate-shaped AIEgen-based luminescent MOF with high quantum yield as self-enhanced ECL tags: mechanism insights and biosensing application, Small 18 (2022) 2106567, https://doi.org/10.1002/smll.202106567.
[213] A.R. Chapman, A.S.V. Shah, K.K. Lee, A. Anand, O. Francis, P. Adamson, D. A. McAllister, F.E. Strachan, D.E. Newby, N.L. Mills, Long-term outcomes in patients with type 2 myocardial infarction and myocardial injury, Circulation 137 (2018) 1236–1245, https://doi.org/10.1161/CIRCULATIONAHA.117.031806.
[214] N.C. Kerbel, Pulmonary hypertension and portal hypertension, Can. Med. Assoc. J. 87 (1962) 1022–1026.
[215] M. He, J. Dong, J. Wen, Y. Zhang, S.Y. Han, C. Wang, B. Gongol, T.Y.W. Wei, J. Kang, H.Y. Huang, S. Cheng, J.Y.J. Shyy, Epitranscriptomic modification of microRNA increases atherosclerosis susceptibility, Circulation 148 (2023) 1819–1822, https://doi.org/10.1161/CIRCULATIONAHA.123.065455.
[216] D. Sun, Z. Luo, J. Lu, S. Zhang, T. Che, Z. Chen, L. Zhang, Electrochemical dual-aptamer-based biosensor for nonenzymatic detection of cardiac troponin I by nanohybrid electrocatalysts labeling combined with DNA nanotetrahedron structure, Biosens. Bioelectron. 134 (2019) 49–56, https://doi.org/10.1016/j.bios.2019.03.049.
[217] A. Ahmadi, S.M. Khoshfetrat, Z. Mirzaeizadeh, S. Kabiri, J. Rezaie, K. Omidfar, Electrochemical immunosensor for determination of cardiac troponin I using two-dimensional metal-organic framework/Fe_3O_4-COOH nanosheet composites loaded with thionine and p CTAB/DES modified electrode, Talanta 237 (2022) 122911, https://doi.org/10.1016/j.talanta.2021.122911.
[218] S. Wang, Y. Zhao, M. Wang, H. Li, M. Saqib, C. Ge, X. Zhang, Y. Jin, Enhancing luminol electrochemiluminescence by combined use of cobalt-based metal organic frameworks and silver nanoparticles and its application in ultrasensitive detection of cardiac troponin I, Anal. Chem. 91 (2019) 3048–3054, https://doi.org/10.1021/acs.analchem.8b05443.
[219] C. Vitali, A.T. Remaley, M. Cuchel, Is low-density lipoprotein cholesterol the key to interpret the role of lecithin:cholesterol acyltransferase in atherosclerosis? Circulation 138 (2018) 1008–1011, https://doi.org/10.1161/CIRCULATIONAHA.118.035358.
[220] M. Zhao, Y. Li, X. Ma, M. Xia, Y. Zhang, Adsorption of cholesterol oxidase and entrapment of horseradish peroxidase in metal-organic frameworks for the colorimetric biosensing of cholesterol, Talanta 200 (2019) 293–299, https://doi.org/10.1016/j.talanta.2019.03.060.
[221] M. Cao, C. Huang, Y. Zhang, X. Yang, L. Cui, A. Li, J. Xu, J. Liu, Molecularly imprinted sensor based on cascade enzyme system supported by metal-organic framework (UiO-66-NH_2) for sensitive colorimetric detection of cholesterol, Sensors Actuators B Chem. 404 (2024) 135235, https://doi.org/10.1016/j.snb.2023.135235.
[222] T. Bai, P. Xue, S. Shao, S. Yan, X. Zeng, Cholesterol depletion-enhanced ferroptosis and immunotherapy via engineered nanozyme, Adv. Sci. (2024) 2405826, https://doi.org/10.1002/advs.202405826.
[223] F. Lv, H. Fang, L. Huang, Q. Wang, S. Cao, W. Zhao, Z. Zhou, W. Zhou, X. Wang, Curcumin equipped nanozyme-like metal-organic framework platform for the targeted atherosclerosis treatment with lipid regulation and enhanced magnetic resonance imaging capability, Adv. Sci. 11 (2024) 2309062, https://doi.org/10.1002/advs.202309062.
[224] K. Xiang, H. Wu, Y. Liu, S. Wang, X. Li, B. Yang, Y. Zhang, L. Ma, G. Lu, L. He, Q. Ni, L. Zhang, MOF-derived bimetallic nanozyme to catalyze ROS scavenging for protection of myocardial injury, Theranostics 13 (2023) 2721–2733, https://doi.org/10.7150/thno.83543.
[225] R. Gill, M. Al Badr, M. Alghouti, N.A. Mohamed, H. Abou-Saleh, M.M. Rahman, Revolutionizing cardiovascular health with nano encapsulated omega-3 fatty acids: a nano-solution approach, Mar. Drugs 22 (2024) 256, https://doi.org/10.3390/md22060256.
[226] S. Hashemzadeh, F. Bina, H.M. Khounsari, S. Hashemzadeh, Nanotechnology in the development of cardiac stents, J. Drug Deliv. Sci. Technol. 95 (2024) 105596, https://doi.org/10.1016/j.jddst.2024.105596.
[227] S. Sadiq, S. Khan, I. Khan, A. Khan, M. Humayun, P. Wu, M. Usman, A. Khan, A. F. Alanazi, M. Bououdina, A critical review on metal-organic frameworks (MOFs) based nanomaterials for biomedical applications: designing, recent trends, challenges, and prospects, Heliyon 10 (2024) e25521, https://doi.org/10.1016/j.heliyon.2024.e25521.
[228] R. Ossenkoppele, Y.A.L. Pijnenburg, D.C. Perry, B.I. Cohn Sheehy, N.M. E. Scheltens, J.W. Vogel, J.H. Kramer, A.E. van der Vlies, R. La Joie, H.J. Rosen, W.M. van der Flier, L.T. Grinberg, A.J. Rozemuller, E.J. Huang, B.N.M. van Berckel, B.L. Miller, F. Barkhof, W.J. Jagust, P. Scheltens, W.W. Seeley, G. D. Rabinovici, The behavioural/dysexecutive variant of Alzheimer's disease: clinical, neuroimaging and pathological features, Brain 138 (2015) 2732–2749, https://doi.org/10.1093/brain/awv191.
[229] B.R. Bloem, M.S. Okun, C. Klein, Parkinson's disease, Lancet 397 (2021) 2284–2303, https://doi.org/10.1016/S0140-6736(21)00218-X.
[230] M. Barnat, M. Capizzi, E. Aparicio, S. Boluda, D. Wennagel, R. Kacher, R. Kassem, S. Lenoir, F. Agasse, B.Y. Braz, J.P. Liu, J. Ighil, A. Tessier, S.O. Zeitlin, C. Duyckaerts, M. Dommergues, A. Durr, S. Humbert, Huntington's disease alters human neurodevelopment, Science 369 (2020) 787–793, https://doi.org/10.1126/science.aax3338.
[231] J.S. Graves, K.M. Krysko, L.H. Hua, M. Absinta, R.J.M. Franklin, B.M. Segal, Ageing and multiple sclerosis, Lancet Neurol. 22 (2023) 66–77, https://doi.org/10.1016/S1474-4422(22)00184-3.
[232] F.S. Vajedi, R. Rasoolzadeh, L. Angnes, E.C.S. Santos, L.P.C. Silva, Ultrasensitive aptasensing platform for the detection of β-Amyloid-42 peptide based on MOF containing bimetallic porphyrin graphene oxide and gold nanoparticles, ACS Appl. Bio Mater. 7 (2024) 2218–2239, https://doi.org/10.1021/acsabm.3c01201.
[233] A.L.L. Brand, P.E.E. Lawler, J.G.G. Bollinger, Y. Li, S.E.E. Schindler, M. Li, S. Lopez, V. Ovod, A. Nakamura, L.M. Shaw, H. Zetterberg, O. Hansson, R.J. J. Bateman, The performance of plasma amyloid beta measurements in identifying amyloid plaques in Alzheimer's disease: a literature review, Alzheimers Res. Ther. 14 (2022) 195, https://doi.org/10.1186/s13195-022-01117-1.
[234] R. Xu, S. Zhang, P. Wang, R. Zhang, P. Lin, Y. Wang, L. Gao, H. Wei, X. Zhang, D. Ling, X. Yan, K. Fan, Nanozyme-based strategies for efficient theranostics of brain diseases, Coord. Chem. Rev. 501 (2024) 215519, https://doi.org/10.1016/j.ccr.2023.215519.
[235] G. Lv, Y. Shen, W. Zheng, J. Yang, C. Li, J. Lin, Fluorescence detection and dissociation of amyloid-β species for the treatment of Alzheimer's disease, Adv. Therap. 2 (2019) 1900054, https://doi.org/10.1002/adtp.201900054.
[236] J. Zhou, P. Jangili, S. Son, M.S. Ji, M. Won, J.S. Kim, Fluorescent diagnostic probes in neurodegenerative diseases, Adv. Mater. 32 (2020) 2001945, https://doi.org/10.1002/adma.202001945.
[237] X.Z. Wang, J. Du, N.N. Xiao, Y. Zhang, L. Fei, J.D. LaCoste, Z. Huang, Q. Wang, X. R. Wang, B. Ding, Driving force to detect Alzheimer's disease biomarkers: application of a thioflavine T@Er-MOF ratiometric fluorescent sensor for smart detection of presenilin 1, amyloid β-protein and acetylcholine, Analyst 145 (2020) 4646–4663, https://doi.org/10.1039/d0an00440e.
[238] J. Qin, M. Cho, Y. Lee, Ferrocene-encapsulated Zn zeolitic imidazole framework (ZIF-8) for optical and electrochemical sensing of amyloid-β oligomers and for the early diagnosis of Alzheimer's disease, ACS Appl. Mater. Interfaces 11 (2019) 11743–11748, https://doi.org/10.1021/acsami.8b21425.
[239] Q. Fan, J. Wang, J.M. Biazik, S. Geng, F. Mazur, Y. Li, P.C. Ke, R. Chandrawati, UiO-66-NH2 metal-organic framework for the detection of Alzheimer's biomarker Aβ (1-42), ACS Appl. Bio Mater. 7 (2024) 182–192, https://doi.org/10.1021/acsabm.3c00768.
[240] X. Dong, G. Zhao, X. Li, J. Fang, J. Miao, Q. Wei, W. Cao, Electrochemiluminescence immunosensor of "signal-off" for β-amyloid detection based on dual metal-organic frameworks, Talanta 208 (2020) 120376, https://doi.org/10.1016/j.talanta.2019.120376.
[241] J. Miao, X. Li, Y. Li, X. Dong, G. Zhao, J. Fang, Q. Wei, W. Cao, Dual-signal sandwich electrochemical immunosensor for amyloid β-protein detection based on cu-Al_2O_3-g-C_3N_4-Pd and UiO-66@PANI-MB, Anal. Chim. Acta 1089 (2019) 48–55, https://doi.org/10.1016/j.aca.2019.09.017.
[242] J. Fang, G. Zhao, X. Dong, X. Li, J. Miao, Q. Wei, W. Cao, Ultrasensitive electrochemiluminescence immunosensor for the detection of amyloid-β proteins based on resonance energy transfer between g-C_3N_4 and Pd NPs coated NH_2-MIL-53, Biosens. Bioelectron. 142 (2019) 111517, https://doi.org/10.1016/j.bios.2019.111517.
[243] S.Y. Yin, G. Song, Y. Yang, Y. Zhao, P. Wang, L.M. Zhu, X. Yin, X.B. Zhang, Persistent regulation of tumor microenvironment via circulating catalysis of $MnFe_2O_4$@metal-organic frameworks for enhanced photodynamic therapy, Adv. Funct. Mater. 29 (2019) 1901417, https://doi.org/10.1002/adfm.201901417.
[244] Y. Wang, W. Wu, J. Liu, P.N. Manghnani, F. Hu, D. Ma, C. Teh, B. Wang, B. Liu, Cancer-cell-activated photodynamic therapy assisted by cu(II)-based metal-organic framework, ACS Nano 13 (2019) 6879–6890, https://doi.org/10.1021/acsnano.9b01665.
[245] X. Wan, H. Zhong, W. Pan, Y. Li, Y. Chen, N. Li, B. Tang, Programmed release of dihydroartemisinin for synergistic cancer therapy using $CaCO_3$ mineralized metal-organic framework, Angew. Chem. Int. Ed. 58 (2019) 14134–14139, https://doi.org/10.1002/anie.201907388.
[246] Z. Xu, P. Li, H. Chen, X. Zhu, Y. Zhang, M. Liu, S. Yao, Picomolar glutathione detection based on the dual-signal self-calibration electrochemical sensor of ferrocene-functionalized copper metal-organic framework via solid-state electrochemistry of cuprous chloride, J. Colloid Interface Sci. 628 (2022) 798–806, https://doi.org/10.1016/j.jcis.2022.08.107.
[247] D. Zhang, H. Zhang, H. Sun, Y. Yang, W. Zhong, Q. Chen, Q. Ren, G. Jin, Y. Zhang, Differential identification of GSH for acute coronary syndrome using a colorimetric sensor based on nanoflower-like artificial nanozymes, Talanta 266 (2024) 124967, https://doi.org/10.1016/j.talanta.2023.124967.
[248] S. Tajahmadi, H. Molavi, F. Ahmadijokani, A. Shamloo, A. Shojaei, M. Sharifzadeh, M. Rezakazemi, A. Fatehizadeh, T.M. Aminabhavi, M. Arjmand, Metal-organic frameworks: a promising option for the diagnosis and treatment of Alzheimer's disease, J. Control. Release 353 (2023) 1–29, https://doi.org/10.1016/j.jconrel.2022.11.002.

[249] P. Horcajada, T. Chalati, C. Serre, B. Gillet, C. Sebrie, T. Baati, J.F. Eubank, D. Heurtaux, P. Clayette, C. Kreuz, J.S. Chang, Y.K. Hwang, V. Marsaud, P. N. Bories, L. Cynober, S. Gil, G. Ferey, P. Couvreur, R. Gref, Porous metal-organic-framework nanoscale carriers as a potential platform for drug delivery and imaging, Nat. Mater. 9 (2010) 172–178, https://doi.org/10.1038/NMAT2608.
[250] J. Zhao, F. Yin, L. Ji, C. Wang, C. Shi, X. Liu, H. Yang, X. Wang, L. Kong, Development of a tau-targeted drug delivery system using a multifunctional nanoscale metal-organic framework for Alzheimer's disease therapy, ACS Appl. Mater. Interfaces 12 (2020) 44447–44458, https://doi.org/10.1021/acsami.0c11064.
[251] H.X. Ren, Y.B. Miao, Y. Zhang, An aptamer based fluorometric assay for amyloid-β oligomers using a metal-organic framework of type Ru@MIL-101(Al) and enzyme-assisted recycling, Microchim. Acta 187 (2020) 114, https://doi.org/10.1007/s00604-019-4092-3.
[252] S. Zhang, Y. Zhang, H. Wang, Y. Wang, H. Ma, D. Wu, Z.F. Gao, D. Fan, X. Ren, Q. Wei, Magnetic photoelectrochemical sensor array utilizing addressing sensing strategy for simultaneous detection of amyloid-β 42 and microtubule-associated protein tau, Anal. Chim. Acta 1298 (2024) 342407, https://doi.org/10.1016/j.aca.2024.342407.
[253] G. Zhao, Y. Wang, X. Li, Q. Yue, X. Dong, B. Du, W. Cao, Q. Wei, Dual-quenching electrochemiluminescence strategy based on three-dimensional metal-organic frameworks for ultrasensitive detection of amyloid-β, Anal. Chem. 91 (2019) 1989–1996, https://doi.org/10.1021/acs.analchem.8b04332.
[254] Y. Xiong, S. Chen, F. Ye, L. Su, C. Zhang, S. Shen, S. Zhao, Synthesis of a mixed valence state Ce-MOF as an oxidase mimetic for the colorimetric detection of biothiols, Chem. Commun. 51 (2015) 4635–4638, https://doi.org/10.1039/c4cc10346g.
[255] L. Yin, Y. Wang, R. Tan, H. Li, Y. Tu, Determination of β-amyloid oligomer using electrochemiluminescent aptasensor with signal enhancement by AuNP/MOF nanocomposite, Microchim. Acta 188 (2021) 53, https://doi.org/10.1007/s00604-021-04710-7.
[256] G. Wang, S. Tang, Y. Dong, F. Zou, J. Jiao, Y. Xiang, Template-controllable rolling circle amplification for dual protein sensitive analysis, J. Mater. Chem. B 12 (2024) 1523–1529, https://doi.org/10.1039/d3tb02478d.
[257] F. Chakari Khiavi, A. Mirzaie, B. Khalilzadeh, H. Yousefi, R. Abolhasan, A. Kamrani, R. Pourakbari, K. Shahpasand, M. Yousefi, M.R. Rashidi, Application of Pt@ZIF-8 nanocomposite-based electrochemical biosensor for sensitive diagnosis of tau protein in Alzheimer's disease patients, Sci. Rep. 13 (2023) 16163, https://doi.org/10.1038/s41598-023-43180-0.
[258] X. Chen, Y. Huang, S. Yang, S. Wang, L. Chen, X. Yu, N. Gan, S. Huang, In-situ nanozyme catalytic amplification coupled with a universal antibody orientation strategy based electrochemical immunosensor for AD-related biomarker, Biosens. Bioelectron. 266 (2024) 116738, https://doi.org/10.1016/j.bios.2024.116738.
[259] A.H. Valekar, B.S. Batule, M.I. Kim, K.H. Cho, D.Y. Hong, U.H. Lee, J.S. Chang, H. G. Park, Y.K. Hwang, Novel amine-functionalized iron trimesates with enhanced peroxidase-like activity and their applications for the fluorescent assay of choline and acetylcholine, Biosens. Bioelectron. 100 (2018) 161–168, https://doi.org/10.1016/j.bios.2017.08.056.
[260] N. Chauhan, S. Tiwari, T. Narayan, U. Jain, Bienzymatic assembly formed @Pt nano sensing framework detecting acetylcholine in aqueous phase, Appl. Surf. Sci. 474 (2019) 154–160, https://doi.org/10.1016/j.apsusc.2018.04.056.
[261] G. Ashraf, M. Asif, A. Aziz, T. Iftikhar, Z.T. Zhong, S. Zhang, B. Liu, W. Chen, Y. D. Zhao, Advancing interfacial properties of carbon cloth via anodic-induced self-assembly of MOFs film integrated with α-MnO2: a sustainable electrocatalyst sensing acetylcholine, J. Hazard. Mater. 426 (2022) 128133, https://doi.org/10.1016/j.jhazmat.2021.128133.
[262] C. Jia, J. Bai, Z. Liu, S. Gao, Y. Han, H. Yan, Application of a titanium-based metal-organic framework to protein kinase activity detection and inhibitor screening, Anal. Chim. Acta 1128 (2020) 99–106, https://doi.org/10.1016/j.aca.2020.06.065.
[263] G. Zhang, M. Li, K. Yu, H. Chai, S. Xu, T. Xu, L. Qu, X. Zhang, Two-dimensional metalloporphyrinic framework nanosheet-based dual-mechanism-driven ratiometric electrochemiluminescent biosensing of protein kinase activity, ACS Appl. Bio Mater. 4 (2021) 1616–1623, https://doi.org/10.1021/acsabm.0c01453.
[264] Amer Diabet Assoc, Diagnosis and classification of diabetes mellitus, Diabetes Care 28 (2005) S37–S42, https://doi.org/10.2337/dc14-S081.
[265] B. Biondi, G.J. Kahaly, R.P. Robertson, Thyroid dysfunction and diabetes mellitus: two closely associated disorders, Endocr. Rev. 40 (2019) 789–824, https://doi.org/10.1210/er.2018-00163.
[266] F.J. van Spronsen, N. Blau, C. Harding, A. Burlina, N. Longo, A.M. Bosch, Phenylketonuria, Nat. Rev. Dis. Prim. 7 (2021) 36, https://doi.org/10.1038/s41572-021-00267-0.
[267] J. Zhang, X. Zhuang, W. Meng, B. Tong, L. Liu, Y. Wang, C. Han, Dual-confinement regulating ternary metal-oxide activity sites derived from co-MOF for enhanced electrocatalytic activity for glucose oxidation, Chem. Eng. J. 489 (2024) 151398, https://doi.org/10.1016/j.cej.2024.151398.
[268] Y. Sun, Y.S. Zhang, H.T. Ren, H.X. Qiu, S.H. Zhang, Q. Lu, Y.J. Hu, Highly sensitive SERS sensors for glucose detection based on enzyme@MOFs and ratiometric Raman, Talanta 271 (2024) 125647, https://doi.org/10.1016/j.talanta.2024.125647.
[269] M. Asaduzzaman, O. Faruk, A.A. Samad, H. Kim, M.S. Reza, Y. Lee, J.Y. Park, A MOFs-derived hydroxyl-functionalized hybrid nanoporous carbon incorporated laser-scribed graphene-based multimodal skin patch for perspiration analysis and electrocardiogram monitoring, Adv. Funct. Mater. 34 (2024), https://doi.org/10.1002/adfm.202405651.
[270] J.H. Zhu, H. Wang, J. Guo, J. Zhao, Z. Gao, Y.Y. Song, C. Zhao, Homochiral light-sensitive metal-organic framework photoelectrochemical gated transistor for enantioselective discrimination of monosaccharides, Biosens. Bioelectron. 258 (2024) 116336, https://doi.org/10.1016/j.bios.2024.116336.
[271] W. Li, L. Liu, X. Li, H. Ren, L. Zhang, M.K. Parvez, M.S. Al Dosari, L. Fan, J. Liu, A Ni(II)MOF-based hypersensitive dual-function luminescent sensor towards the 3-nitrotyrosine biomarker and 6-propyl-2-thiouracil antithyroid drug in urine, J. Mater. Chem. B 12 (2024) 11800–11809, https://doi.org/10.1039/D4TB01618A.
[272] B. Kabak, E. Kendüzler, Europium metal-organic frameworks: synthesis, characterization, and application as fluorescence sensors for the detection of Cu^{2+}, Ni^{2+} cations and T_3, T_4 hormones, Talanta 266 (2024) 124944, https://doi.org/10.1016/j.talanta.2023.124944.
[273] X. Chen, H. Zhu, X. Huang, P. Wang, F. Zhang, W. Li, G. Chen, B. Chen, Novel iodinated gold nanoclusters for precise diagnosis of thyroid cancer, Nanoscale 9 (2017) 2219–2231, https://doi.org/10.1039/c6nr07656d.
[274] J. Chen, X. Yu, Y. Qu, X. Wang, Y. Wang, K. Jia, Q. Du, J. Han, H. Liu, X. Zhang, X. Wang, Z. Nie, High-performance metabolic profiling of high-risk thyroid anodules by ZrMOF hybrids, ACS Nano 18 (2024) 21336–21346, https://doi.org/10.1021/acsnano.4c05700.
[275] M. Ko, L. Mendecki, A.M. Eagleton, C.G. Durbin, R.M. Stolz, Z. Meng, K.A. Mirica, Employing conductive metal-organic frameworks for voltammetric detection of neurochemicals, J. Am. Chem. Soc. 142 (2020) 11717–11733, https://doi.org/10.1021/jacs.9b13402.
[276] S. Sargazi, I. Fatima, M.H. Kiani, V. Mohammadzadeh, R. Arshad, M. Bilal, A. Rahdar, A.M. Diez Pascual, R. Behzadmehr, Fluorescent-based nanosensors for selective detection of a wide range of biological macromolecules: a comprehensive review, Int. J. Biol. Macromol. 206 (2022) 115–147, https://doi.org/10.1016/j.ijbiomac.2022.02.137.
[277] J. Cheng, Y. Wu, L. Zhu, S. Lin, Y. Liu, K. Huang, W. Xu, Uric acid biosensors based on molecular recognition: classifications, advances, and prospects, Trac, Trends Anal. Chem. 179 (2024) 117887, https://doi.org/10.1016/j.trac.2024.117887.
[278] J. Han, Y. Zhang, X. Lv, D. Fan, S. Dong, A facile, low-cost bimetallic iron–nickel MOF nanozyme-propelled ratiometric fluorescent sensor for highly sensitive and selective uric acid detection and its smartphone application, Nanoscale 16 (2024) 1394–1405, https://doi.org/10.1039/D3NR05028A.
[279] X. Lin, D. Song, T. Shao, T. Xue, W. Hu, W. Jiang, X. Zou, N. Liu, A multifunctional biosensor via MXene assisted by conductive metal-organic framework for healthcare monitoring, Adv. Funct. Mater. 34 (2024) 2311637, https://doi.org/10.1002/adfm.202311637.
[280] W. Qi, L. Zheng, S. Wang, F. Huang, Y. Liu, H. Jiang, J. Lin, A microfluidic biosensor for rapid and automatic detection of Salmonella using metal-organic framework and raspberry Pi, Biosens. Bioelectron. 178 (2021) 113020, https://doi.org/10.1016/j.bios.2021.113020.
[281] J. Liang, Z. Huang, K. Wang, L. Zhang, Y. Wan, T. Yang, H. Zeng, Ultrasensitive visual detection of the food-borne pathogen via MOF encapsulated enzyme, Talanta 259 (2023) 124503, https://doi.org/10.1016/j.talanta.2023.124503.
[282] S. De Marchi, D. Garcia Lojo, G. Bodelon, J. Perez Juste, I. Pastoriza Santos, Plasmonic Au@ag@mSiO$_2$ nanorattles for in situ imaging of bacterial metabolism by surface-enhanced Raman scattering spectroscopy, ACS Appl. Mater. Interfaces 13 (2021) 61587–61597, https://doi.org/10.1021/acsami.1c21812.
[283] Z. Sun, Y. Peng, M. Wang, Y. Lin, M. Jalalah, S.A. Alsareii, F.A. Harraz, J. Yang, G. Li, Electrochemical deposition of cu metal-organic framework films for the dual analysis of pathogens, Anal. Chem. 93 (2021) 8994–9001, https://doi.org/10.1021/acs.analchem.1c01763.
[284] G. Dai, Z. Li, F. Luo, Y. Lu, Z. Chu, J. Zhang, F. Zhang, Q. Wang, P. He, Simultaneous electrochemical determination of nuc and mecA genes for identification of methicillin-resistant Staphylococcus aureus using N-doped porous carbon and DNA-modified MOF, Microchim. Acta 188 (2021) 39, https://doi.org/10.1007/s00604-020-04698-6.
[285] J.Y. Tian, X. Liu, S. Zhang, K. Chen, L. Zhu, Y. Song, M. Wang, Z. Zhang, M. Du, Novel aptasensing strategy for efficiently quantitative analyzing Staphylococcus aureus based on defective copper-based metal-organic framework, Food Chem. 402 (2023) 134357, https://doi.org/10.1016/j.foodchem.2022.134357.
[286] Y. Lou, Q. Jia, F. Rong, S. Zhang, Z. Zhang, M. Du, Universal biosensing platform based on polyMn-MOF nanosheets for efficient analysis of foodborne pathogens from diverse foodstuffs, Food Chem. 395 (2022) 133618, https://doi.org/10.1016/j.foodchem.2022.133618.
[287] W.C. Hu, J. Pang, S. Biswas, K. Wang, C. Wang, X.H. Xia, Ultrasensitive detection of bacteria using a 2D MOF nanozyme-amplified electrochemical detector, Anal. Chem. 93 (2021) 8544–8552, https://doi.org/10.1021/acs.analchem.1c01261.
[288] F. Chai, D. Wang, F. Shi, W. Zheng, X. Zhao, Y. Chen, C. Mao, J. Zhang, X. Jiang, Dual functional ultrasensitive point-of-care clinical diagnosis using metal-organic frameworks-based immunobeads, Nano Lett. 23 (2023) 9056–9064, https://doi.org/10.1021/acs.nanolett.3c02828.
[289] P. Wang, X. Wang, W. Li, Z. Leng, Z. Lu, K. Zhai, D. Xiang, Simultaneous detection of four specific DNAs fragments based on two-dimensional bimetallic MOF nanosheets, Microchem. J. 182 (2022) 107918, https://doi.org/10.1016/j.microc.2022.107918.
[290] B.P. Xie, G.H. Qiu, P.P. Hu, Z. Liang, Y.M. Liang, B. Sun, L.P. Bai, Z.H. Jiang, J. X. Chen, Simultaneous detection of dengue and Zika virus RNA sequences with a three-dimensional cu-based zwitterionic metal–organic framework, comparison of single and synchronous fluorescence analysis, Sensors Actuators B Chem. 254 (2018) 1133–1140, https://doi.org/10.1016/j.snb.2017.06.085.

[291] L. Wang, K. Liang, W. Feng, C. Chen, H. Gong, C. Cai, Molecularly imprinted polymers based on magnetically fluorescent metal-organic frameworks for the selective detection of hepatitis a virus, Microchem. J. 164 (2021) 106047, https://doi.org/10.1016/j.microc.2021.106047.
[292] A. Vojdani, H. Asaadi, Z. Meshkat, E. Aryan, S.B.T. Sany, H. Farsiani, J. Dorazehi, B. Hatamluyi, S. Abolbashari, A robust bioplatform based on DNA-gated nanoscale porous carbon derived from a metal-organic framework for specific detection of herpes simplex virus type 1, Sensors Actuators B 411 (2024) 135707, https://doi.org/10.1016/j.snb.2024.135707.
[293] W. Yang, D. Li, L. Chen, S. You, L. Chen, Hybridization-driven fluorometric platform based on metal-organic frameworks for the identification of the highly homologous viruses, Microchem. J. 187 (2023) 108403, https://doi.org/10.1016/j.microc.2023.108403.
[294] X. Wei, L. Zheng, F. Luo, Z. Lin, L. Guo, B. Qiu, G. Chen, Fluorescence biosensor for the H_5N_1 antibody based on a metal-organic framework platform, J. Mater. Chem. B 1 (2013) 1812–1817, https://doi.org/10.1039/c3tb00501a.
[295] Q. Lu, T. Su, Z. Shang, D. Jin, Y. Shu, Q. Xu, X. Hu, Flexible paper-based Ni-MOF composite/AuNPs/CNTs film electrode for HIV DNA detection, Biosens. Bioelectron. 184 (2021) 113229, https://doi.org/10.1016/j.bios.2021.113229.
[296] Z. Su, D. Tang, X. Yang, Y. Peng, B. Wang, X. Li, J. Chen, Y. Hu, X. Qin, Selective and fast growth of CdS nanocrystals on zinc (II) metal-organic framework architectures for photoelectrochemical response and electrochemical immunosensor of foot-and-mouth disease virus, Microchem. J. 174 (2022) 107038, https://doi.org/10.1016/j.microc.2021.107038.
[297] B. Perk, Y. Tepeli Büyüksünetçi, S. Bachraoui Bouzaien, M.F. Diouani, Ü. Anik, Fabrication of metal-organic framework based electrochemical Leishmania immunosensor, Microchem. J. 192 (2023) 108958, https://doi.org/10.1016/j.microc.2023.108958.
[298] Antimicrobial Resistance Anonymous, Collaborators., Global burden of bacterial antimicrobial resistance in 2019: a systematic analysis, Lancet 400 (2022) 1102, https://doi.org/10.1016/S0140-6736(21)02653-2.
[299] Y. Guo, Z. Han, H. Min, Z. Chen, T. Sun, L. Wang, W. Shi, P. Cheng, A europium-organic framework sensing material for 2-Aminoacetophenone, a bacterial biomarker in water, Inorg. Chem. 60 (2021) 9192–9198, https://doi.org/10.1021/acs.inorgchem.1c01251.
[300] M.M. Pan, D. Feng, Y. Ouyang, D. Yang, X. Yu, L. Xu, I. Willner, MOF-templated synthesis of cobalt-doped zinc oxide superparticles for detection of the 3-hydroxy-2-butanone microbial biomarker, Sensors Actuators B 358 (2022) 131482, https://doi.org/10.1016/j.snb.2022.131482.
[301] X.Z. Guo, B. Lin, G.Z. Xiong, R. Krishna, Z.R. Zhang, Q.Z. Liu, Z.X. Zhang, L. Fan, J. Zhang, B. Li, Construction of negative electrostatic sugared gourd pore within nickel-based metal-organic framework for one-step purification acetylene from ethylene and carbon dioxide mixture, Chem. Eng. J. 498 (2024) 154734, https://doi.org/10.1016/j.cej.2024.154734.
[302] Y. Sun, C. Zhao, J. Niu, J. Ren, X. Qu, Colorimetric band-aids for point-of-care sensing and treating bacterial infection, ACS Central Sci. 6 (2020) 207–212, https://doi.org/10.1021/acscentsci.9b01104.
[303] L. Zhang, M. Ouyang, Y. Zhang, L. Zhang, Z. Huang, L. He, Y. Lei, Z. Zou, F. Feng, R. Yang, The fluorescence imaging and precise suppression of bacterial infections in chronic wounds by porphyrin-based metal-organic framework nanorods, J. Mater. Chem. B 9 (2021) 8048–8055, https://doi.org/10.1039/d1tb01649k.
[304] K. Yuan, K. Huang, Y.Q. Yang, Y.X. Lin, Y.H. Liu, F.P. Li, Y.K. Liang, H.S. Chang, Y.H. Chen, T.T. Tang, S.B. Yang, Multi-roles of nanoscale bismuth metal-organic frameworks infectious photoacoustic probe and inhibitor of antibiotics tolerant bacteria via targeting endogenous H_2S, Nano Today 47 (2022) 101683, https://doi.org/10.1016/j.nantod.2022.101683.
[305] X. Liu, H. Xu, H. Peng, L. Wan, D. Di, Z. Qin, L. He, J. Lu, S. Wang, Q. Zhao, Advances in antioxidant nanozymes for biomedical applications, Coord. Chem. Rev. 502 (2024) 215610, https://doi.org/10.1016/j.ccr.2023.215610.
[306] N.O. Mishra, A.S. Quon, A. Nguyen, E.K. Papazyan, Y. Hao, Y. Liu, Constructing physiological defense systems against infectious disease with metal-organic frameworks: a review, ACS Appl. Bio. Mater. 6 (2023) 3052–3065, https://doi.org/10.1021/acsabm.3c00391.
[307] W. Hu, Q.O. Yang, C. Jiang, S. Huang, N.E. Alireza, D. Guo, J. Liu, Y. Peng, Biomedical metal–organic framework materials on antimicrobial therapy: perspectives and challenges, Mater. Today Chem. 41 (2024) 102300, https://doi.org/10.1016/j.mtchem.2024.102300.
[308] Q. Huang, Y. Chen, M. Ye, S. Zhuang, A. Zhong, J. Liu, G. Maduraiveeran, Y. Peng, Y. Huang, Metal-organic framework-based dressings: application and opportunities in wound healing, Mater. Today Chem. 40 (2024) 102235, https://doi.org/10.1016/j.mtchem.2024.102235.
[309] X. Zhu, H. Zheng, X. Wei, Z. Lin, L. Guo, B. Qiu, G. Chen, Metal-organic framework (MOF): a novel sensing platform for biomolecules, Chem. Commun. 49 (2013) 1276–1278, https://doi.org/10.1039/c2cc36661d.
[310] L. Chen, H. Zheng, X. Zhu, Z. Lin, L. Guo, B. Qiu, G. Chen, Z.N. Chen, Metal-organic frameworks-based biosensor for sequence-specific recognition of double-stranded DNA, Analyst 138 (2013) 3490–3493, https://doi.org/10.1039/c3an00426k.
[311] L. Qin, L.X. Lin, Z.P. Fang, S.P. Yang, G.H. Qiu, J.X. Chen, W.H. Chen, A water-stable metal-organic framework of a zwitterionic carboxylate with dysprosium: a sensing platform for ebolavirus RNA sequences, Chem. Commun. 52 (2016) 132–135, https://doi.org/10.1039/c5cc06697b.
[312] D.I. Osman, S.M. El Sheikh, S.M. Sheta, O.I. Ali, A.M. Salem, W.G. Shousha, S. F. EL Khamisy, S.M. Shawky, Nucleic acids biosensors based on metal-organic framework (MOF): paving the way to clinical laboratory diagnosis, Biosens. Bioelectron. 141 (2019) 111451, https://doi.org/10.1016/j.bios.2019.111451.
[313] J.M. Fang, F. Leng, X.J. Zhao, X.L. Hu, Y.F. Li, Metal-organic framework MIL-101 as a low background signal platform for label-free DNA detection, Analyst 139 (2014) 801–806, https://doi.org/10.1039/c3an01975f.
[314] S.P. Yang, W. Zhao, P.P. Hu, K.Y. Wu, Z.H. Jiang, L.P. Bai, M.M. Li, J.X. Chen, Lanthanum-based metal-organic frameworks for specific detection of Sudan virus RNA conservative sequences down to single-base mismatch, Inorg. Chem. 56 (2017) 14880–14887, https://doi.org/10.1021/acs.inorgchem.7b02107.
[315] D. Wu, Q. Cai, J. Zhang, F. Guo, G. Jie, Multifunctional spatial-potential resolved electrochemiluminescence biosensor for dual-channel simultaneous detection of hepatitis a virus and hepatitis C virus DNA, Sensors Actuators B 422 (2025) 136597, https://doi.org/10.1016/j.snb.2024.136597.
[316] G.Y. Wang, C. Song, D.M. Kong, W.J. Ruan, Z. Chang, Y. Li, Two luminescent metal-organic frameworks for the sensing of nitroaromatic explosives and DNA strands, J. Mater. Chem. A 2 (2014) 2213–2220, https://doi.org/10.1039/c3ta14199c.
[317] M. Mehmandoust, Z.P. Gumus, M. Soylak, N. Erk, Electrochemical immunosensor for rapid and highly sensitive detection of SARS-CoV-2 antigen in the nasal sample, Talanta 240 (2022) 123211, https://doi.org/10.1016/j.talanta.2022.123211.
[318] Y. Li, W. Wang, W. Yue, Q. Lei, Z. Zhao, Y. Sun, H. Xu, W. Zhang, L. Chen, J. K. Kim, J. Hu, Construction of highly sensitive electrochemical immunosensor based on au and Co_3O_4 nanoparticles functionalized Ni/co bimetal conductive MOF for quantitative detection of HBsAg, Chem. Eng. J. 483 (2024) 149087, https://doi.org/10.1016/j.cej.2024.149087.
[319] L. Luo, F. Zhang, C. Chen, C. Cai, Molecular imprinting resonance light scattering nanoprobes based on pH-responsive metal-organic framework for determination of hepatitis a virus, Microchim. Acta 187 (2020) 140, https://doi.org/10.1007/s00604-020-4122-1.
[320] Y. Wang, Y. Hu, Q. He, J. Yan, H. Xiong, N. Wen, S. Cai, D. Peng, Y. Liu, Z. Liu, Metal-organic frameworks for virus detection, Biosens. Bioelectron. 169 (2020) 112604, https://doi.org/10.1016/j.bios.2020.112604.
[321] G. Férey, C. Serre, C. Mellot Draznieks, F. Millange, S. Surblé, J. Dutour, I. Margiolaki, A hybrid solid with giant pores prepared by a combination of targeted chemistry, simulation, and powder diffraction, Angew. Chem. Int. Ed. 43 (2004) 6296–6301, https://doi.org/10.1002/anie.200460592.
[322] G. Férey, C. Mellot Draznieks, C. Serre, F. Millange, J. Dutour, S. Surblé, I. Margiolaki, A chromium terephthalate-based solid with unusually large pore volumes and surface area, Science 309 (2005) 2040–2042, https://doi.org/10.1126/science.1116275.
[323] R. Singh, J.F. White, M. de Vries, G. Beddome, M. Dai, A.G. Bean, X. Mulet, D. Layton, C.M. Doherty, Biomimetic metal-organic frameworks as protective scaffolds for live-virus encapsulation and vaccine stabilization, Acta Biomater. 142 (2022) 320–331, https://doi.org/10.1016/j.actbio.2022.02.002.
[324] B.R. Martins, Y.O. Barbosa, C.M.R. Andrade, L.Q. Pereira, G.F. Simao, C.J. de Oliveira, D. Correia, R.T.S. Oliveira Jr., M. da Silva, A.C.A. Silva, N.O. Dantas, V. Rodrigues Jr., R.A.A. Munoz, R.P. Alves-Balvedi, Development of an electrochemical immunosensor for specific detection of visceral leishmaniasis using gold-modified screen-printed carbon electrodes, Biosensors-Basel 10 (2020) 81, https://doi.org/10.3390/bios10080081.
[325] N. Rispail, L. De Matteis, R. Santos, A.S. Miguel, L. Custardoy, P.S. Testillano, M. C. Risueno, A. Perez-de-Luque, C. Maycock, P. Fevereiro, A. Oliva, R. Fernandez-Pacheco, M. Ricardo Ibarra, J.M. de la Fuente, C. Marquina, D. Rubiales, E. Prats, Quantum dot and superparamagnetic nanoparticle interaction with pathogenic fungi: internalization and toxicity profile, ACS Appl. Mater. Interfaces 6 (2014) 9100–9110, https://doi.org/10.1021/am501029g.
[326] J. Rosário, L.L. da Luz, R. Geris, J.G.S. Ramalho, A.F. da Silva, S. Alves, M. Malta, Photoluminescent organisms: how to make fungi glow through biointegration with lanthanide metal-organic frameworks, Sci. Rep. 9 (2019) 7302, https://doi.org/10.1038/s41598-019-43835-x.
[327] A.A.M. El Shafey, M.H.A. Hegab, M.M.E. Seliem, A.M.A. Barakat, N.E. Mostafa, H. A. Abdel Maksoud, R.M. Abdelhameed, Curcumin@metal organic frameworks nano-composite for treatment of chronic toxoplasmosis, J. Mater. Sci. Mater. Med. 31 (2020) 90, https://doi.org/10.1007/s10856-020-06429-y.
[328] A. Sosa Arroniz, A. Lopez Monteon, R. Pena Rodriguez, J.M. Rivera Villanueva, J. Torres Montero, A. Ramos Ligonio, Efficacy of a Zn-based metalorganic framework doped with benznidazole on acute experimental Trypanosoma cruzi infection, Drug. Deliv. Transl. Res. (2024) 2190–2393, https://doi.org/10.1007/s13346-024-01664-0.
[329] B. Ran, L. Ran, Z. Wang, J. Liao, D. Li, K. Chen, W. Cai, J. Hou, X. Peng, Photocatalytic antimicrobials: principles, design strategies, and applications, Chem. Rev. 123 (2023) 12371–12430, https://doi.org/10.1021/acs.chemrev.3c00326.
[330] F. Paknia, M. Roostaee, E. Isaei, M.S. Mashhoori, G. Sargazi, M. Barani, A. Amirbeigi, Role of metal-organic frameworks (MOFs) in treating and diagnosing microbial infections, Int. J. Biol. Macromol. 262 (2024) 130021, https://doi.org/10.1016/j.ijbiomac.2024.130021.
[331] L. Su, Y. Li, Y. Liu, R. Ma, Y. Liu, F. Huang, Y. An, Y. Ren, H.C. van der Mei, H. J. Busscher, L. Shi, Antifungal-inbuilt metal-organic-frameworks eradicate Candida albicans biofilms, Adv. Funct. Mater. 32 (2022) 2202895, https://doi.org/10.1002/adfm.202202895.
[332] J.I. Shin, K.H. Lee, Y.H. Joo, J.M. Lee, J. Jeon, H.J. Jung, M. Shin, S. Cho, T. H. Kim, S. Park, B.Y. Jeon, H. Jeong, K. Lee, K. Kang, M. Oh, H. Lee, S. Lee, Y. Kwon, G.H. Oh, A. Kronbichler, Inflammasomes and autoimmune and rheumatic diseases: a comprehensive review, J. Autoimmun. 103 (2019) 102299, https://doi.org/10.1016/j.jaut.2019.06.010.

[333] N. Brodszki, A. Frazer Abel, A.S. Grumach, M. Kirschfink, J. Litzman, E. Perez, M. R.J. Seppanen, K.E. Sullivan, S. Jolles, European society for immunodeficiencies (ESID) and european reference network on rare primary immunodeficiency, autoinflammatory and autoimmune diseases (ERN RITA) complement guideline: deficiencies, diagnosis, and management, J. Clin. Immunol. 40 (2020) 576–591, https://doi.org/10.1007/s10875-020-00754-1.

[334] L. Zhao, J. Zhou, P. Li, S. Huang, X. Zhu, Y. Zhang, M. Liu, S. Yao, Target-induced photoelectrochemistry and colorimetric dual-mode platform for HIgG based on Ag_2S/SnO_2 composites and CoOOH nanoflakes, Sensors Actuators B Chem. 409 (2024) 135638, https://doi.org/10.1016/j.snb.2024.135638.

[335] J. Chen, J. Qi, C. Chen, J. Chen, L. Liu, R. Gao, T. Zhang, L. Song, D. Ding, P. Zhang, C. Liu, Tocilizumab-conjugated polymer nanoparticles for NIR-II photoacoustic-imaging-guided therapy of rheumatoid arthritis, Adv. Mater. 32 (2020) 2003399, https://doi.org/10.1002/adma.202003399.

[336] L. Li, X. Wang, R. Gao, B. Zhang, Y. Liu, J. Zhou, L. Fu, J. Wang, Inflammation-triggered supramolecular nanoplatform for local dynamic dependent imaging-guided therapy of rheumatoid arthritis, Adv. Sci. 9 (2022) 2105188, https://doi.org/10.1002/advs.202105188.

[337] F. Colombo, P. Durigutto, L. De Maso, S. Biffi, B. Belmonte, C. Tripodo, R. Oliva, P. Bardini, G.M. Marini, E. Terreno, G. Pozzato, E. Rampazzo, J. Bertrand, B. Feuerstein, J. Javurek, J. Havrankova, C. Pitzalis, L. Nunez, P. Meroni, F. Tedesco, D. Sblattero, P. Macor, Targeting $CD34^+$ cells of the inflamed synovial endothelium by guided nanoparticles for the treatment of rheumatoid arthritis, J. Autoimmun. 103 (2019) 102288, https://doi.org/10.1016/j.jaut.2019.05.016.

[338] L. Guo, S. Zhong, P. Liu, M. Guo, J. Ding, W. Zhou, Radicals scavenging MOFs enabling targeting delivery of siRNA for rheumatoid arthritis therapy, Small 18 (2022) 2202604, https://doi.org/10.1002/smll.202202604.

[339] B. Wang, X.Q. Zhou, L. Li, Y.X. Li, L.P. Yu, Y. Chen, Ratiometric fluorescence sensor for point-of-care testing of bilirubin based on tetraphenylethylene functionalized polymer nanoaggregate and rhodamine B, Sensors Actuators B 369 (2022) 132392, https://doi.org/10.1016/j.snb.2022.132392.

[340] C. Xia, Y. Xu, M.M. Cao, Y.P. Liu, J.F. Xia, D.Y. Jiang, G.H. Zhou, R.J. Xie, D. F. Zhang, H.-L. Li, A selective and sensitive fluorescent probe for bilirubin in human serum based on europium(III) post-functionalized Zr(IV)-based MOFs, Talanta 212 (2020) 120795, https://doi.org/10.1016/j.talanta.2020.120795.

[341] W. Hou, W. Mao, D. Yu, Y. Pan, W. Shen, J. Zhang, D. Kong, L. Zang, H. Dai, F. Yang, H.K. Lee, S. Tang, Photo-crosslinked hydrogel as a sensing platform for sensitive detection of free bilirubin in urine samples, Sensors Actuators B 411 (2024) 135663, https://doi.org/10.1016/j.snb.2024.135663.

[342] H. Lin, Y. Yan, C. Deng, N. Sun, Engineered bimetallic MOF-crafted bullet aids in penetrating serum metabolic traits of chronic obstructive pulmonary disease, Anal. Chem. 96 (2024) 14688–14696, https://doi.org/10.1021/acs.analchem.4c03681.

[343] W. Zhang, J. Ren, J. Lu, P. Li, W. Zhang, H. Wang, B. Tang, Elucidating the relationship between ROS and protein phosphorylation through in situ fluorescence imaging in the pneumonia mice, Anal. Chem. 93 (2021) 10907–10915, https://doi.org/10.1021/acs.analchem.1c01690.

[344] X. Huang, S. Zhang, Y. Tang, X. Zhang, Y. Bai, H. Pang, Advances in metal-organic framework-based nanozymes and their applications, Coord. Chem. Rev. 449 (2021) 214216, https://doi.org/10.1016/j.ccr.2021.214216.

[345] Y. Huo, M. Bu, Z. Ma, J. Sun, Y. Yan, K. Xiu, Z. Wang, N. Hu, Y. Li, Flexible, non-contact and multifunctional humidity sensors based on two-dimensional phytic acid doped co-metal organic frameworks nanosheets, J. Colloid Interface Sci. 607 (2022) 2010–2018, https://doi.org/10.1016/j.jcis.2021.09.189.

[346] Q. Lin, J. Huang, Y. Zhang, M. Chen, Y. Xu, X. Zou, S. Liu, Z. Dai, A smartphone-assisted "all-in-one" paper chip for one-pot noninvasive detection of salivary glucose level, Chem. Eng. J. 468 (2023) 143608, https://doi.org/10.1016/j.cej.2023.143608.

[347] A. Khan, Z. Riahi, J.T. Kim, J.W. Rhim, Gelatin/carrageenan-based smart packaging film integrated with cu-metal organic framework for freshness monitoring and shelf-life extension of shrimp, Food Hydrocoll. 145 (2023) 109180, https://doi.org/10.1016/j.foodhyd.2023.109180.

[348] Z. Xu, Z. Cheng, Q. Tang, K. Huang, H. Li, Z. Zou, Ammonia-sensitive cellulose acetate-based films incorporated with co-BIT microcrystals for smart packaging application, Carbohydr. Polym. 316 (2023) 121045, https://doi.org/10.1016/j.carbpol.2023.121045.

[349] Y. Kang, D. Zhao, D. Cai, B. Jia, J. Fu, X. Li, J. Hu, L. Li, Novel copper-based metal–organic skeleton smart tags that respond to ammonia for real-time visual freshness monitoring of shrimp, Chem. Eng. J. 495 (2024) 153388, https://doi.org/10.1016/j.cej.2024.153388.

[350] H. O'Brien, T. Davoodian, M.D.L. Johnson, The promise of copper ionophores as antimicrobials, Curr. Opin. Microbiol. 75 (2023) 102355, https://doi.org/10.1016/j.mib.2023.102355.

[351] Z. You, M. Zhao, H. Lu, H. Chen, Y. Wang, Eye-readable and wearable colorimetric sensor arrays for in situ monitoring of volatile organic compounds, ACS Appl. Mater. Interfaces 16 (2024) 19359–19368, https://doi.org/10.1021/acsami.4c00312.

[352] D. Zhang, Z. Yang, S. Yu, Q. Mi, Q. Pan, Diversiform metal oxide-based hybrid nanostructures for gas sensing with versatile prospects, Coord. Chem. Rev. 413 (2020) 213272, https://doi.org/10.1016/j.ccr.2020.213272.

[353] D. Zhang, J. Liu, C. Jiang, A. Liu, B. Xia, Quantitative detection of formaldehyde and ammonia gas via metal oxide-modified graphene-based sensor array combining with neural network model, Sensors Actuators B 240 (2017) 55–65, https://doi.org/10.1016/j.snb.2016.08.085.

[354] S. Okur, Z. Zhang, M. Sarheed, P. Nick, U. Lemmer, L. Heinke, Towards a MOF e-nose: a SURMOF sensor array for detection and discrimination of plant oil scents and their mixtures, Sensors Actuators B 306 (2020) 127502, https://doi.org/10.1016/j.snb.2019.127502.

[355] S. Okur, P. Qin, A. Chandresh, C. Li, Z. Zhang, U. Lemmer, L. Heinke, An enantioselective e-nose: an array of nanoporous homochiral MOF films for stereospecific sensing of chiral odors, Angew. Chem. Int. Ed. 60 (2021) 3566–3571, https://doi.org/10.1002/anie.202013227.

[356] D. Wang, D. Zhang, Y. Yang, Q. Mi, J. Zhang, L. Yu, Multifunctional latex/polytetrafluoroethylene-based triboelectric nanogenerator for self-powered organ-like MXene/metal-organic framework-derived CuO nanohybrid ammonia sensor, ACS Nano 15 (2021) 2911–2919, https://doi.org/10.1021/acsnano.0c09015.